ERDC/CRREL TR-04-17

Cold Regions Research and Engineering Laboratory

US Army Corps of Engineers®
Engineer Research and Development Center

Blast-Sound-Absorbing Surfaces

A Joint Project of the ERDC and the Netherlands Ministry of Defense

Keith Attenborough, Alan Cummings, Piyush Dutta, Paul Schomer, Erik Salomons, Edwin Standley, Olga Umnova, Frank Van Den Berg, Frits Van Der Eerden, Pieter Van Der Weele, and Eric Védy

September 2004

ERDC/CRREL TR-04-17
September 2004

Blast-Sound-Absorbing Surfaces

A Joint Project of the ERDC and the Netherlands Ministry of Defense

Keith Attenborough, Alan Cummings, Piyush Dutta,
Paul Schomer, Erik Salomons, Edwin Standley,
Olga Umnova, Frank Van Den Berg, Frits Van Der Eerden,
Pieter Van Der Weele, and Eric Védy

Prepared for OFFICE OF THE CHIEF OF ENGINEERS and
THE NETHERLANDS DEFENSE COORDINATOR FOR SPATIAL PLANNING AND ENVIRONMENT

ABSTRACT

This research investigated methods of absorbing blast sound, including the development of analytical theories, numerical simulations, laboratory experiments, and a field trial. Prior to this research, no theory existed for the design of sound-absorbing surfaces at low frequencies in a highly non-linear shock environment. The work includes developments of (1) a theory for the non-linear response of rigid-porous materials to high amplitude sound, allowing for a linear variation of flow resistivity with flow velocity (Forchheimer's non-linearity); (2) a time-domain non-linear theory that assumes low frequencies, semi-infinite media, and weak shocks and gives explicit results for incident triangular shock waveforms; (3) an alternative time-domain formulation that enables predictions for a finite layer but requires numerical integration; and (4) a further non-linear theory that predicts the response of multiple rigid-porous layers to continuous high-intensity sound. Numerical work has been carried out to predict the surface impedance of a porous and elastic layer subject to continuous high-intensity sound and including Forchheimer's non-linearity. Measurements have been made on the propagation constant, characteristic impedance, and reflection coefficients for finite-amplitude, low-frequency continuous sound waves incident on porous concrete, porous aluminum, sand, gravel stones, perforated panels, and open-cell polymer foams. In addition, shock tube systems based on membrane rupture have been used to look at the acoustic shock response of materials. Finally, the far-field propagation is modeled using parabolic equation method. A full-scale field test using high explosives was conducted at Ft. Drum, NY. The primary purpose was to test predictions of the blast reflection from and attenuation into a porous medium, and a secondary objective was to test the effect of plowing the ground surface over a larger area. Charges of C4 were exploded over two candidate blast sound-absorbing test surface sections filled with gravel stones. The non-linear theory for response of rigid-porous layers to continuous high amplitude sound has been found to give predictions in good agreement with impedance tube data. The most interesting behavior is that the reflection coefficient decreases at first as incident sound pressure increases. The non-linear theory for the impulse response of single rigid-porous layers has been found to give predictions in good agreement with laboratory measurements of shock wave reflection and transmission. The predictions of the plane wave non-linear theories have been found to be in reasonable agreement with reflection and transmission data from Ft. Drum.

CONTENTS

LIST OF ILLUSTRATIONS

LIST OF TABLES

LIST OF ACRONYMS

ACS(IM)	Assistant Chief of Staff (Installation and Management)
AMC	Army Materiel Command
COE	Corps of Engineers
CROMD	Coordinator for Spatial Planning and Environment
CRREL	Cold Regions Research and Engineering Laboratory
DAT	Data
dB	Decibel unit
DCSOPS	Deputy Chief of Staff for Operations
ERDC	Engineer Research and Development Center
FCT	Flux corrected transport code
FORSCOM	Forces Command
NCEJ	*Noise Control Engineering Journal*
NH	New Hampshire
NL MOD	Netherlands Ministry of Defense
NPE	Non-linear parabolic equation; also name of code
NY	New York
OBCF	Octave band center frequency
PE	Parabolic equation
SEL	Sound exposure level
TNO	The Netherlands Organization of Scientific Research
TPD	The Institute of Applied Physics of TNO
U.S. DOD	U.S. Department of Defense
USA	United States of America

EXECUTIVE SUMMARY

The noise generated by military testing and training causes considerable annoyance to the surrounding civilian communities and results in a large number of complaints. The conflict between the need to train and good relationships with the off-post civilian community is severely affecting training and readiness missions in the U.S. and Europe. The primary Army noise source is the high-energy impulsive noise generated by large weapons (e.g. armor, artillery, or demolition). Measures are most effective if they are placed near the source. Standard noise attenuation techniques such as barriers and partial enclosures might offer some reduction, particularly if placed close to the source. However, noise from large guns has considerable energy in the frequency range from 15 to 125 Hz. At the lowest frequencies, for example at 15 Hz, a barrier would need to be 50 m tall. The creation of local sound-absorbing surfaces at firing locations represents a potential means for large weapon noise mitigation. However, the interaction of high blast sound pressure levels close to the weapon with barriers and sound-absorbing material cannot be described by the usual linear models. The basic research described here represents a joint effort to investigate methods of absorbing blast sound, local to its generation, by the U.S. (ERDC with support from the University of Hull, UK) and the Netherlands (NL-MOD, Coordinator for Spatial Planning and Environment, with support from TNO, The Netherlands Organization of Scientific Research). The work by the contributors from the Netherlands has extended also to predict audio-frequency blast sound levels at longer ranges. The work reported here includes the development of analytical theories, numerical simulations, laboratory experiments, and a field trial.

Prior to this research effort, no theory existed for the design of sound-absorbing surfaces at low frequencies in a highly non-linear shock environment. An important parameter that controls the linear acoustical properties of rigid-porous materials is the flow resistivity or air permeability. The following are new theoretical developments:

- A theory has been developed for the non-linear response of rigid-porous materials to high-amplitude continuous sound, which allows for a linear variation of flow resistivity with flow velocity (Forchheimer's non-linearity). This theory enables predictions of the acoustic reflection coefficient at the surface of a hard-backed rigid-porous layer as a function of incident sound pressure as well as frequency.
- A time-domain non-linear theory has been developed also, since transient wave motion is the primary consideration of the project. The theory assumes low frequencies, semi-infinite media, and weak shocks and gives explicit results for incident triangular shock waveforms.

- An alternative time-domain formulation has been derived from the frequency-domain solution. It enables predictions for a finite layer but requires numerical integration.
- A further non-linear theory has been derived that predicts the response of multiple rigid-porous layers to continuous high-intensity sound.

Numerical work has been carried out also on predicting the surface impedance of a porous *and elastic* layer subject to continuous high-intensity sound and including Forchheimer's non-linearity.

An impedance tube system has been constructed at the University of Hull in which a layer of test material is placed. This system has been used to test theory on a range of materials, including those of particular interest for the project objectives. Measurements have been made on the propagation constant, characteristic impedance, and reflection coefficients for finite-amplitude, low-frequency continuous sound waves incident on porous concrete, porous aluminum, sand, gravel stones of two mean sizes, perforated panels, and open- cell polymer foams. In addition, two shock tube systems based on membrane rupture have been constructed: a large system containing five PCB transducers at ERDC/CRREL and a smaller system at the University of Hull. These have been used to look at the acoustic shock response of materials. The tube at Hull has also been used to investigate acoustic shock transmission through and into various rigid-porous materials, both as single layers and in triple-layer configurations, and the frame displacement by means of a magnetic technique, in the case of flexible materials.

In the Netherlands a computational fluid dynamics method [the Flux Corrected Transport (FCT) method] for calculating shock waves at short ranges, typically 1–15 m from explosions, has been modified to allow for interaction with porous structures. It is based on the multi-dimensional Euler equations. In this project the applicability of using the FCT technique for the case of gun muzzle blast propagation has been investigated. In using this approach, an explosion at the muzzle is chosen as a starting condition.

A theory is needed to describe the degeneration of a blast wave into an acoustical wave. A non-linear propagation code (non-linear parabolic equation, NPE) for moderate distances from the weapon has been developed, based on an equation for non-linear propagation. It is restricted to isentropic processes, such as pressure waves with shocks that are not too strong (less than 10 kPa). Atmospheric refraction and dissipation can be taken into account using these calculations. In NPE the flow resistivity and porosity can be included for the ground as an additional boundary condition at the air–ground interface. The ground is then also included in the code. However, no satisfactory results have been found yet.

Finally, the far-field propagation is modeled using PE. The PE or parabolic equation method is based on a numerical integration of the linear wave equation in the frequency domain. Atmospheric refraction and ground absorption can be explicitly accounted for when using the PE. The PE method works in the frequency domain. To use the blast wave, which is described in the time domain by the FCT and NPE method, for the PE method, it has to be decomposed into Fourier components. Wave propagation is then described for each component with the PE method for several hundreds of meters.

The coupling between these models can be solved sequentially, since we only consider waves traveling outwards from the source; there is only a "one-way coupling." Thus, in addition to describing the near-field flow of the muzzle numerically, another main innovative aspect to this project is the coupling of different propagation codes into one approach.

A full-scale field campaign using high explosives has been conducted at Ft. Drum. The primary purpose was to test predictions of the blast reflection from and attenuation into a porous medium. A secondary objective was to test the effect of plowing the ground surface over a larger area.

Charges of C4 ranging from 71 g (eighth stick) to 567 g (one stick) were exploded at a height of 2 m over two candidate blast-sound-absorbing test surface sections consisting of 3.45-m-square × 1.5-m-deep pits filled with gravel stones. Because of cost limitations, smaller test sections were used than would be required for substantial noise reduction at long range. A grass-covered control site was used as a reference. The multi-layering of Pit 1 was intended to give good absorption at 50 Hz. For comparison with predictions and simplicity of analytical analysis, Pit 2 was filled entirely with pea gravel.

Measurements were made of the reflections from these test surfaces and the attenuation into the test surfaces. Measurements of linear ground impedance were made over the pits, undisturbed grass-covered soil, and plowed ground. In addition, acoustic data were gathered at farther distances ranging from 15 to 250 m. Meteorological data including wind and temperature profiles were collected at 100 m from the explosions. The longer-range and meteorological measurements were intended to enable to test sound propagation computations.

The non-linear theory for the response of rigid-porous layers to continuous high-amplitude sound has been found to give predictions in good agreement with impedance tube data. In particular, both theory and experiment have shown that non-linearity has a strong influence on the acoustic behavior near the layer resonance and that two types of behavior are possible depending on the porous material characteristics. The most interesting behavior from the point of view of the blast sound absorbers project is that in which the reflection coefficient decreases at first as incident sound pressure increases. The non-linear theory for the

impulse response of single rigid-porous layers has been found to give predictions in good agreement with laboratory measurements of shock wave reflection and transmission. The non-linear theory for response of multiple layers of rigid-porous materials has been found to give good agreement with impedance tube measurements on double and triple layers. In particular, it has been found that configurations designed to give optimum absorption at linear amplitudes may not continue to do so as the incident sound pressure is increased. The predictions of the plane wave non-linear theories have been found to be in reasonable agreement with reflection and transmission data from Ft. Drum Pit 2. Calculations made using the FCT-code have been found to correspond well with results found in the literature. FCT calculations have been found to agree also with waveform data above and near Pit 2 from the Ft. Drum trial. Further FCT calculations indicate that a larger pit will yield greater absorption beyond the pit.

Ft. Drum data show that Pit 2 gives good absorption between 8 and 500 Hz. However, only Pit 1 leads to slight reductions at 15 and 250 m. The quarter-stick data indicate that a shorter distance between the blast source and the absorbing surface (1 m instead of 2 m) leads to greater absorption.

The plowed field test yielded a noticeable effect. The main absorption occurs at short distances (up to 50 m) and occurs even below 100 Hz. At 250 m absorption occurs at the higher frequencies (over 100 Hz). Both pit and plowed field data showed behavior at low frequencies that is not predicted by rigid-porous material approaches, and it is suggested that the elasticity of the ground and pit materials is implicated through acoustic-to-seismic coupling.

Since the basic ability to design and optimize blast source sound-absorbing surfaces has been developed from the work reported here, it is recommended that further research be conducted to provide requisite proof of concept and bread-board validation. The FCT code and the analytical methods can be extended to enable optimization of the size, shape, extent, and material makeup of absorbing surface. For practical configurations, such topics as starting conditions and muzzle brake effects must be considered. Optimizing the standoff distance for a given source should be considered also. There should be field trials of candidate materials to ensure minimal damage and to investigate benefits from non-planar surfaces and practical configurations for armor fire. Finally, a full-scale test would compare data with theory leading to a design method protocol and corresponding manual.

PREFACE

This report was prepared by Keith Attenborough, University of Hull, UK; Alan Cummings, University of Hull, UK; Piyush Dutta, USA/ERDC-CRREL; Paul Schomer, Schomer and Associates, Inc., USA; Erik Salomons, TNO TPD; Edwin Standley, University of Hull, UK; Olga Umnova, University of Hull, UK; Frank van den Berg, TNO TPD, NL; Frits van der Eerden, TNO TPD, NL; Pieter van der Weele, Netherlands MOD-CROMD; and Eric Védy, TNO TPD, NL.

The authors of this report and researchers in this study gratefully acknowledge the excellent support provided by Ft. Drum for the conduct of the full-scale field test. First, they thank the Environmental Office and Jim Haynes, the Airfield and Joe White, and the Range Control Office and Al Schwark for their cooperation and coordination that made this study at Ft. Drum possible. Secondly, they acknowledge and thank the following individuals and groups for their active assistance in the setup and conduct of this test: Al Schwark, Range Control, for overall support and guidance; Joe Donnally, Range Control, for coordination and interface with airfield and with ammo supply; Tom Lent, Range Control–ITAM Program, for site layout and construction; ITAM Program, Range Control, for site construction; and 46th Engineers, for setting charges and other site logistical support.

This project was funded by the Office of the Chief of Engineers and by the Netherlands Ministry of Defense Coordinator for Spatial Planning and Environment.

This report was prepared under the general supervision of Dr. Justin Berman, Chief, Applied and Military Engineering Branch; and James L. Wuebben, Acting Director, CRREL.

The commander of the Engineering Research and Development Center is COL James R. Rowan. The director is Dr. James R. Houston.

Blast-Sound-Absorbing Surfaces

A Joint Project of the ERDC and the Netherlands Ministry of Defense

KEITH ATTENBOROUGH, ALAN CUMMINGS, PIYUSH DUTTA,
PAUL SCHOMER, ERIK SALOMONS, EDWIN STANDLEY,
OLGA UMNOVA, FRANK VAN DEN BERG, FRITS VAN DER EERDEN,
PIETER VAN DER WEELE, AND ERIC VÉDY

1 INTRODUCTION

Background

The noise generated by military testing and training results in annoyance in and complaints from the off-post civilian community that surrounds military installations. This conflict between the need to train and the off-post civilian community is negatively affecting the U.S. DOD and The Netherlands (NL) MOD training and readiness mission. This is certainly the case for land forces of the MOD and for the U.S. Army, where, for both, weapons noise is one of their most major problems. In the Netherlands, the increasing demands from noise regulations lessen the ability to train. In the U.S., the Air Force has stated that noise is the number one issue affecting their ability to train, and when the Navy instituted their supersonic flight training area at Naval Air Station Fallon, noise was the chief issue negotiated between the Secretary of the Navy and the Governor of Nevada.

In addition, improvements in conventional arms have resulted in noisier weapons that fire at more distant targets than in the past. To accommodate increased target distances, training area operators must site these weapons close to the boundary, further raising the impulsive noise levels in neighboring communities. Also, over the years planners have sought to optimize land use, which has resulted in dwellings being closer to established firing ranges. All of these factors exacerbate the noise problem.

Much environmental research by the U.S. DOD and the NL-MOD has concentrated on predicting the noise impact. Consequently, that research has

been concerned with the physics of sound propagation, methods to quantify community response to noise, and computerized models for land use compatibility studies and noise assessment. The primary Army noise source is the high-energy impulsive noise generated by large weapons (e.g. armor, artillery, or demolition). It is well known that large-weapon noise creates conflict with the off-post community. What is needed is the means to mitigate the noise. Reducing training opportunities and the number of firing locations is not a good long-term noise mitigation solution and is not in the best interest of the Army.

Large-weapon noise is particularly difficult to mitigate. Mitigation measures are most effective if they are placed near the source. Due to the high blast sound pressure levels close to the weapon, the interaction of the sound field with barriers and sound-absorbing material cannot be described by the usual linear models. Noise from large guns has considerable energy in the frequency range from 15 to 125 Hz. Standard noise attenuation techniques such as barriers and partial enclosures might offer some reduction, particularly if placed close to the source. However, the long wavelengths corresponding to the lowest of these frequencies make them impracticable. For example, a barrier would need to be tens of meters tall to be effective at 15 Hz. And to make matters more difficult, near the source, the acoustic wave is in the form of a shock wave. This means that commonly used linear theories are not applicable. Thus, to date, little has been done to mitigate large-weapon noise because of a lack of basic theories and technology.

One obvious potential means for large-weapon noise mitigation is the creation of local sound absorbing surfaces at firing locations. According to the ISO dose–response relationship, the nature of community response to blast noise means that a 3-dB reduction in the C-weighted sound exposure level (CSEL) is equivalent to up to a 6-dB reduction in terms of annoyance. Other dose–response relationships also suggest that such a reduction is very significant. But prior to this research effort, no theory existed for the design of sound-absorbing surfaces at low frequencies—especially in a highly non-linear shock environment. There had been relatively little research into the behavior of porous materials at large sound amplitudes or at frequencies down to 10 Hz.

Technical Objectives

The objective of this work was to develop theories for large-amplitude, low-frequency wave interactions with porous materials and finite impedance surfaces. Overall, this project is concerned with theories that describe the interaction of gun blasts with local ground surfaces, both natural and artificial, and with methods for exploiting this interaction. This involves suitable characterization of the source, the interacting surfaces, and the propagation from the source to a receiver near to the ground in the presence of structures intended to achieve passive noise

control. Since design and testing of a full-scale blast-absorbing surface is applied rather than basic research, it has not been attempted here.

Approach

This work has been accomplished as a cooperative effort between the U.S. Army Corps of Engineers Engineer Research and Development Center (USACOE/ERDC) and the Netherlands Ministry of Defense Coordinator for Spatial Planning and Environment (N-MOD/CROMD). The CROMD was supported by TNO-TPD (TNO is The Netherlands Organization of Scientific Research and TPD is their Institute of Applied Physics). ERDC was supported by the University of Hull and Schomer and Associates, Inc. The following milestones have been accomplished and are separated into two complementary sets, each funded and accomplished by the indicated organization.

ERDC—Theory for large-amplitude wave interactions with porous materials—Milestones

- Review and improve existing theories for the non-linear acoustical and mechanical behavior of porous materials.
- Extend these theories to predict absorption properties at appropriate amplitudes and frequencies.

CROMD—Blast and associated sound wave generation—Milestones

- Develop theories that describe the generation of a muzzle blast wave with arbitrary starting conditions.
- Improve or adapt theories that describe the propagation of a blast shock wave in free air.
- Implement these theories in numerical schemes for predicting shock muzzle blast generation and propagation.
- Couple the combined theory with a linear sound field extrapolation model in order to be able to predict sound levels in the environment. Meteorological influences on the sound propagation can then be taken into account.

ERDC and CROMD—Joint Milestones

- Couple the blast shock wave generation and propagation theories with non-linear propagation theory for rigid porous materials.

This study has coupled theory with experiment. Theory includes the development of analytical methods by ERDC, the development of numerical methods by

CROMD, and the testing of both against experimental data. Experimental data come from shock tube measurements by ERDC and a full-scale blast test at Ft. Drum, NY, that was conducted jointly by ERDC and CROMD.

Organization of this Report

This report is organized into six parts:

1. Introduction
2. ERDC theoretical development and shock tube experiments
3. CROMD numerical methods development
4. Conduction of the full-scale test at Ft. Drum
5. Results from the full-scale test
6. Conclusions and recommendations

Sections 2 and 3 are based on journal papers—mainly published in the November–December 2002 Special Issue of *Noise Control Engineering Journal* (NCEJ). Sections 4 and 5 are based in part on draft journal papers—mainly to be published in a second special issue of *Noise Control Engineering Journal*. In addition there are two papers, one of which will be published in the *Journal of the Acoustical Society of America*, and the other has been submitted to *Applied Acoustics*.

Future Research

This project leads directly to the ability of ERDC to perform applied research and development on noise-absorbing surfaces for large-weapon firing positions—a topic that is critical to maintaining installation capability and readiness. Specifically, this research has developed theories and corresponding analytical models for noise mitigation in the near-field from blast waves. Follow-on research can examine practical implementations of the theories developed here. This will include the development of pressure and blast wind-tolerant material mixes and structures and their testing in laboratory and field setting. Following successful research, demonstration validation and training workshops can be accomplished in conjunction with a variety of potential end users, including (but not limited to) ACS(IM), DCSOPS, FORSCOM, AMC, and specific installations.

Surfaces that absorb low-frequency sound could have many other significant applications. For example, the low-frequency noise from ground operations is a subject of great concern around commercial airports and to the Navy and Air Force. Sound-absorbing engine run-up pads could reduce noise. Similarly, diesel train engines generate significant low-frequency energy. Sound-absorbing track beds could provide noise reduction in urban areas.

The Netherlands MOD will use these results for better insight into the blast field environment close to the source and in a model for the transition from blast wave to the sound field. This will enable the design of more effective sound barriers. It will enable measurement of the source strength close to the weapon, thus avoiding disturbances by meteorological and ground effects. Finally, this knowledge may assist in the design or optimization of muzzle blast suppressors.

2 ERDC THEORETICAL DEVELOPMENT AND SHOCK TUBE EXPERIMENTS

Natural ground surfaces are, by their nature, both porous and elastic. It has become widely accepted, in studies of outdoor sound propagation related to noise prediction, that porous ground surfaces may be treated as rigid-framed. However, ground elasticity is likely to be of some significance at the low frequencies involved in gunfire spectra (10–125 Hz). There are many porous and elastic materials used for passive noise control. These include the flexible polymer foams used in building acoustics, porous duct liners, and the porous concrete and asphalt pavements used to reduce noise from highways. For many low-stiffness materials, the flexibility of the solid phase of the material is of minor importance at higher frequencies. However, the materials most likely to withstand blast over pressures are rigid-porous materials.

Sound absorption at low acoustic amplitudes by rigid-framed porous media is fairly well understood. The governing properties are the flow resistivity, porosity, tortuosity, pore size distribution, and layering. At low frequencies the most important of these are flow resistivity and layering. At high sound pressures i.e. at sound levels in excess of about 140 dB, non-linear hydrodynamic effects take place in the fluid contained in the material. The latter effects occur principally because of the appearance of an additional quasi-steady fluid drag term in the momentum equation, caused by "inertial" (as opposed to viscous) fluid forces on the solid frame. This extra term is quadratic in the acoustic particle velocity, in contrast to the linear viscous term. It may be simulated by assuming that the flow resistivity of the material is a function of fluid velocity. This is known as a Forchheimer non-linearity (Forchheimer 1901).

Various workers have investigated the inertial fluid drag effect in the case of rigid-framed porous media. It has been shown that sinusoidal waves suffer additional attenuation in a bulk porous medium at high sound pressure amplitudes, and an empirical expression involving a steady flow resistivity parameter may be used successfully to explain this extra attenuation (Kuntz and Blackstock 1987). A theory that includes the quasi-steady Forchheimer equation in a formulation for the acoustic properties of porous media at high amplitudes has been developed (Wilson et al. 1988), and this was shown to be in good agreement with measured data. A numerical technique was also reported to yield the high-amplitude surface impedance of a layer of porous material against a rigid backing (Wilson et al. 1988). This has been employed by Cummings (1989) in predicting the behavior of layers of absorbents in cavities at high sound pressure amplitudes. By studying data on the dynamic flow impedance of several materials (McIntosh et al. 1990), McIntosh and Lambert (1990) have concluded that flow

resistivity has a quadratic dependence on (peak) particle velocity for low velocities and a linear dependence at high velocities. They described the transition between the two behaviors by a critical particle velocity. They concluded also that non-linear thermal effects are relatively unimportant (McIntosh and Lambert 1990) and have verified this for sound pressures up to 160 dB. As alternatives to a numerical solution of the non-linear equations of motion for propagation in a rigid porous material, Lambert and McIntosh (1990) developed approximate analytical solutions. Auregan and Pachebat (1999) proposed a model that combines the equivalent fluid model of Johnson et al. (1987) with effective flow resistivity values dependent on the Reynolds number to explain the nonlinear behavior of rigid porous materials.

During this project a model (*nonlinear model 1*) for the propagation of high-amplitude continuous sound through hard-backed rigid-porous layers has been developed to allow for linear variation of flow resistivity with flow velocity and hence incident pressure. The model is an alternative to that previously published (Auregan and Pachebat 1999). However, instead of assuming that the flow through the sample is constant, which is not applicable to a layered situation, the model enables prediction the acoustical properties of hard-backed porous layers at high intensities and allows for changes in the particle velocity in the pores. Thermal effects are accounted for by the linear complex compressibility function. The model for continuous sound requires a five-parameter description of the rigid porous material. The parameters are porosity, flow resistivity, tortuosity, viscous characteristic length, and the nonlinearity parameter. The model enables prediction of the acoustical properties of hard-backed porous layers at high intensities. The nonlinearity associated with Forchheimer's correction is shown to be particularly important in the range of frequencies around layer resonance. Nonlinear model 1 has been used to derive analytical expressions for surface impedance and reflection coefficient as a function of incident pressure amplitude. Depending on the material parameters, sample thickness, and frequency range, the model predicts either growth or decrease of reflection coefficient with sound amplitude. Good agreement between model predictions and data for rigid-porous materials has been demonstrated (Umnova et al. 2003).

A time-domain analytical formulation (*nonlinear theory 2*) also has been developed, since transient wave motion is the primary consideration. However, the analytical derivation requires a low-frequency assumption and omits dependence on the viscous characteristic length parameter. Moreover, it is limited to semi-infinite media since it only allows for forward-traveling shocks (Umnova et al. 2002). As an alternative, a time-domain formulation of nonlinear model 2 has been derived from the frequency-domain solution (excluding the viscous characteristic dimension) and requires numerical integration over frequency. This allows prediction of reflection by, or transmission through, a layer.

A further model (*nonlinear theory 3*) has been developed to predict the response of multiple rigid-porous layers to continuous high-intensity sound and has been validated against laboratory measurements of impedance. As with a single, hard-backed, rigid-porous layer, the nonlinear acoustical behavior of a multilayered absorber exhibits either growth or decrease of the reflection coefficient with sound amplitude. However, the change of behavior in this case results from the change in the relative thickness of the layers for a given total thickness. The parameters that optimize the sound absorption of a multilayered material at linear amplitudes are not the same as those that give optimum performance at high amplitudes.

Work has been carried out also on predicting the surface impedance of a porous and elastic layer subject to continuous high-intensity sound and including Forchheimer's nonlinearity (*nonlinear model 4*). However, the complexity of the equations precludes an analytical solution for time-domain problems or extensions to include the nonlinear response of the elastic frame.

The acoustical properties of porous materials at high intensities were measured in a standing wave apparatus. Several authors have used a modified version of the impedance tube (McIntosh et al. 1990) to study the complex flow impedance of porous materials subject to continuous sound at high intensities. In this apparatus, a thin section of the material to be tested is placed near a velocity maximum in the standing wave tube, and the pressure is measured on both sides of the sample. Such a system has been used to obtain data for open-cell polymer foam down to 10 Hz. A large loudspeaker system has been constructed at the University of Hull (Fig. 1) in which a layer of test material is place at the closed end of the tube and the standing wave field is measured by a transfer function method. This has been used to test theory and to extend the range of materials that have been studied previously to include those that might be of interest for our objectives. Measurements were made on the propagation constant, the characteristic impedance, and reflection coefficients for finite-amplitude, low-frequency continuous sound waves incident on porous concrete, porous aluminum, soil samples, a variety of gravel stone, perforated panels, and open-cell polymer foams. In addition, since transient waves are of primary interest here, two shock tube systems based on membrane rupture have been constructed: a large system containing five PCB transducers at ERDC/CRREL (Fig. 2) and a smaller system at the University of Hull (Fig. 3). These have been used to look at the acoustic shock response of eight materials (one of which was available in two configurations), including the frame displacement in the case of flexible materials. In addition, the tube at Hull has been used to investigate acousticshock transmission through and into various rigid-porous materials, both as single layers and in triple-layer configurations.

Figure 1. Large loudspeaker impedance tube.

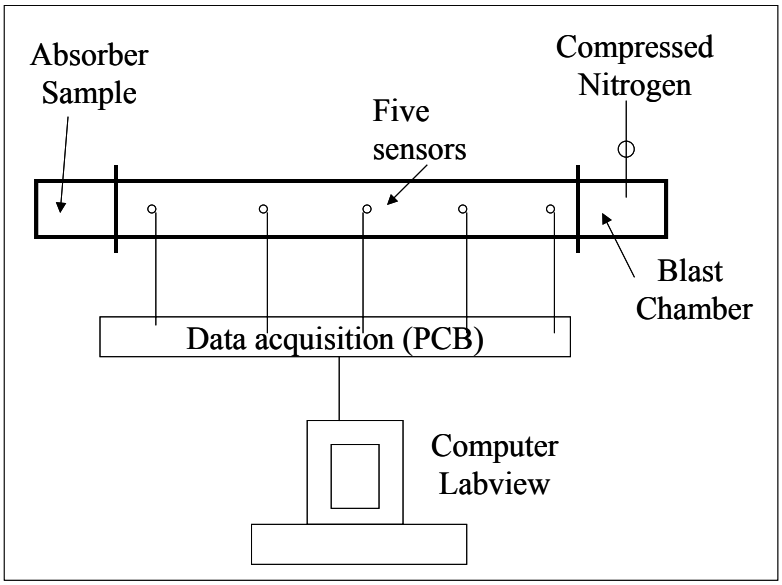

a. Schematic.

b. Shock tube.

Figure 2. Large-diameter shock tube (CRREL).

Figure 3. Small-diameter shock tube (Hull).

More detail on the work described in this section is available in papers by Umnova et al. (2002, 2003) and Standley et al. (2002). The paper by Umnova et al. (2003), based on non-linear model 1, shows that it is possible to design materials to be good absorbers at low frequencies and high pressures, and, as Figure 4 taken from this paper shows, it is possible to design materials such that the absorption *increases* with pressure in a pressure region of interest. The conclusions from this paper state:

"A new model which combines Forchheimer's nonlinearity with an equivalent fluid model has been developed and tested successfully against data for three types of hard backed rigid porous layers (lead shot, porous aluminum and porous concrete). The model is shown to give valid predictions of both impedance and reflection coefficient behavior at high sound amplitudes (up to 500 Pa) over a wide range of frequencies. Particular attention has been paid to the reflection coefficient behavior near layer resonance. Depending on material parameters and layer thickness, either growth or decrease of reflection coefficient with pressure amplitude is predicted and measured. The criterion derived in the paper allows predictions of the nonlinear behavior at resonance based on the material linear parameters assuming that resonant frequency is relatively high. It has been tested against data and has proved satisfactory."[*]

[*] For the medium-size gravel used in Pit 2 at Ft. Drum, the criterion will be valid as long as the resonant frequency is higher than 7 Hz. Since the first resonance frequency of a 1.5-m-deep pit is around 50 Hz, the restriction on the use of the criterion presents no problem.

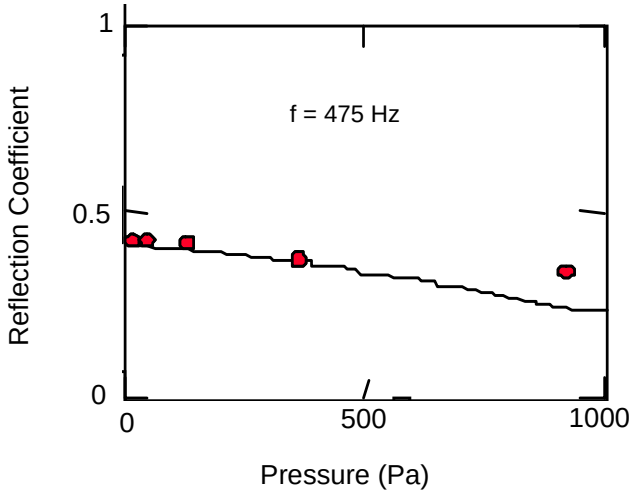

Figure 4. Decrease in reflection coefficient for increasing pressure for 15-cm-thick hard-backed 9-mm gravel at 475 Hz. The line show predicted values; the points show measured values. (From Umnova et al. 2003.)

3 CROMD/TNO NUMERICAL DEVELOPMENT

The muzzle blast of a large weapon (e.g., a 155-mm howitzer) is characterized by a non-linear shock wave with a peak overpressure of several tens of kPa's at a few meters from the weapon. The amplitude of such a wave decays with increasing distance and can be considered linear for distances greater than about 200 m. For acoustic purposes, non-linear effects can be avoided by making use of an effective linear emission spectrum based on measurements in the linear region. Noise levels at large distances can be computed from this emission spectrum and a linear propagation model. This approach does not work, however, for estimating the effects of measures close to the weapon (barriers, sound-absorbing materials, etc.). The efficiency of a noise barrier may be considerably reduced by non-linear effects, in particular the effect of *self refraction* (when a blast wave refracts itself over a barrier). To describe blast near the muzzle, a gas-dynamical code has to be used to give a solution to the multi-dimensional Euler equations.

At larger distances from the muzzle, the meteorological situation can affect the propagation of the blast wave. McDonald et al. (1994) reported on a numerical technique that can take into account atmospheric refraction and dissipation. This model is restricted to isentropic processes such as pressure waves and shock waves that are not too strong (less than 10 kPa of overpressure) and only for propagation over hard surfaces. For pressure waves less then 1 kPa of overpressure, linear models can be used [for instance, the PE (parabolic equation) code reported by Gilbert and White (1989)]. Atmospheric refraction and dissipation can be taken into account, including ground effects described by a complex soil impedance.

The coupling between these models can be solved sequentially, since we only consider waves traveling outwards from the source; there is only a "one-way coupling." This is the explicit assumption in the use of the PE to approximate the hyperbolic wave equation.

The interaction with an absorbing material cannot be solved separately because there is a strong "two-way" coupling between the pressure wave in the absorber and in free air. These interactions must be solved simultaneously using the same numerical code. Thus, in addition to describing the near-field flow of the muzzle numerically, another main innovative aspect to this project is the coupling of different propagation codes into one approach.

This effort started with investigation of the Boris (1976) description of a solution of the multi-dimensional Euler equations. The shock wave propagation is described by use of the Flux-Corrected Transport (FCT) technique, and this project investigates the applicability of using the FCT technique for the case of

gun muzzle blast propagation. In using this approach, an explosion at the muzzle is chosen as a starting condition.

A theory is needed to describe the degeneration of a blast wave into an acoustical wave. As a starting point, the method described by McDonald et al. (1994) has been used. This numerical method is based on a numerical integration of an equation for non-linear propagation of a blast wave, and it is restricted to isentropic processes, such as pressure waves with shocks that are not too strong (less than 10 kPa). Atmospheric refraction and dissipation can be taken into account using these calculations. To implement this, TNO has developed a non-linear propagation code (NPE) for moderate distances from the weapon. This numerical calculation is based on the parabolic equation approach used so successfully in the linear region.

Finally, the far-field propagation is modeled using PE. The PE method is based on a numerical integration of the linear wave equation in the frequency domain (Gilbert and White 1989). Atmospheric refraction and ground absorption can be explicitly accounted for when using the PE. The PE method works in the frequency domain. To use the blast wave, which is described in the time domain by the FCT and NPE method, for the PE method, it has to be decomposed into Fourier components. Wave propagation is then described for each component with the PE method.

The FCT technique has been implemented numerically and is performing correctly. The details have been published in papers by Védy (2002a, b). These papers show good comparison between measurements and calculations. In particular, comparisons are made with shock-tube results (one-dimensional calculations) and with published two-dimensional results (Fig. 5). Section 5 contains comparisons between field measurements at Ft. Drum and FCT calculations (three-dimensional calculations in which cylindrical symmetry is assumed).

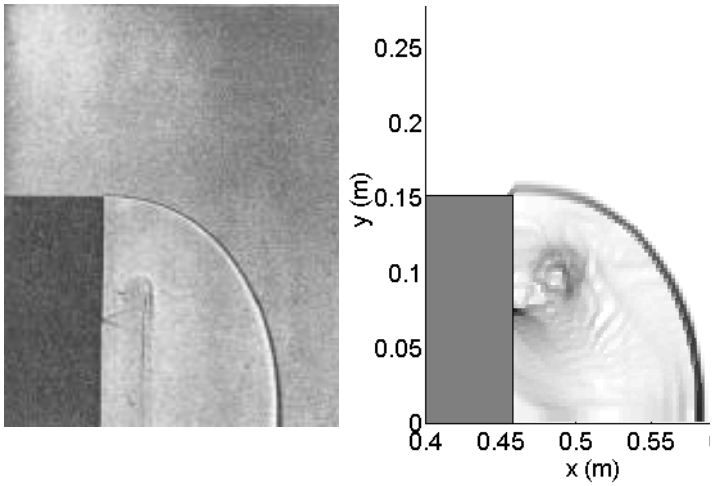

a. Experiment. **b. Numerical result.**

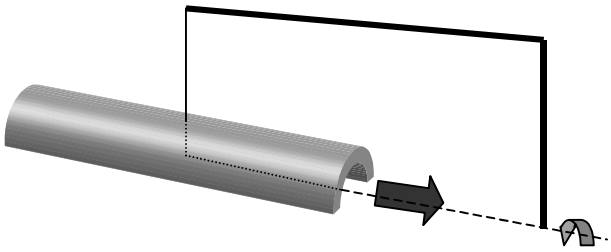

c. Axis of symmetry around the gun barrel.

Figure 5. Shadowgraph of the blast wave field at 200 μs. The abscissa is the gun barrel axis of symmetry, and the black rectangle is the end of the gun barrel. In a and b the horizontal axis corresponds to the centerline of the gun barrel. (From Védy 2002b.)

4 FULL-SCALE TEST AT FT. DRUM

Introduction

The purpose of these measurements was to test several of the analytical and computational methods developed by this research program. In particular, analytical methods have been developed to model the interaction of plane blast waves with a porous medium. Computational methods using the FCT-technique have been developed to model the three-dimensional blast reflection from and attenuation into a porous medium. In this field test, blasts were set off over two candidate blast-sound-absorbing test surface sections. In and near the material, measurements were made of (1) the surface reflections from high-pressure blasts impinging on these test surfaces and (2) the attenuation as these high-pressure blasts propagated into the test surfaces. In addition, data were gathered at distances ranging from 15 to 250 m so that TNO could test the complete sound transmission computational method as it transitions from FCT methods to nonlinear PE methods and finally to normal PE methods. Because of cost limitations, only relatively small test sections were used, so no large attenuation of the blast pulses was expected at these further distances. However, they still provided the ability to measure small amounts of attenuation. These small amounts of attenuation provide the proof that the effects of attenuating surfaces near a blast can be realized at farther distances. Two factors should make this far-field attenuation larger: (1) making the absorbing surface larger, and (2) moving the blast source closer to the absorbing surface.

This first set of experiments was designated Test I. It included three side-by-side blast sites. The middle site was a grass-covered control site. Each of the side sites contained a pit filled with the blast-sound-absorbing test section. Pressure measurements were made in and near the pits and control site and in a line from the blast sites out to 250 m. C-4 explosives were used as the blast source, with charge sizes ranging from 71 g (eighth stick) to 567 g (one stick).

The second set of experiments was designated Test II. It was designed to measure the ability of a ground surface impedance change to attenuate propagating blast sound. Here, linear theory and earlier studies by Albert and Orcutt (1990) and Albert (2002)**,** using a pistol noise source and C-4 explosions, respectively, indicated the possible efficacy of this method. This test used the grass-covered control portion of the Test I site and a parallel, adjacent, like-sized test section where the ground surface was freshly plowed ground instead of grass. As in Test I, pressure measurements were made near the explosive source and at distances ranging from 15 to 250 m. For Test II, C-4 was again used as the blast

source, and the charge sizes ranged from 142 g (quarter stick) to 2270 g (four sticks).

Test Site Requirements

The first requirements for the test sites were that we would be able to set off C-4 explosives, that the area would be free of loud competing noise sources, and that our tests would not be affected by other nearby activities. The second requirement was that the site be a flat open area extending to at least a distance of 250–300 m. This distance was required so that the blasts would be attenuating to the linear region. In that way two effects could be observed. First, any effect caused by the source-absorbing surfaces could be observed. Second, any effect caused by a relatively large extent of plowed ground could be observed. The operational requirements of the test suggested the need for a military installation where the local command and range personnel would cooperate and assist. Because of previous research by ERDC at Ft. Drum, it was known that Ft. Drum had the requisite test site and willingness to support this study.

Figure 6 shows the general area of the test site. It was just east of Ft. Drum's Wheeler Sac Airfield on an edge of the training area that is close to the main built-up part of the installation. (The airfield cooperated with the test by keeping aircraft away from the test area during testing.) Figure 7 shows a close-up photograph of the test site. The blasting and pressure sensors were located approximately in the indicated area, which was flat, grass-covered land, with very few small trees or shrubs and no nearby reflecting surfaces.

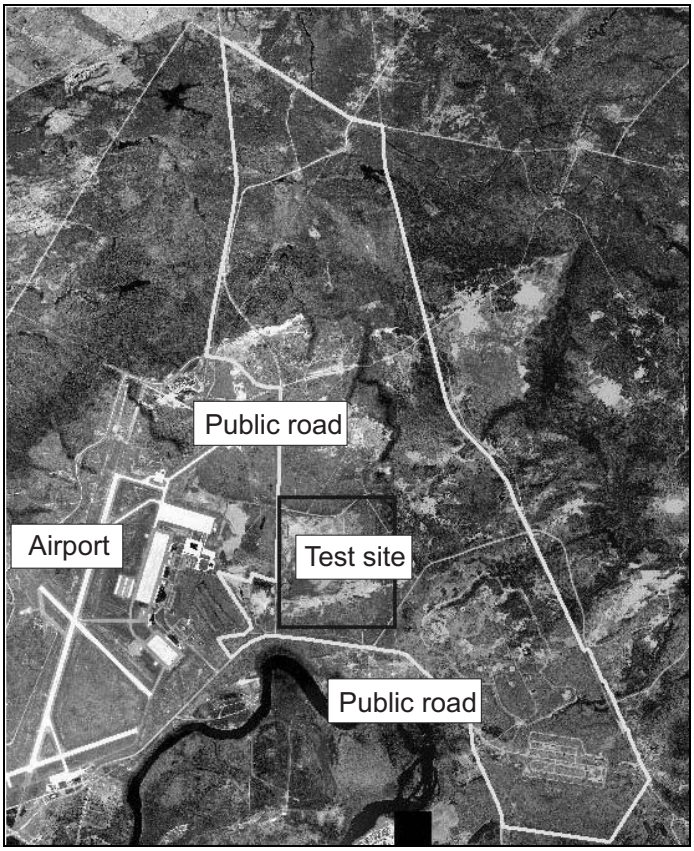

Figure 6. Square test area at Ft. Drum.

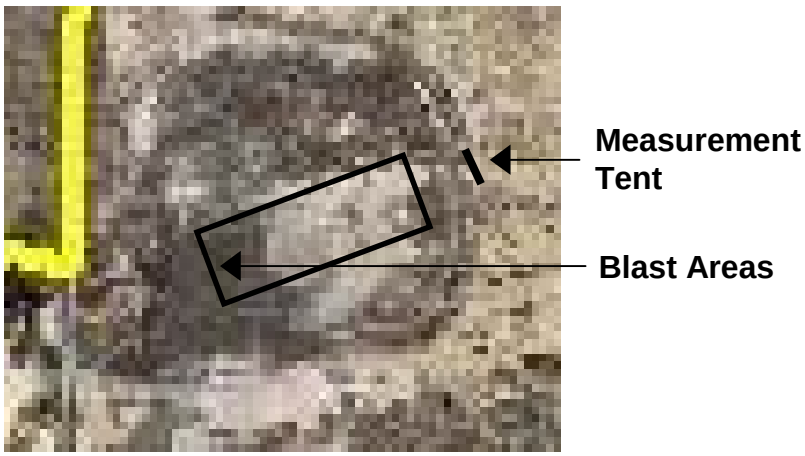

Figure 7. Test site at Ft. Drum (zoomed).

Test I Site Design

Blast Site Layout and Blast Sensors

Test I was designed to develop data with which to test the analytical and FCT calculations near and in blast-sound-absorbing material and to test the TNO transitions from FCT, to non-linear PE, and finally to the PE solutions in the linear region (about 250 m from the source). Because of financial limitations, the test sound-absorbing surfaces were not designed to yield the full potential sound mitigation benefits in the far field. Rather, they were designed to be between a quarter and a half wavelength in diameter at the peak frequency of the blast spectrum. Design and testing of a full-scale blast-absorbing surface is not basic research and should be undertaken as part of applied research and development.

The Test I design allowed for the testing of two different blast-sound-absorbing surfaces in close proximity to a grass-covered control surface. Time and financial constraints prevented the testing of more than two surfaces. Figure 8 shows the basic test layout in the vicinity of the blast sites. The two test material "surfaces" were built into the test pits, which were 1.5 m deep. The blast location for each pit and for the grass-covered control site was on a 15-m radius from the "15-m" pressure sensor. Pressure sensors were locate at the top surface of each pit, at the air–ground interface of the control surface, and at a height of 1 m and a radial distance of about 2.5 m from each blast site. In addition, pressure sensors were place 0.5 m down from the top surface of each pit and at the base of Pit 1. Figure 9 shows the elevation view of Pit 1. It was planned to set off all explosives at a distance of 2 m above the pit's top surface or above the control ground surface. Since, during the test, no surface damage or movement was observed, some charges were set at a height of 1 m. Appendix A contains the detailed design of a pit.

At distances of 50, 100, and 250 m, there was a single line of microphones. There were two microphones at each distance, one at a height of 1 m above the ground surface and the other at a height of 5 m above the ground surface. Figure 10 shows the overall Test I site layout. The overall site was such that the prevailing wind was in line with the outgoing line of sensors.

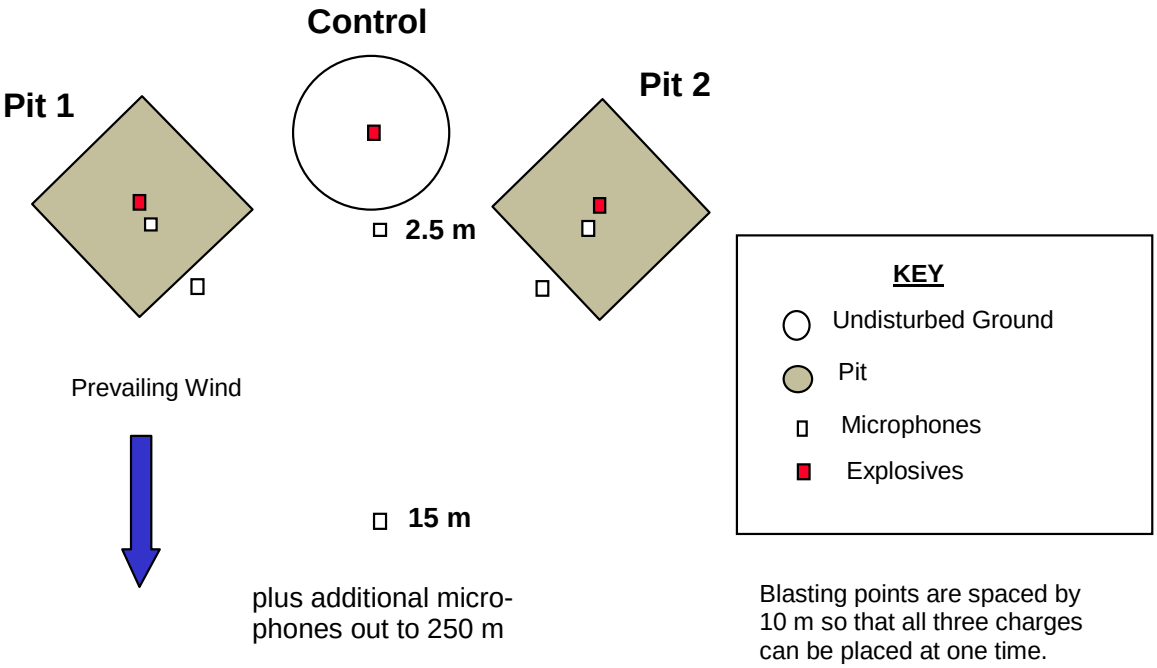

Figure 8. Plan view of the blast site area for Test I.

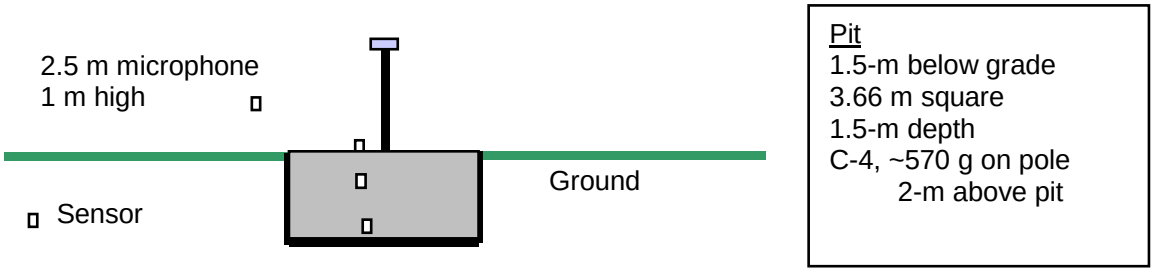

Figure 9. Elevation view of Pit 1. Pit 2 is the same except that there was no sensor at the bottom of Pit 2.

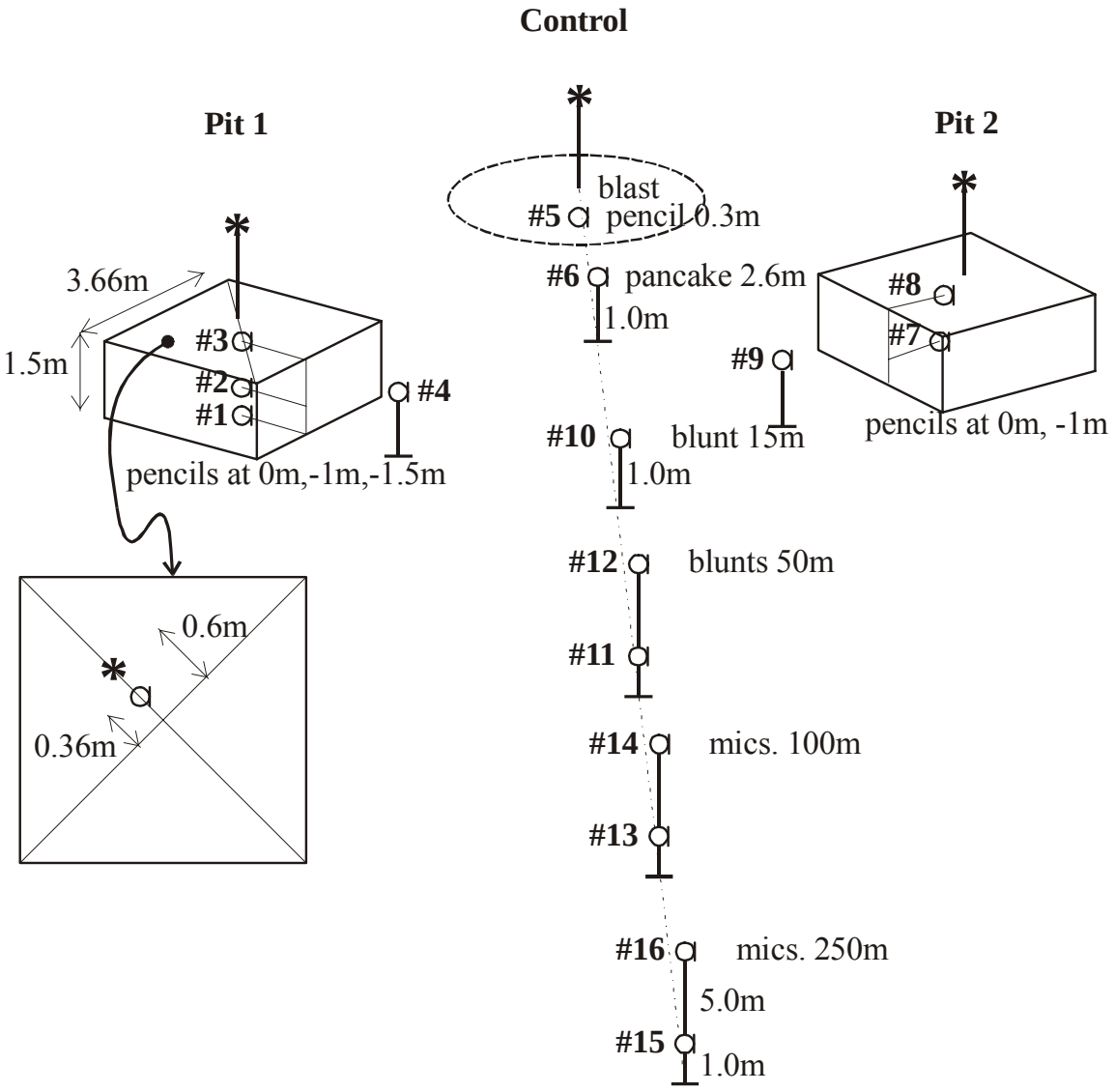

Figure 10. Overall Test I site layout. The numbers by each gauge are channel numbers for data recording and analysis.

The blast sensors in the pits and at the surface beneath the blast were piezo-resistive pressure sensors mounted in a "pencil gauge" housing (Fig. 11). This housing is optimum for a blast impinging normally on the gauge with no reflected pulse, as was the case here. As indicated in Figure 10, the blast holder was situated 0.6 m back from the center of the pit, and the blast sensors were mounted 0.3 m from this holder to mechanically isolate the blast sensor holders from the blast holder.

a. Photograph.

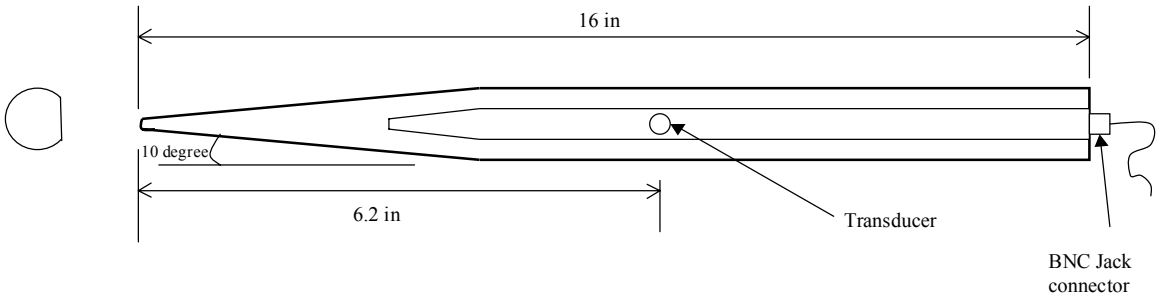

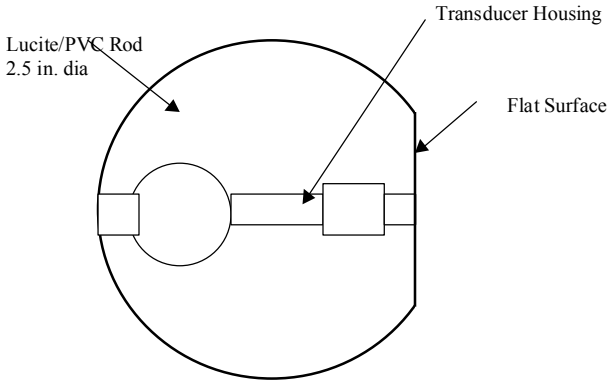

b. Diagram.

Figure 11. Pencil gauge.

There was a sensor at 2.6 m from the blast holder. This sensor, mounted 1 m above the ground, received both a direct and a reflected pulse, so it was a piezo-resistive pressure sensors mounted in a "pancake gauge" housing (Fig. 12). This housing is optimum for blasts impinging from anywhere in a single plane. The "pancake" is placed flat into this plane.

Figure 12. Pancake gauge.

The sensors at 15 and 50 m were piezo-resistive pressure sensors mounted in "blunt gauge" housings. The blunt gauge housings were cylinders that were about 1.2 cm in diameter and 13 cm long. The sensing element is mounted flush in the center of one end of the cylinder. The blunt gauge is optimum for more random incidence. The single sensor at 15 m was faced up so as to present the same sensitivity to all three blast locations. Regular 12-mm microphones were used at 100 and 250 m. All of the sensors at 50, 100, and 250 m were mounted for essentially grazing incidence with respect to the blast waves, that is, they were mounted horizonally and tangential to the line of blast propagation.

Blast-Sound-Absorbing Materials

The analytical selection of blast-sound-absorbing materials is one of the main thrusts to this whole program, and the methods and testing described in Parts 2 and 3 proved to be sufficiently robust to perform this task. Initially it was believed that materials similar to classical sound-absorbing materials such as mineral fibers or open-celled foams could be used. Early theoretical analysis and shock tube testing showed that the best plan was for a top layer with high porosity and a very low flow resistivity (<1000 Pa-s m^{-2}), followed by a middle layer with higher resistivity (<30,000) and a bottom layer with a still higher resistivity (<100,000). At the same time the porosity was to decrease from about 0.9 to about 0.4, with the middle layer having a porosity of about 0.5 to 0.6.

Many materials were considered, including some exotics such as foam aluminum (which theoretically will work but costs in excess of $10,000 per cubic meter), common acoustical absorbing materials, and porous concrete. Remarkably the most suitable material for testing was gravel. Gravel allows control of the flow resistivity and nonlinearity parameter through grain size at the expense of a porosity only in the vicinity of 0.4. In Pit 1 we used a top layer of nominally 3-cm washed river gravel. The middle layer was nominally 0.9-cm pea gravel, and the bottom layer was fine gravel having a mean grain size of 0.18 cm. For

comparison and simplicity of analytical analysis, the second pit was filled entirely with just the nominal 0.9-cm pea gravel. Figure 13 portrays Pit 1. Pit 2 was the same but filled only with pea gravel.

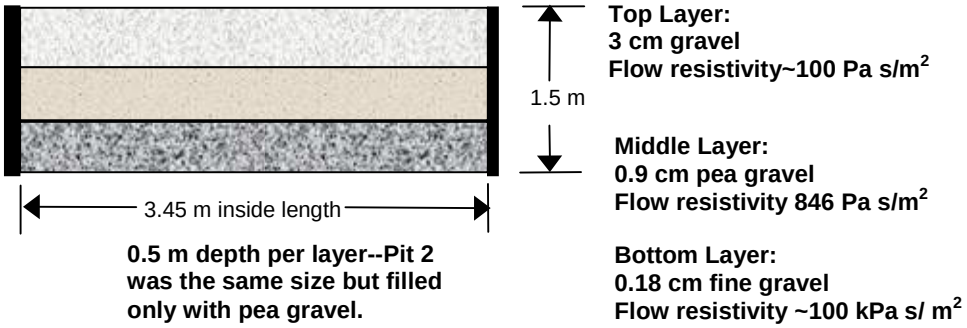

Figure 13. General dimensions and fill of Pit 1. Pit 2 was the same size but filled entirely with what was nominally 0.9-cm pea gravel.

Table 1 and Figure 14 show the size distribution statistics for the three types of gravel.

Table 1. Gravel size distributions (largest particle dimensions in mm).

Statistic	Fine gravel (nominal 3 mm)	Medium gravel (nominal 8 mm)	Large gravel (nominal 25.4 mm)
Mean	1.828	9.02	31.01
Median	1.37	8.91	28.73
Standard deviation	1.408	1.81	11.2

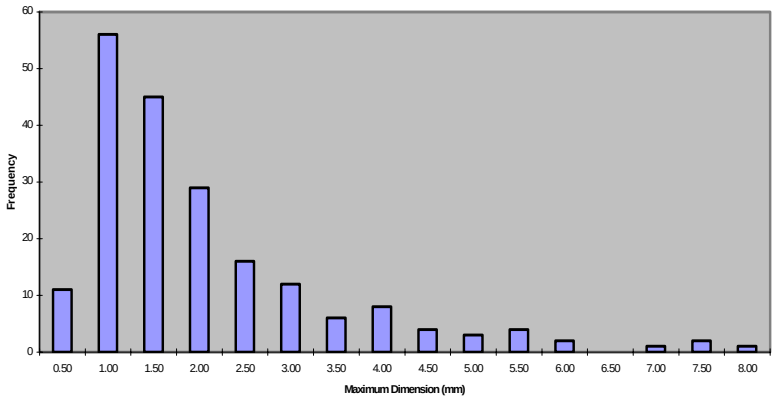

a. Fine gravel

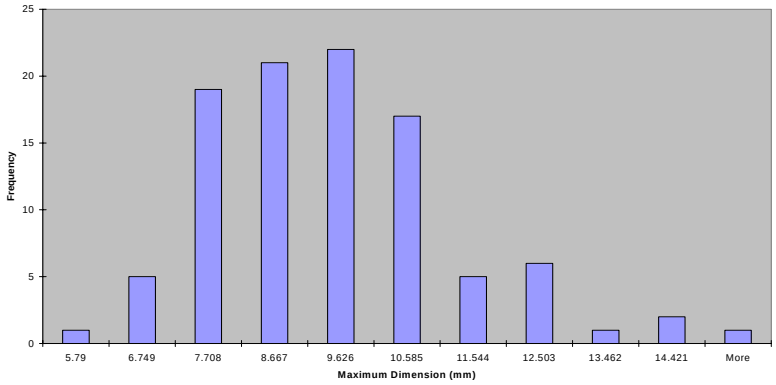

b. Medium gravel.

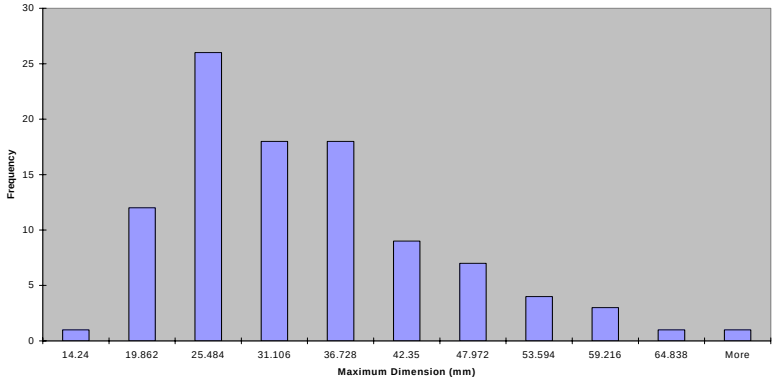

c. Large gravel.

Figure 14. Gravel size distributions.

Blast Testing

The blast test used C-4 plastic explosives. These come in 567-g sticks. The Test I plan was to test with four charge sizes, working up from eighth stick to one stick (eighth, quarter, half, and one stick) and then to replicate the quarter-stick set. The size of charge was gradually increased to be sure that we obtained the maximum data prior to any possible blast damage to the pits. After finding no damage and virtually no motion to the pits or their contents, it was decided during Test I to set off the second sequence of quarter-stick charges at a height of 1 m above the ground instead of the 2 m used for the first four sets.

In Test I each data set consisted of nine like-sized charges. First, charges were set up at each of the three sites, the two pits, and the control site (Fig. 8). These three charges were set off sequentially, remotely from the instrument tent (Fig. 7) in a Pit 1, Control, Pit 2 sequence. The time between blasts was less than one minute. Then a second group of three charges was set up and again detonated sequentially. A similar third group of three charges followed. The time between groups to set up the charges and review data was about 15 minutes. Thus, a data set consisted of three replications of the same basic group of three measurements. The blast sequence and site layout were chosen so that the control was closer in both time and space to each of the two pits than they were to each other.

This Test I plan provided very good control for both weather and terrain effects since the same essential sound path affected propagation from all three blast sites (Test I) and since the same weather was present for all three detonations in a group. Because of the short time between blasts in a group, the meteorological effects on the sound propagation should be essentially the same for the three explosions. Further, each group of three explosions was replicated three times to average out any minor random effects. Therefore, the resulting data can be used to determine acoustical differences between Pit 1, Pit 2, and the control site as a function of charge size.

Pit Material Motion Sensing

One concern was that the blast-absorbing test materials would settle or move, thereby changing the geometry and position of sensors relative to the surface boundaries, etc. To track the layer boundary heights, “tell-tales” as shown in Figure 15 were placed at boundary surfaces, and a high-resolution theodolite was used to check for changes in their elevation.

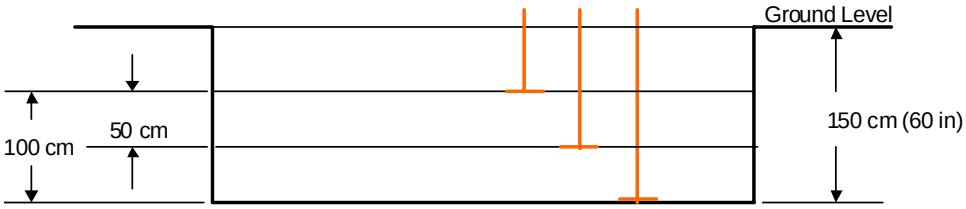

TELL TALES

lengths: 110 cm, 140 cm, and 160 cm

Fiberglass rods marked in 1 or 2 cm spacing, 1/16 in thick.
Base of tell-tale rod is a webbed, 8-prong spider.
Base legs should be 8 in long.
Tell-tales should extend above top layer by 10 cm.

Figure 15. Tell-tale design.

Test II Site Design

Blast Site Layout and Blast Sensors

Test II was designed to test whether changing the ground surface impedance between the source and the receiver could mitigate blast noise in communities. The Test II design involved changing the ground impedance over an area considerably larger than the pits in Test I. Figure 16 shows the overall site layout for Test II. This test consisted of a side-by-side comparison of blast-sound propagation over grass and freshly plowed ground. The plowed ground extended from 15 to 250 m from the blast. The surface was about 60 m wide, and the furrows were transverse to the line of propagation. Each blast site itself was over grass. Pencil gauge sensors as described above were mounted at the base of each blast holder (at a horizontal distance of 30 cm). In addition, there were blunt-gauge sensors at 15 m (at a height of 1 m) and at 50 m (at a height of 1 m). Twelve-millimeter (so-called “half-inch”) microphones were used at 50 m (at a height of 5 m) and at both heights at 100 and 250 m. All three types of gauge are described above. The 1-m-high microphone at 100-m range was not connected to the HP analyzer although it was recorded by DAT. Instead, a third microphone was added to the grass field site at 250 m for a source localization test that was unrelated to this study and is not reported here

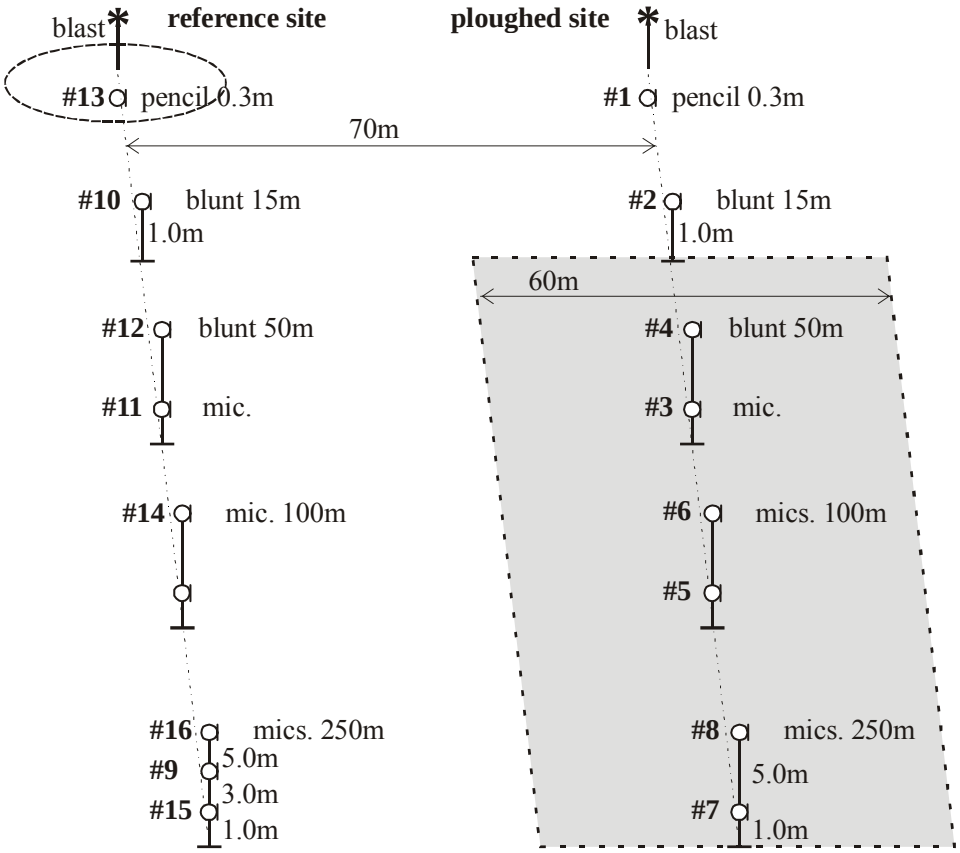

Figure 16. Overall Test II site layout. The numbers by each gauge are channel numbers for HP data analysis.

Figure 17 shows the overall general layout for Tests I and II together. The same control line of sensors was used for both Test 1 and Test II. Also, the direction of sound propagation was laid out as WSW, which is the prevailing wind direction in August during the day at Ft. Drum.

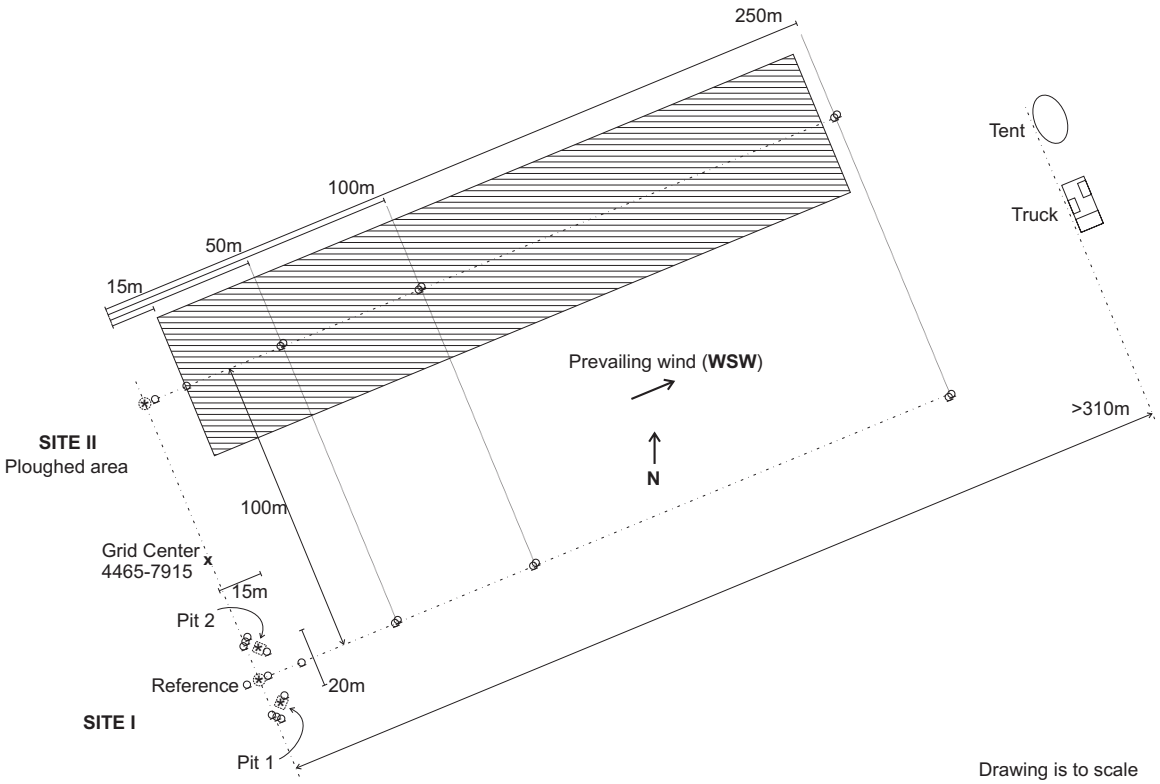

Figure 17. Overall layout for the combined Test I and Test II experiments.

Blast Testing

The Test II plan was to test with three charge sizes, working up from a quarter stick to four sticks (quarter, one, and four sticks). Each data set consisted of six like-sized charges. First, charges were set up at each of the two sites, the grass-field control site and the plowed-field test site (Fig. 16). These two charges were set off sequentially, remotely from the instrument tent (Fig. 7) in a grass field, plowed field sequence. The time between blasts was less than 1 minute. Then a second group of two charges was set up and again detonated sequentially. A similar third group of two charges followed. The time between groups to set up the charges and review data was about 15 minutes. Thus, a data set consisted of three replications of the same basic group of two measurements.

This Test II plan also provided very good control for both weather and blast site effects, since the same essential blast position (grass covered) affected the source for both blast sites and the same weather was present for both detonations in a group. Because of the short time between blasts in a group, the meteorological effects on the sound propagation should be essentially the same for the three explosions. Further, each group of three explosions was replicated three times to

average out any minor random effects. Therefore, the resulting data can be used to determine acoustical differences between the plowed-ground site and the control site as a function of charge size.

Measurements

Weather Sensing

Weather sensors were located on a single mast 125 m downrange from the control blast point and about 50 m to one side, so that it was midway between the two lines of propagation used in Test II. As with the whole site, there were no obstacles nearby. The wind speed was measured at three heights between 1 and 7 m, the temperature was measured at five heights ranging from 0.1 to 7 m, the wind direction was measured at a height of 7.4 m, and the humidity was measured at a height of 3 m (Fig. 18). The data from these sensors were collected into a co-located datalogger. Magnetic declination from the airfield (about 1 km away) was used to adjust the wind-direction device for true north.

Computer simulations such as the PE use weather data for their detailed propagation predictions. However, in terms of comparisons between the two pit sites and the control, close spacing in time and replications are used to control for the minor changes in propagation conditions.

Surface Impedance Measurements

Surface impedance was measured over various areas of the Test Site I grass field, the two pits, and the grass-covered Site I control blast location. Similar measurements were made over the plowed ground and at the blast location for the plowed-ground test. Two forms of data were collected. One form of data was measurements from a loudspeaker set at two heights above the test surface. In this method, microphones measured the source near the loudspeaker and the combined direct and reflected sound a short distance (a few meters) from the loudspeaker. Figures 19 and 20 show measurements being made over Pit 1 and over the plowed ground, respectively. Data were collected on site, and two methods were used to analyze these data back in the laboratory. One was the *Template Method for Measuring Ground Impedance* (American National Standards Institute 1999), and the other was *Direct Impedance Fitting* (Taherzadeh and Attenborough 1999).

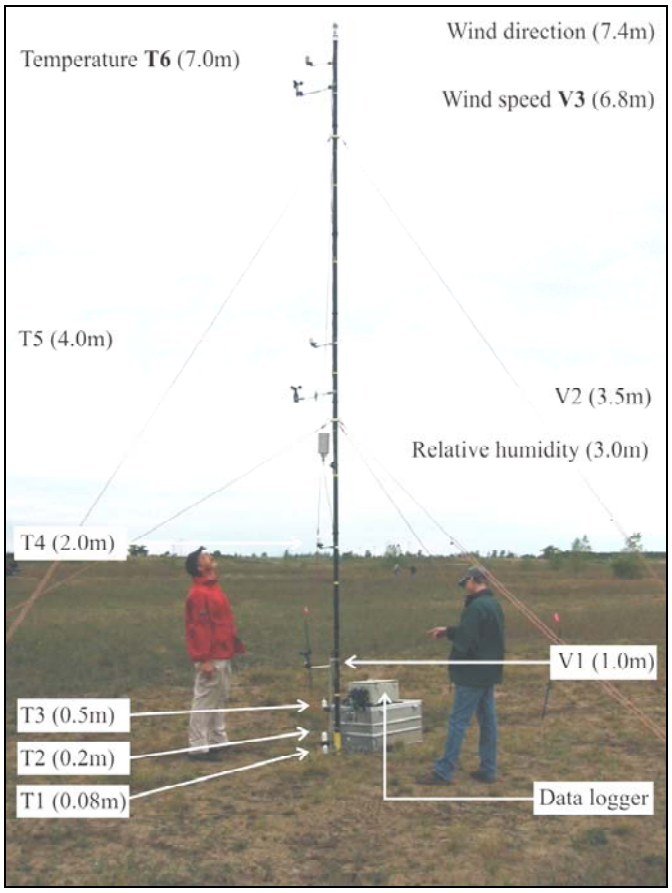

Figure 18. Meteorological sensing.

Figure 19. Impedance measurements of the Pit 1 surface.

Figure 20. Impedance measurements of the plowed-field surface.

The second form of data was recordings made with a gas cannon noise source (Fig. 21). These data were not analyzed because the direct and reflected signals could not be sufficiently separated. Moreover, the loudspeaker method using the two forms of analysis described above proved to be sufficient.

Figure 21. Impedance measurements using the gas cannon.

Basic On-site Data Collection and Analysis

For Test I the gauges recording the 16 channels of acoustical data shown in Figure 10 were all wired directly to recording and analysis equipment that was situated in the instrument tent (Fig. 7), where the equipment was operated with generator-supplied electricity. For Test II the HP analyzer was used to analyze the 16 channels of acoustical data shown in Figure 16. DAT recordings were

made for possible later use, and the 16-channel HP analyzer was used mostly to generate field-analyzed data files. The HP analyzer produced the following for each of the 16 channels for each blast:

- A digital time history with a sample rate of 16,384 samples per second;
- A 1/3-octave-band sound exposure level (SEL) spectrum;
- An octave-band SEL spectrum; and
- Flat-, A-, and C-weighted SELs.

Thus, at the completion of field testing, all of the basic data except for the 100-m microphone at a height of 1 m were initially analyzed and available for further analysis. These data are available as a two-CD set and have been used for all of the analyses that follows (the time histories consume most of the space on the CDs). The DAT recordings were used to extract the data for the 100-m microphone.

As note earlier, the meteorological data were stored in the battery-operated control unit situated at the base of the sensor array. These data were transferred to a computer each day as delimited text files.

The tell-tales were checked after testing with each size of charge. In all cases the cumulative displacement was found to be less than 1 cm (typically 3 mm), even after the one-stick charges. The results are calculated from small changes in angles measured using the theodolite at a distance of 50 m. Table 2 contains the results of these displacement calculations. The results in the table are cumulative changes with respect to the starting condition. The fact that the cumulative changes sometimes decrease over time suggests that these small displacements are largely the result of measurement error. The apparently large displacements for the quarter-stick charges (1 m above the ground) may reflect the fact that these measurements were made one day after the other measurements.

Table 2. Cumulative motion of the tell-tales in meters.

	After 1/8 stick	After 1/4 stick	After 1/2 stick	After one stick	After 1 1/4 stick
Pit 1, 50 cm	0.004	0.004	0.004	0.007	0.008
Pit 1, 100 cm	0.002	0.004	0.003	0.004	0.004
Pit 2, 50 cm	0.000	0.000	0.002	0.004	0.008
Pit 2, 100 cm	0.003	0.001	0.003	0.002	0.005
Pit 2, 12 cm from bottom	0.002	0.001	0.001	0.001	0.002

5 RESULTS FROM THE FULL-SCALE TEST AT FT. DRUM

This chapter of the report is divided into six parts. The first part discusses the pressure–time histories. The second part gives summary results primarily using octave-band SEL data. It also provides summary ground impedance results. The third part gives a more detailed analysis of the Test I pit results. It primarily focuses on the near-field results but also touches on the observed Pit 1 blast sound level reductions that resulted at 15 and 250 m. The fourth part focuses in detail on the results from Test II. The fifth part focuses on a comparison between numerical prediction and measurement near to the blast source using the FCT method, and the last part focuses on the numerical prediction when transitioning from FCT to non-linear PE and then to linear PE.

Pressure–Time Histories

Appendix B contains time histories that were measured at distances of 2.6 and 15 m from the source (1-m receiver height) for the different charge sizes (series 1 through 12) and for quarter-stick charges that were detonated at a height of 1 m above the surface (series 14 and 15). Three pancake gauges were used at the 2.6-m distance for the Pit 1, Control, and Pit 2 sites. A single blunt gauge was used at the 15-m distance, a gauge location that was equidistant from all three explosions. Figure 22 shows a typical one-stick time history measured at 2.6 m. At this distance the direct and reflected pulses can be distinguished.

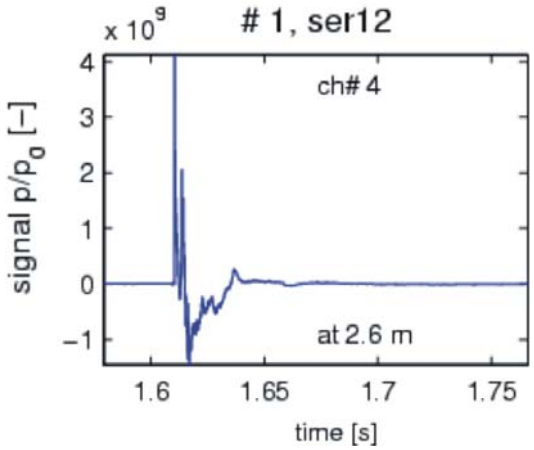

Figure 22. Typical pressure–time history for a pancake gauge (one stick—series 12).

Figure 23 shows the three pancake gauge time histories for quarter-stick charges. Normal blast time histories exhibit a sharp initial pressure rise, but Figure 23 shows that the Pit 1 time histories do not exhibit sharp initial pressure rises for either the direct or the reflected pulses. This same effect is evident in the Pit 1 pancake gauge data for all of the eighth-stick and quarter-stick charges (both charge heights) and for two of the three half-stick charges. Data for one of the three half-stick charges and all three of the one-stick charges exhibit sharp pressure rises and, therefore, are used for further analysis in this report. It seems that the pancake gauge at Pit 1 did not operate properly at lower pressures.

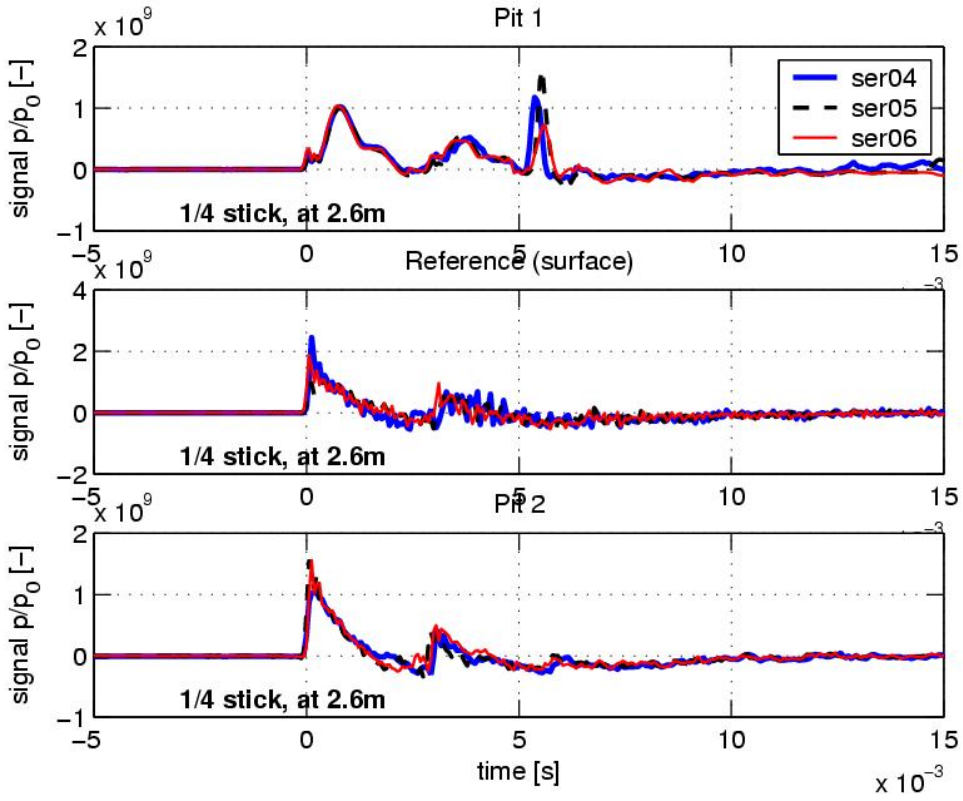

Figure 23. Comparison of three pancake recordings. Time signals have been shifted so that at t = 0, the first pressure rise occurs. Note that for the upper plot a sharp pressure rise is nearly absent.

Blunt gauges were used at 15 m (1 m high—channel 10) and 50 m (1 m high—channel 11 and 5 m high—channel 12). Figure 24 shows typical pressure–time histories for these three gauges. Channels 10 and 12 exhibit proper blast time histories. However, the blunt gauge used for channel 11 does not appear to be working properly; the standard deviation analysis contained in the next section confirms this conclusion.

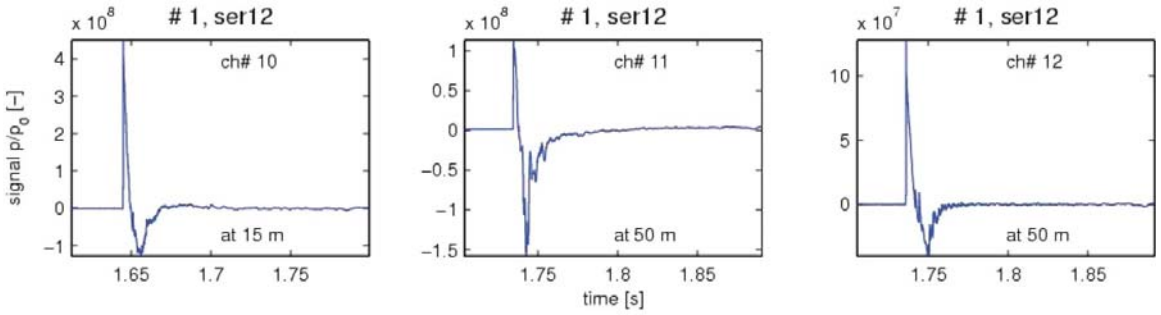

Figure 24. Pressure–time recordings for a blunt gauge for series 12 (one stick).

Figure 25 shows typical results for the four microphones. The microphones were used at 100 and 250 m at 1.0- and 5.0-m heights. At 100 m a peak value of about 154 dB is measured for the one-stick charge. Non-linear effects occur generally above 154 dB (1 kPa) for this blast waveform. At 250 m a peak value of about 141 dB is measured for the one-stick charge. Also, a small increase of the positive phase duration of the blast waveform can be observed at 250 m.

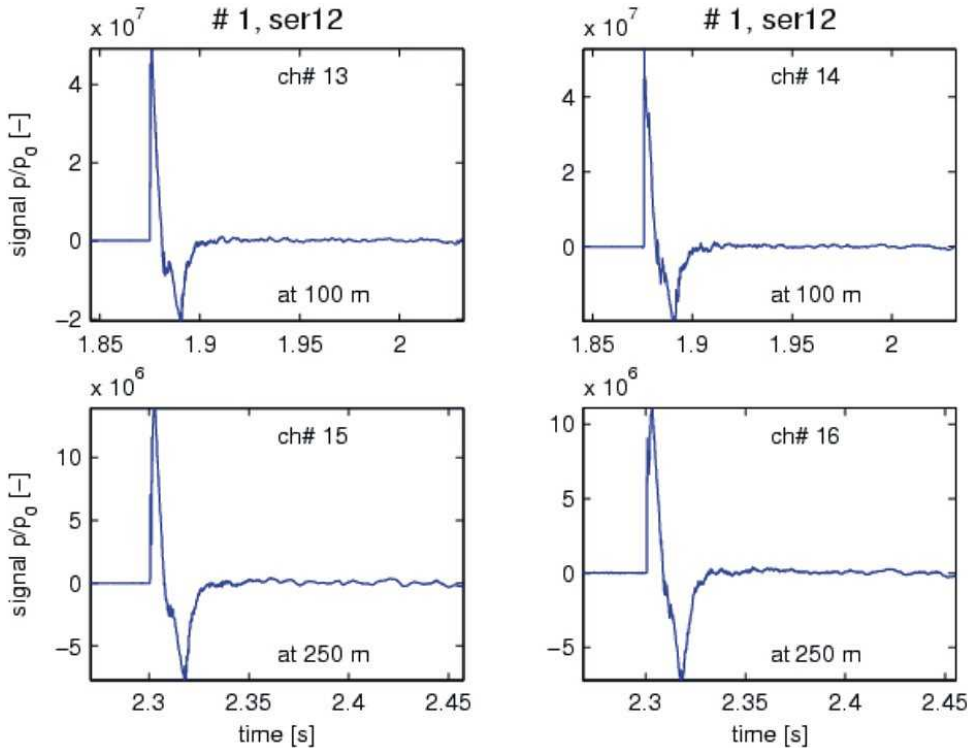

Figure 25. Pressure–time recordings for the microphones for series 12 (one stick) at heights of 1.0 m (left) and 5.0 m (right).

Summary of Sound Exposure Level and Surface Impedance Results

Sound Exposure Level Results for Test I

Test I includes three replications of each blast charge size at the two test pits and the control site. Therefore, one can average the energy of the three replications and examine the standard deviation. This basic analysis has been done for all of the octave band, one-third-octave band, and frequency-weighted SEL data. For CD distributions of this report, these are contained in the five attached Excel files labeled TI-8th, TI-4th (2m), TI-4th (1m), TI-half, and TI-one, where the charge size is given, and for the quarter-stick charge size, the height of the charge above ground is indicated.

Table 3 contains the average standard deviation for each set of three replications. The numbers represent the average for all sensors relevant to that blast site for the octave bands from 16 through 250 Hz and for just the 15- through 250-m sensors. In general these averages are about 1 dB, indicating that these data replicated well. However, two of the sensors consistently exhibited higher standard deviations. The air–grass interface pencil gauge sensor at the base of the control site nearly always exhibited a much higher standard deviation (typically about 7 dB), and the 1-m-high blunt gauge sensor at 50 m exhibited a somewhat higher standard deviation (typically 1–3 dB). The pencil gauge did not function properly and cannot be used. The blunt gauge appears to be variable but in an unbiased

Table 3. Average standard deviations in decibels for octave-band SEL data in the frequency range from 16 through 250 Hz.

Charge (height)	Blast source	All sensors	Sensors at 15–250 m	Problems
eighth (2 m)	Pit 1	0.9	0.9	50 m (1 m high)
	Control	1.0	0.9	50 m (1 m high), 0 m (0 m high)
	Pit 2	1.7	0.9	50 m (1 m high)
1/4 (1 m)	Pit 1	1.0	0.8	50 m (1 m high)
	Control	1.4	1.0	50 m (1 m high), 0 m (0 m high)
	Pit 2	1.4	1.6	50 m (1 m high)
1/4 (2 m)	Pit 1	0.7	0.6	50 m (1 m high)
	Control	1.0	1.1	50 m (1 m high), 0 m (0 m high)
	Pit 2	0.6	0.6	50 m (1 m high)
1/2 (2 m)	Pit 1	1.0	0.9	50 m (1 m high); Pancake a little high
	Control	1.2	1.1	50 m (1 m high), 0 m (0 m high)
	Pit 2	0.9	1.1	50 m (1 m high)
1 (2 m)	Pit 1	1.2	0.9	50 m (1 m high); Pancake a little high
	Control	1.6	1.1	50 m (1 m high), 0 m (0 m high)
	Pit 2	0.7	0.6	50 m (1 m high)

manner. All of the other sensors typically exhibited standard deviations that were in the 0.3- to 0.9-dB range. The standard deviations sometimes are a little larger at 250 m, but this is believed to be the result of meteorological effects and not related to the gauges. As noted earlier in the time-domain waveform discussion, the pancake gauge at 2.6 m for Pit 1 gave repeatable but incorrect waveforms. Only the half-stick and one-stick data are used for this gauge.

Given the three-replication energy averages, the differences between the blast sites for the same or corresponding sensor positions can be examined. As an example, these comparisons have been made for the 2.6-m pancake gauge for each blast site and for all of the sensors ranging from 15 through 250 m. The three basic comparisons are "Control minus Pit 1," "Control minus Pit 2," and "Pit 1 minus Pit 2." If a pit is attenuating the blast sound, then the difference between the control level and the pit level should be positive. A remarkable result is that when the near-field result at the 2.6-m pancake gauge is examined, Pit 2 is attenuating and Pit 1 is not. However, at the farther distance of 15 m, the opposite is true: Pit 1 is attenuating and Pit 2 is "amplifying" relative to the control site. The same trend that is evident at 15 m also is evident at 250 m but to a lesser extent. The next chapter gives a theoretical interpretation of these results.

Table 4 lists the results for the 2.6-m pancake gauge. In interpreting these result, there are two factors to consider: the size of the differences and the sign of the differences. For example, for the "Control minus Pit 2" data in Table 4, the average difference is about 3.5 dB. Considering the size of the average standard deviations (Table 3), great precision cannot be attached to this difference: the 95% confidence interval will be on the order of 1.5–5.5 dB. But the signs of the differences indicate a very certain result. There is virtually no doubt that Pit 2 is attenuating the sound level measured at the 2.6-m sensor. If there were no attenuation, then the signs of the differences would be random. On average, half would be positive and half would be negative. The following question can be posed: What is the probability that there is no effect yet we measure 25 positive differences? Statistically, it is the same as the probability that 25 coin tosses yield heads every time. In this case, the probability is 2^{25}, or 1 chance in 32,000,000. As noted above, much of the Pit 1 data for the 2.6-m gauge are unreliable. The remaining data are shown in Table 4. For the "Pit 1 minus Pit 2" data, the average difference is over 5 dB. In this case all ten differences are positive, and the probability of ten consecutive tosses of heads is 2^{10}, or 1 in 1024. For the "Control minus Pit 1" data, there at eight negative differences and two positive differences. The probability of two heads in ten coin tosses is calculated using the well-known binomial expansion. In this case, the probability is about 45 chances in 1024, or less than 5 in 100. Overall, one can clearly conclude that there is a very significant statistical difference between the measured levels for Pit 1, Pit 2, and the control site.

Table 4. Differences in measured level for the cases indicated at the 2.6-m pancake gauge.

Frequency (Hz)	1/4 charge 1 m	eighth charge 2 m	1/4 charge 2 m	1/2 charge 2 m	Full charge 2 m
Control – Pit 1 (Mainly negative)					
16				–6.1	–2.5
31				–5.8	–3.5
63				–1.3	–1.3
125				–3.2	–3.7
250				1.3	2.1
Control – Pit 2 (All positive)					
16	8.9	2.9	7.2	8.8	7.0
31	4.9	1.9	3.7	3.7	2.1
63	3.9	2.3	3.0	3.3	2.1
125	3.0	1.8	2.3	2.1	0.6
250	2.0	2.4	2.4	1.7	2.2
Pit 1 – Pit 2 (All positive)					
16				14.8	9.5
31				9.8	5.7
63				5.2	3.4
125				6.1	4.3
250				0.4	0.1

Table 5 gives the measured results for the 15-m sensor. Looking at just the size of the difference, one might erroneously conclude that there was no difference between the control and pit data, but this would be a mistake. The differences are small but real, and the sign tests prove this. The chance that a "Control minus Pit 1" POSITIVE difference does not exist is less than 1 in 10,000; the chance that a "Control minus Pit 2" NEGATIVE difference does not exist is less that 1 in 1,000,000; and the chance that a "Pit 1 minus Pit 2" POSITIVE difference does not exist is less than 1 in 32,000,000. Thus, there is no doubt that the relative effect reverses between the near-field measurement at the 2.5-m sensors and the more distant result at the 15-m sensor.

Table 5. Differences in measured level for the cases indicated at the 15-m sensor.

Frequency (Hz)	1/4 charge 1 m	eighth charge 2 m	1/4 charge 2 m	1/2 charge 2 m	Full charge 2 m
Control – Pit 1 (Mainly positive)					
16	1.2	0.3	0.6	0.6	–0.3
31	1.0	0.5	0.6	0.8	0.2
63	1.4	1.2	1.0	0.5	1.1
125	2.9	1.1	1.3	–0.1	0.5
250	–1.3	0.7	0.7	0.4	0.0
Control – Pit 2 (Mainly negative)					
16	–0.7	–1.4	–1.4	–0.2	–1.4
31	–0.6	–0.7	–1.0	0.1	–0.6
63	–0.8	–0.4	–1.3	–0.3	–0.4
125	–1.0	–0.6	–1.9	–0.2	–1.2
250	–2.6	–1.1	–1.9	–1.6	–1.7
Pit 1 – Pit 2 (All negative)					
16	–2.0	–1.6	–2.0	–0.8	–1.1
31	–1.6	–1.2	–1.6	–0.7	–0.8
63	–2.2	–1.6	–2.3	–0.8	–1.4
125	–3.9	–1.7	–3.2	–0.1	–1.7
250	–1.3	–1.8	–2.6	–2.0	–1.7

Table 6 lists data collected at the 250-m microphones (1 and 5 m high). Here an effect from Pit 1 is seen primarily when the blast was 1 m rather than 2 m from the blast-sound-absorbing pit surface. This is to be expected, since the relative size of the source area, according to ISO 9613-2, is linearly proportional to the height of the source above the surface. There is also an indication of some effect with the eighth-stick charge. This also is to be expected, since the same size source area should work better at higher frequencies than at lower frequencies. In Table 6 we are dealing with only 10 differences per charge size and configuration. The probability of all tails with 10 coin tosses is 1 in 1024, the probability of no more than 1 heads is 11 in 1024 or about 1 in a hundred, and the probability of no more than two heads is 56 in 1024 or about 1 in 20. Therefore, conclusions drawn from Table 6 are much less certain than those drawn from Tables 4 and 5. Nevertheless, there is clearly an effect from Pit 1 and Pit 2 on the received levels with the quarter-stick charge located at a height of 1 m. Just like the result overall at 15 m, Pit 1 reduced blast levels and Pit 2 increased blast levels at 250 m.

Figures 26 through 28 show the results at the 2.6-, 15-, and 250-m sensors.

Table 6. Differences in measured level for the cases indicated at the 250-m sensors.

Frequency (Hz)	1/4 charge 1 m		eighth charge 2 m		1/4 charge 2 m		1/2 charge 2 m		Full charge 2 m	
	1 m	5 m	1 m	5 m	1 m	5 m	1 m	5 m	1 m	5 m
Control – Pit 1 (Mostly positive for 1/4 – 1 m)										
16	0.1	0.3	–1.2	0.0	–0.6	–0.7	0.4	0.4	–0.7	–0.8
31	0.3	0.2	0.7	0.5	–0.1	–0.2	1.2	1.0	–0.1	–0.1
63	0.8	0.3	1.6	1.6	0.1	–0.1	0.9	0.5	0.5	0.4
125	1.7	–0.5	1.0	1.0	–0.5	–0.6	1.8	0.7	1.3	1.4
250	4.7	3.9	–0.7	0.0	0.5	–0.3	0.6	–0.1	–0.3	0.4
Control – Pit 2 (All negative for 1/4 – 1 m)										
16	–0.4	–0.3	–1.0	–0.3	–0.8	–0.9	0.1	0.2	–1.1	–1.2
31	–0.6	–0.4	0.1	0.0	0.2	0.1	0.4	0.3	–0.1	–0.1
63	–1.5	–1.0	0.4	0.7	0.4	0.3	0.1	–0.3	–0.2	–0.2
125	–1.3	–1.2	–0.4	0.3	0.9	0.0	1.4	1.1	0.4	0.4
250	–4.0	–3.4	–2.0	–0.9	0.0	–1.8	1.0	1.1	–1.5	–1.7
Pit 1 – Pit 2 (All negative for 1/4 – 1 m and mostly negative for 1.8 – 2 m)										
16	–0.5	–0.6	0.2	–0.3	–0.2	–0.2	–0.3	–0.2	–0.4	–0.4
31	–0.9	–0.5	–0.6	–0.6	0.3	0.3	–0.8	–0.7	0.0	0.0
63	–2.2	–1.2	–1.2	–0.9	0.4	0.4	–0.8	–0.8	–0.7	–0.6
125	–3.0	–0.7	–1.4	–0.8	1.4	0.7	–0.4	0.4	–0.8	–1.0
250	–8.8	–7.4	–1.3	–0.9	–0.5	–1.5	0.4	1.3	–1.1	–2.0

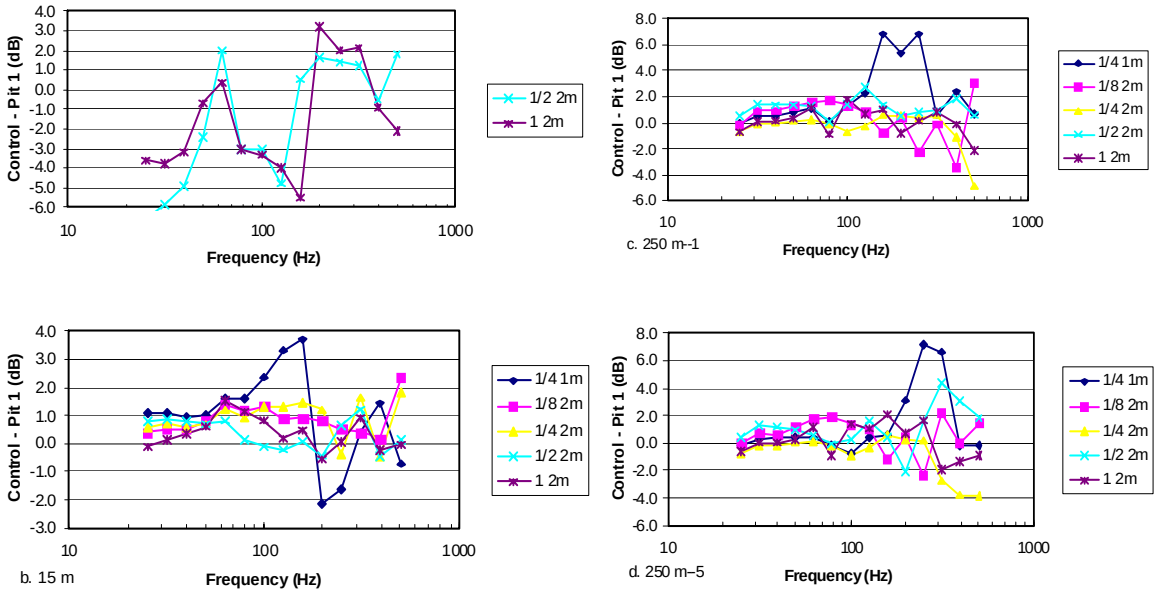

Figure 26. Plots of Control minus Pit 1 values as functions of frequency for the charge indicated. Note that the quarter-stick charge at a height of 1 m clearly departs from the other data at both 15 and 250 m.

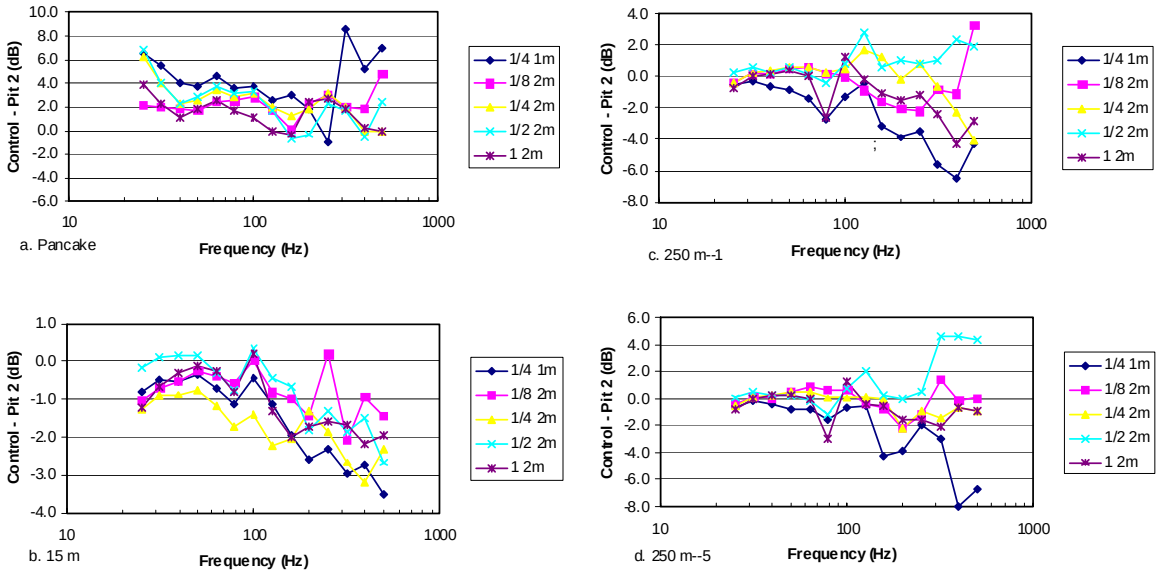

Figure 27. Plots of Control minus Pit 2 values as functions of frequency for the charge indicated. Again, the quarter-stick charge at a height of 1 m clearly departs from the other data, this time at both 2.5 and 250 m.

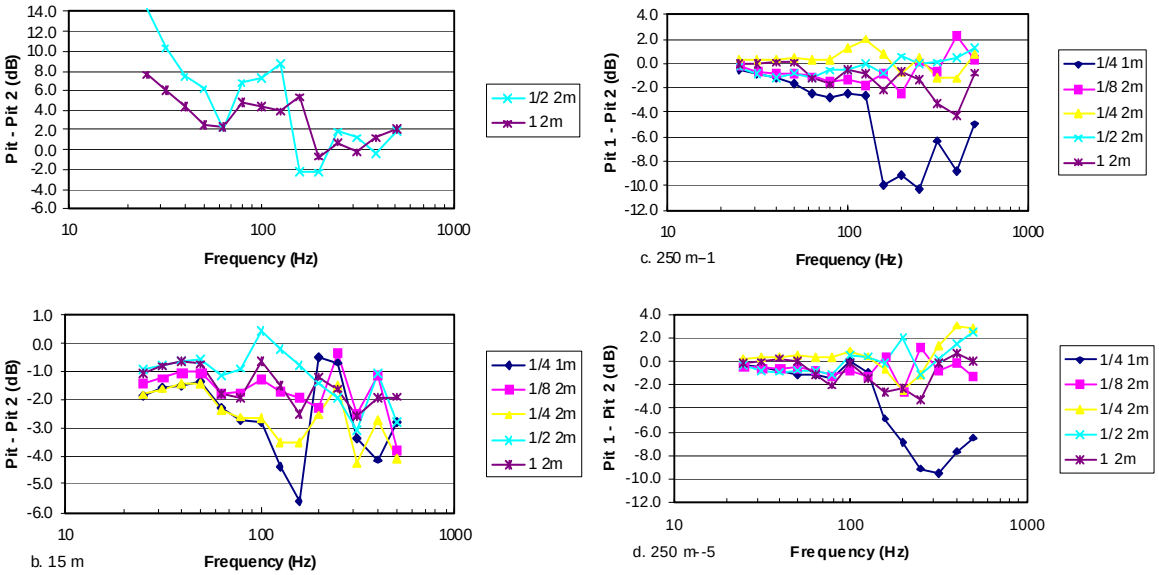

Figure 28. Plots of Pit 1 minus Pit 2 values as functions of frequency for the charge indicated. Here, the quarter-stick charge at a height of 1 m clearly departs from the other data at all three distances.

Sound Exposure Level Results for Test II

Test II includes three replications of each blast charge size at the grass-covered control site and the plowed-field site. As with the Test I data, an energy average of the three replications and the standard deviation to the replications has been done for all of the octave, one-third octave, and frequency-weighted SEL data.

Table 7 contains the average standard deviations for each set of three replications. The numbers represent the average for all sensors relevant to that blast site for the octave bands from 16 through 250 Hz. The number in parenthesis represents the standard deviation when problem sensor data are removed from the average. These improved averages are about 0.4–0.9 dB, indicating that the data at most sensors replicated well. However, the results from two of the sensors consistently exhibit a higher standard deviation than do the results for the others. The results for the air–grass interface pencil gauge sensor at the base of the plowed-field blast site nearly always exhibits a much higher standard deviation. Also, the results for the 1-m-high blunt gauge sensor at 15 m exhibit a higher standard deviation at the very low frequencies in the 16- and 31-Hz octave bands, but because this is a low-frequency effect, it is not noticeable in the data of Table 7. The data for these two sensors do not appear to be usable. In addition, the data at the control site for the 5-m-high sensor at 250 m for the quarter-stick case exhibit a standard deviation of 30 dB and are totally unusable. The results for all of the other sensors typically exhibited standard deviations that were in the 0.3- to 0.9-dB range. The standard deviations sometimes are a little larger at 250 m, but this is believed to be caused by normal atmospheric variation and not related to the gauges.

Table 7. Average standard deviations for octave-band SEL data in the frequency range from 16 through 250 Hz.

Charge size (sticks)	Blast source	Standard deviation	Problems
1/4	Control	5.0 (0.8)	250-m (5-m high) sd~30
	Plowed	0.9	OK
1	Control	0.5	OK
	Plowed	1.5 (1.0)	0-m sensor sd~6
4	Control	0.4	OK
	Plowed	1.0 (0.9)	0-m sensor sd~1.1

Given the three-replication energy averages, differences between the blast sites for like sensor positions may be examined. Overall, the results are that the plowed ground attenuates at all frequencies out to 100 m, but at farther distances,

the propagation is attenuated for frequencies above 100 Hz and the propagation is enhanced for frequencies below 100 Hz. A theoretical interpretation of these results is presented later in the this chapter. Table 8 and Figure 29 portray these results.

Table 8. Differences between the control (grass) field and the plowed field for various frequencies in Test II.

Distance	Charge	16 Hz	31 Hz	63 Hz	125 Hz	250 Hz	500 Hz	1000 Hz	A (weighted)	C (weighted)
					5-m height					
50	1/4	0.7	1.1	3.3	5.4	3.6	1.3	1.9	2.8	3.4
	1	1.2	1.0	2.0	3.7	3.3	2.4	2.7	2.7	2.1
	4	1.4	1.5	1.4	2.2	2.3	2.1	2.5	2.3	1.6
	Average	1.1	1.2	2.3	3.7	3.1	1.9	2.4	2.6	2.3
100	1/4	2.0	1.0	3.6	8.5	4.9	1.9	1.2	2.3	3.9
	1	2.6	0.9	1.9	6.3	3.0	3.5	2.5	3.0	2.1
	4	3.0	1.5	1.2	3.3	1.0	1.2	1.0	1.2	1.7
	Average	2.5	1.1	2.2	6.0	2.9	2.2	1.6	2.2	2.6
250	1/4	–	–	–	–	–	–	–	–	–
	1	–4.0	–3.0	–0.8	11.4	5.9	2.9	1.8	2.9	–1.1
	4	–3.6	–2.2	–0.4	7.7	4.8	4.7	4.1	4.4	–1.2
	Average	–3.8	–2.6	–0.6	9.5	5.4	3.8	3.0	3.7	–1.1
					1-m height					
50	1/4	12.1	9.0	7.1	7.8	16.2	10.9	7.7	9.1	8.1
	1	13.0	9.3	6.7	6.2	13.5	12.1	8.3	9.3	7.5
	4	12.1	8.7	4.7	0.7	3.4	5.1	1.7	2.6	4.9
	Average	12.4	9.0	6.2	4.9	11.0	9.4	5.9	7.0	6.8
250	1/4	–4.1	–2.7	0.4	15.1	24.4	8.6	1.1	7.9	1.0
	1	–3.8	–3.2	–2.1	10.9	14.9	9.2	1.4	5.0	–1.8
	4	–3.1	–2.2	–1.8	6.5	18.2	12.7	4.7	5.7	–1.6
	Average	–3.7	–2.7	–1.1	10.8	19.1	10.2	2.4	6.2	–0.8

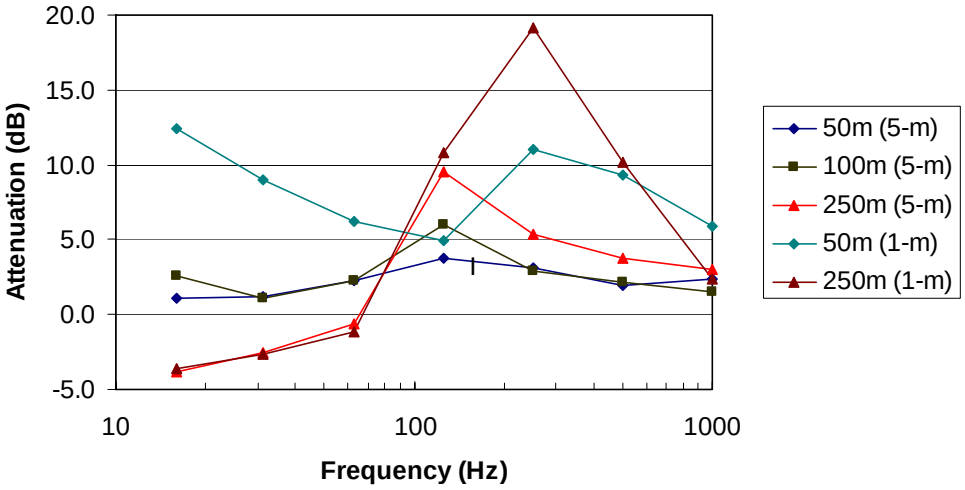

Figure 29. Plots of the average differences between the control (grass) field and the plowed field from Table 8.

Impedance Measurement Results

As noted earlier, surface impedance measurements were made at various positions in the Test Site I grass field, on the two pits, and near the 250-m mast in grass-covered Test II site before plowing. Measurements of complex excess attenuation were made using a source consisting of a mid-range Hi-Fi driver in a cylindrical cabinet and an MLSSA (Half Blackman Harris window) for signal acquisition and analysis (Fig. 19 and 20). Similar measurements were made over the plowed ground. The analysis uses both a method similar to the *Template Method for Measuring Ground Impedance* (American National Standards Institute 1999) and the method of *Direct Impedance Fitting* (Taherzadeh and Attenborough 1999). The template method uses only the magnitude of the measured excess attenuation spectra, whereas the direct impedance fitting requires the *complex* excess attenuation measurements. Figures 30 through 34 show typical results. In each case the left-hand graph shows the data and results of impedance model fitting. For the template method, three impedance models have been used: a two-parameter semi-empirical model [Delany and Bazley (1970) hard-backed layer], a two-parameter (variable porosity) model by Attenborough (1992), and a five-parameter rough porous layer model (with two of the parameters viz. porosity and tortuosity fixed) by Attenborough and Waters-Fuller (2000). The black continuous lines represent the loudspeaker-gathered data, the red broken lines represent predictions using the two-parameter model, and the blue dotted lines represent predictions using the five-parameter model. In Figure 30, the brown dash–dot lines represent predictions using the two-parameter Delany and Bazley model. The right-hand graphs in each of Figures 30 through 34 show the directly

deduced impedance spectra as black continuous lines. The other lines represent the various impedance model predictions using the best-fit parameter values deduced from the excess attenuation spectra.

For the unplowed ground, the data and fits obtained near the 250-m mast in the Test II area suggest a lower flow resistivity than those obtained near the 50-m mast in the Test I area. However, the directly deduced impedance spectra at both sites are quite similar. The best-fit parameters at the 250-m mast site before plowing give the best fits to the directly deduced impedance spectra.

Although it is not the only model that gives tolerable agreement with the measured excess attenuation spectra, the five-parameter model consistently gives best agreement with the directly deduced impedance spectra, particularly for the plowed ground and gravel pits. Gravel Pit 1 contained three layers of gravel within a total depth of 1.5 m. For the purposes of the template fitting for ground impedance, Pit 1 has been treated as a single layer and the "effective" depth adjusted for best fit. With this simplification, the apparent flow resistivity is smaller than the measured flow resistivity for Pit 2, which is consistent with the larger stone size in the surface layer of Pit 1. In the case of gravel Pit 2, template fitting (after fixing the flow resistivity at the measured value for the 8-mm gravel) has been applied with both hard-backing and sandy soil backing. The latter slightly reduces the oscillations in the predictions observed at low frequencies. The directly deduced (linear) impedance spectra for both gravel pits suggest more or less pure resistance.

Table 9 summarizes the parameter values for all of the surfaces according to five-parameter model.

Table 9. Summary of parameters deduced from measured surface impedance. In all cases the porosity has been assumed to be 0.4 and the tortuosity = 1/porosity

Location	Flow resistivity (kPa s m^{-2})	Layer depth (m)	Roughness height (m)	Roughness spacing (m)
Unplowed ground near 250 m site in test II area	150	0.05	0.015	0.05
Plowed ground (across furrows)	20	∞	0.04	0.1
Pit 1	0.5	4.5	0.01	0.05
Pit 2 (non-hard back)	0.85	1.5	0.005	0.02

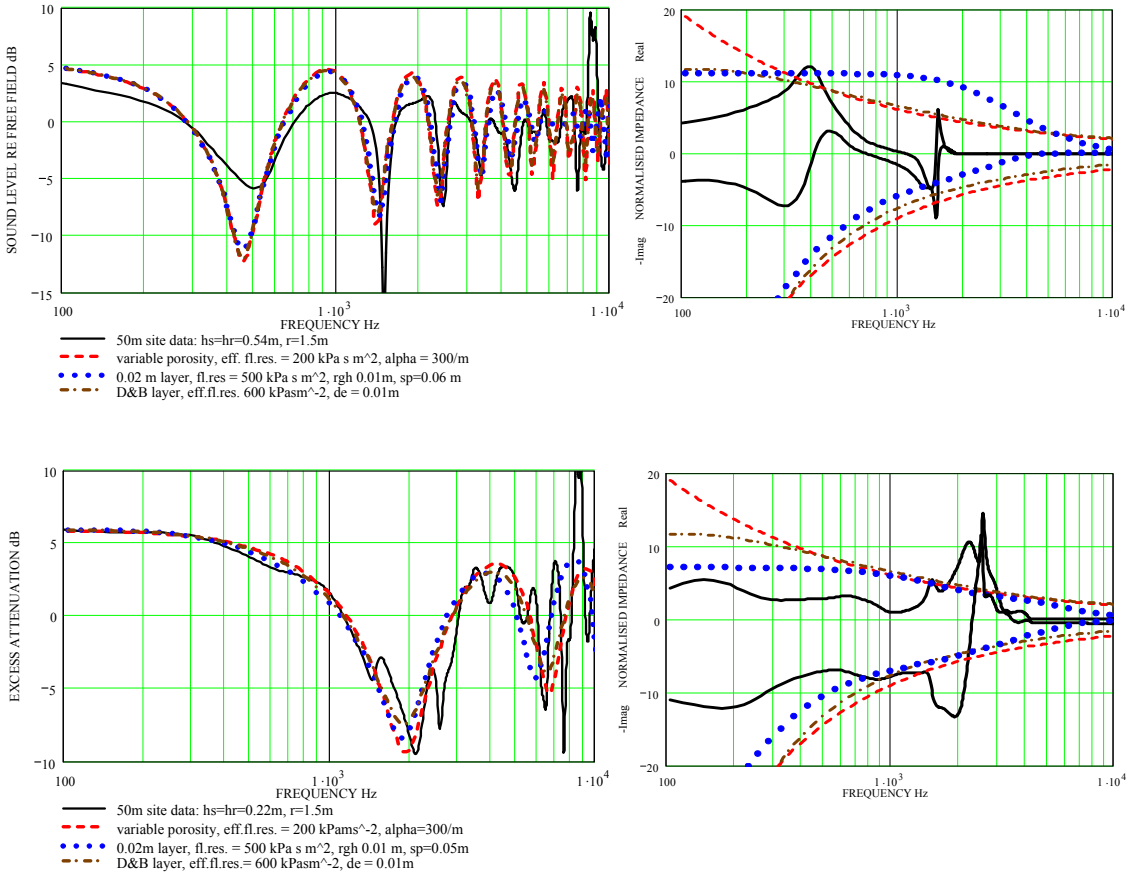

Figure 30. Two examples of the results from measurements near the 50-m mast site in the Test I area. The two graphs on the left are measured excess attenuation spectra, and the two graphs on the right are the corresponding impedance fit. (Fit parameters at the 50-m area: *2-para*: σe = 200 kPa s m^{-2}; a = 300/m; *rough 5-para*: σ = 500 kPa s m^{-2}; Ω = 0.4, T = 1/Ω, rgh ht = 0.015 m, sp = 0.05 m, d = 0.05 m; *Delany & Bazley* σe = 600 kPa s m^{-2}; de = 0.01 m.)

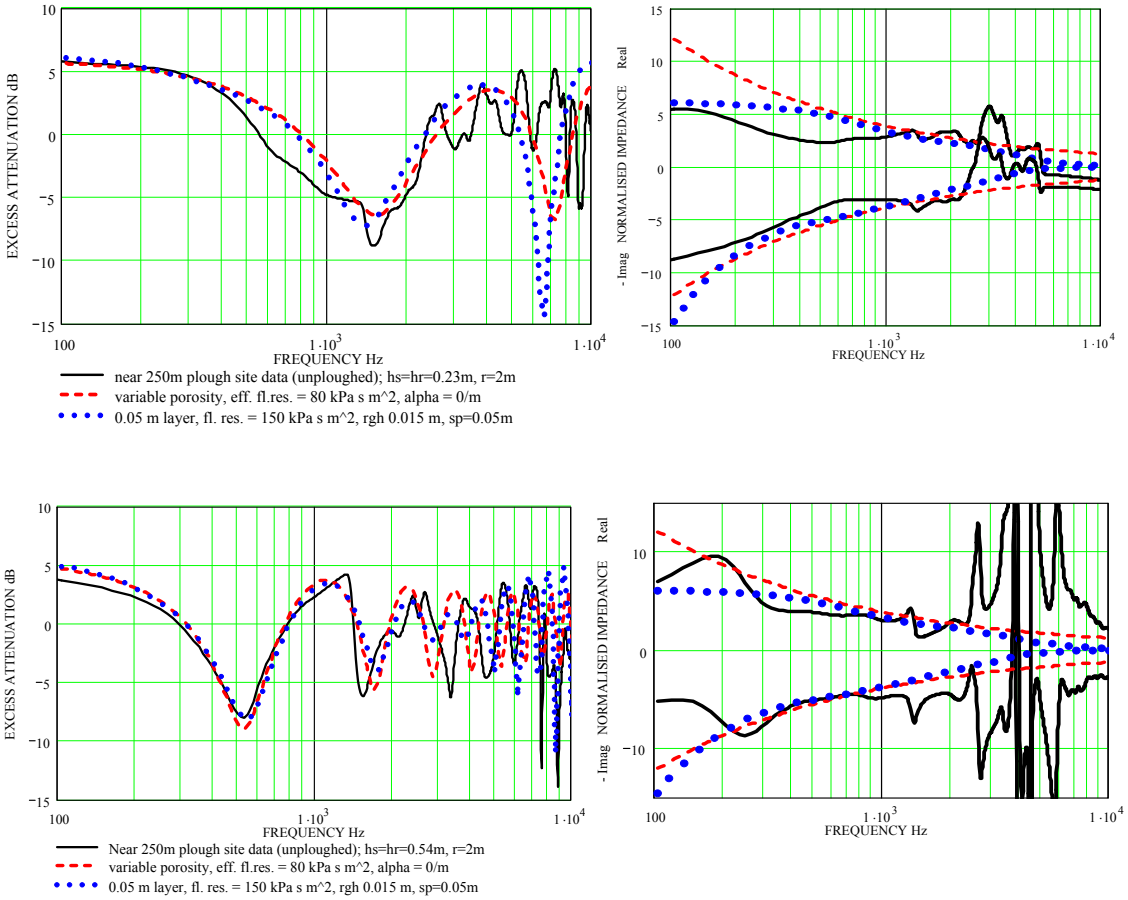

Figure 31. Two examples of measurements near the 250-m mast site in the Test II area (before plowing) and various model predictions. The two graphs on the left are measured and predicted excess attenuation spectra, and the two graphs on the right are corresponding impedance fits.

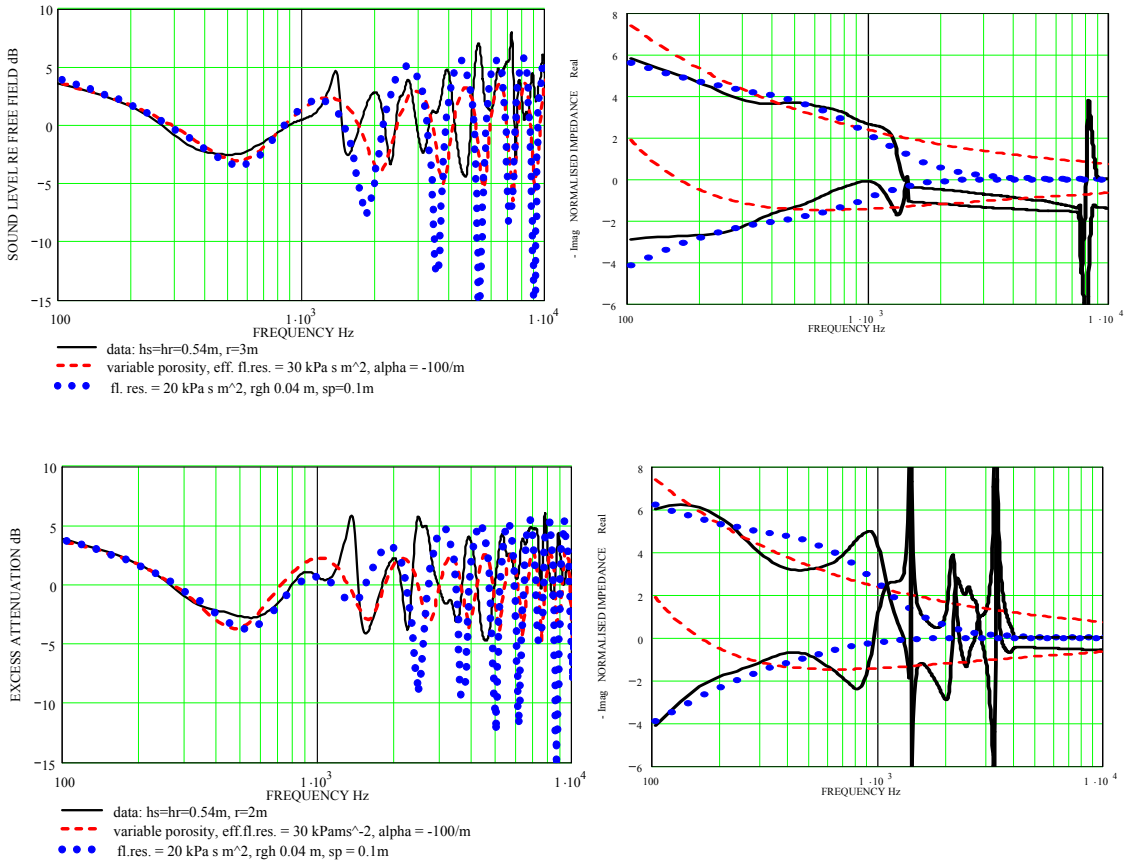

Figure 32. Excess attenuation and directly fitted impedance spectra obtained across (i.e. at right angles to) furrows of plowed sandy soil during Test II. The two graphs on the left are measured and predicted excess attenuation spectra, and the two graphs on the right are corresponding impedance fits.

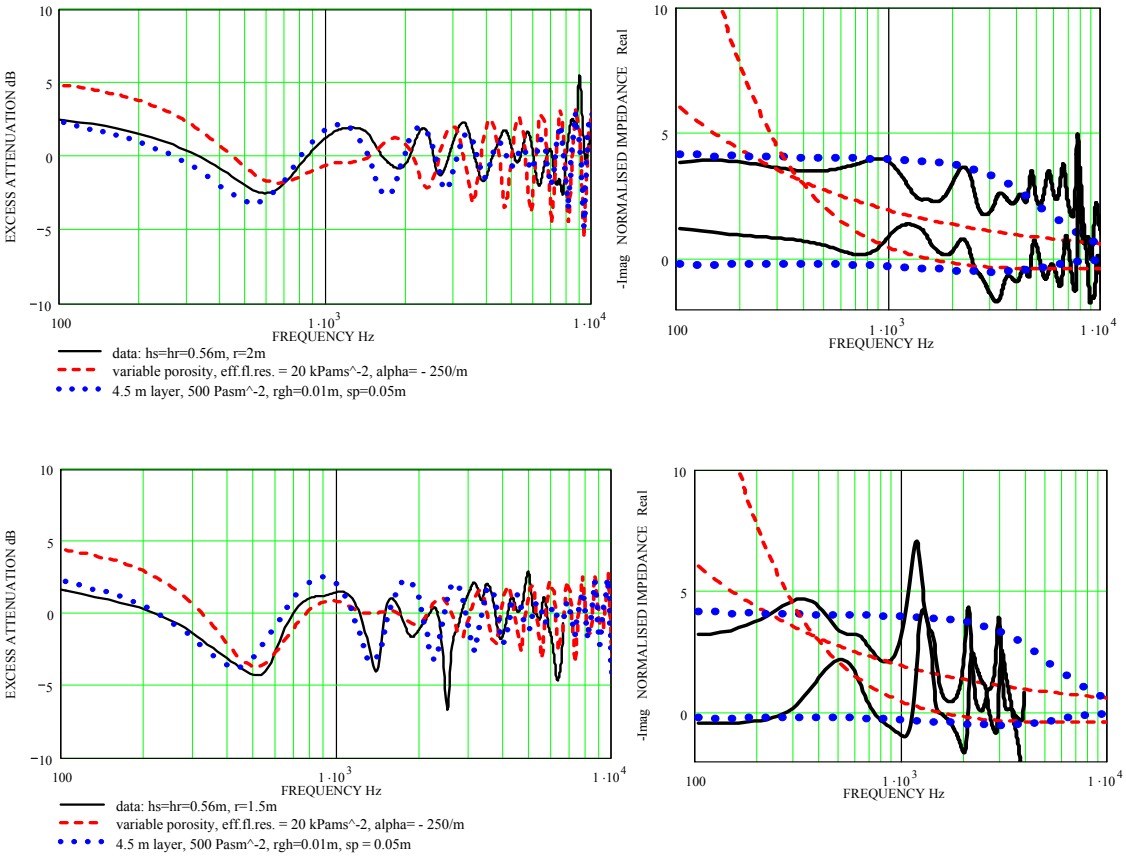

Figure 33. Excess attenuation and directly fitted impedance spectra obtained at Gravel Pit 1.

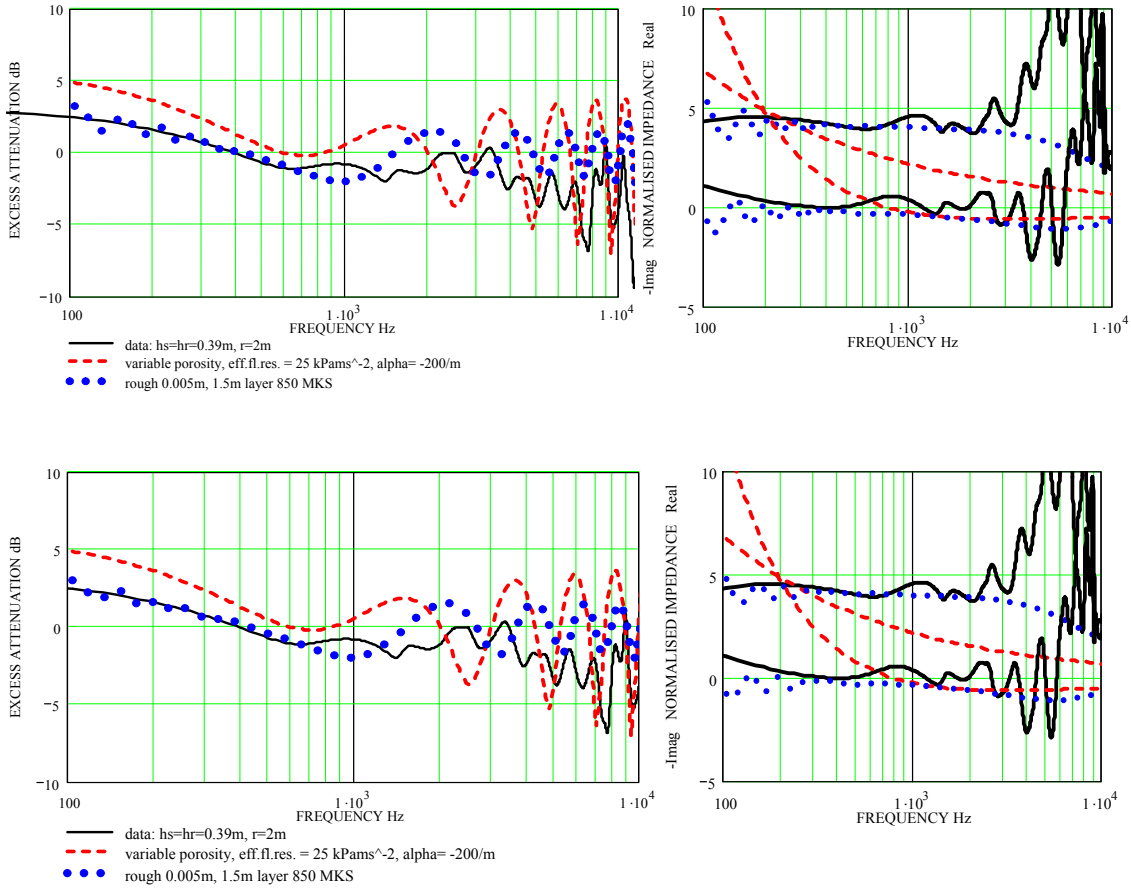

Figure 34. Excess attenuation and directly fitted impedance spectra obtained at Gravel Pit 2 using measured flow resistivity (850 Pa s m^{-2}). The top two graphs assume a hard-backed layer, and the bottom two graphs assume a non-hard-backed layer.

Discussion of Test I Results Near the Pits

The conclusions drawn from Test I data are that

- Pit 1 has a negligible near-field effect on the blast sound compared with the reference site but has some effect in the far field; and
- Pit 2 has a significant blast sound reduction effect in the near-field compared with the reference site but has a slightly negative effect in the far field.

The comparisons with predictions of the numerical codes are discussed in a later section. For comparison with theoretical predictions, first it is necessary to note that the analytical nonlinear theories that have been developed are weak shock theories. Secondly, they are for plane waves, whereas the field trials involved "point" sources. In this section, non-linear theory 2 for reflection of

high-amplitude plane wave pulses from a rigid-porous layer is used for comparison with near-field data for Pit 2. Predictions for Pit 1 have not been made since the parameters for the top layer are not known.

For data obtained at ranges longer than 2.6 m from the source, it is necessary to take into account the discontinuous nature of the ground surface. This can be done numerically but not with the theoretical nonlinear models. On the other hand, *linear* predictions of the effects of changing the pit dimensions are made and discussed.

Pit Near-Field Effects

Comparisons with Data Received by Surface-Mounted Receiver at Pit 2. Data measured by the sensors on the ground at the reference site (Channel 5) may be compared with those recorded by the sensors at the surface of Pit 2 (Channels 3 and 8). For these sensors the blast sound wave was almost normally incident. To compare with plane wave predictions for Pit 2, the waveform measured on the surface of the pit is considered to be the sum of incident and pit-reflected pulses. To calculate the reflected pulse for the waveform normally incident at the surface, it is necessary to estimate the pressure and duration of the incident waveform. For this purpose, use is made of the signal received by Channel 9 (height 1 m, 2.6 m from blast), which consists of identifiable direct and reflected pulses. The direct pulse travels approximately 2.79 m from the blast point. The distance between the blast point and receiver 8 is 2 m. To reconstruct the incident pulse on the surface, the direct arrival at Channel 9 is assumed to be triangular. Then the combination of losses due to hydrodynamic nonlinearity in the air and spherical spreading at distance x1 from the source can be expressed in terms of the peak amplitude and duration of the pulse measured at distance x0 from the source. Hence

$$p(x1) = \frac{p(x0)}{\sqrt{1 + 1.2\dfrac{p(x0)x0}{c^2\rho_0 t(x0)}\ln\left(\dfrac{x1}{x0}\right)}}\frac{x0}{x1} \tag{1}$$

$$t(x1) = t(x0)\sqrt{1 + 1.2\frac{p(x0)x0}{c^2\rho_0 t(x0)}\ln\left(\frac{x1}{x0}\right)}\,. \tag{2}$$

Assuming that x0 = 2.789 m, x1 = 2 m, p(x0) = 31000 Pa (values for series 5 and 6), t(x0) = 1.8 ms (estimate of the duration for series 5 and 6), and spherical spreading, it can be calculated that p(x1) = 55500Pa and t(x1) = 1.4 ms at a dis-

tance corresponding to that of the pit surface from the blast. The estimate of duration at 2.6 m is approximate since the real pulse is not triangular. The resulting estimate of change in duration with distance is approximate also. Assuming plane waves, the direct pulse measured by Channel 9 with amplitude increased to 55500 Pa (and unchanged duration) has been used as the incident pulse in predicting the reflected pulse at the surface of Pit 2. The combination of the assumed incident pulse and the predicted reflected pulse is compared with the measured waveform at the sensor mounted on the surface of the gravel in Pit 2 in Figure 35.

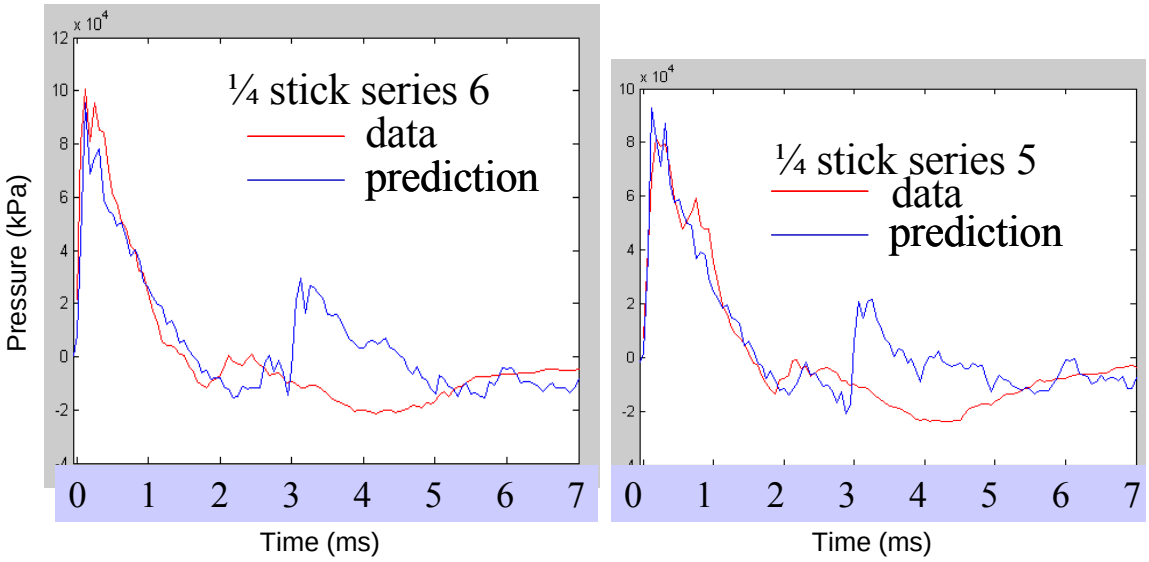

a. Quarter stick, series 6 prediction data. **b. Quarter stick, series 5 prediction data.**

Figure 35. Measured and predicted blast waveforms for the quarter-stick charge at the sensor mounted on the surface of the gravel in Pit 2 without adjustment of the estimated incident pulse duration.

The spectral comparisons are shown in Figure 36, and the results of allowing for the estimated change in the duration of the incident pulse are shown in Figure 37 and 38.

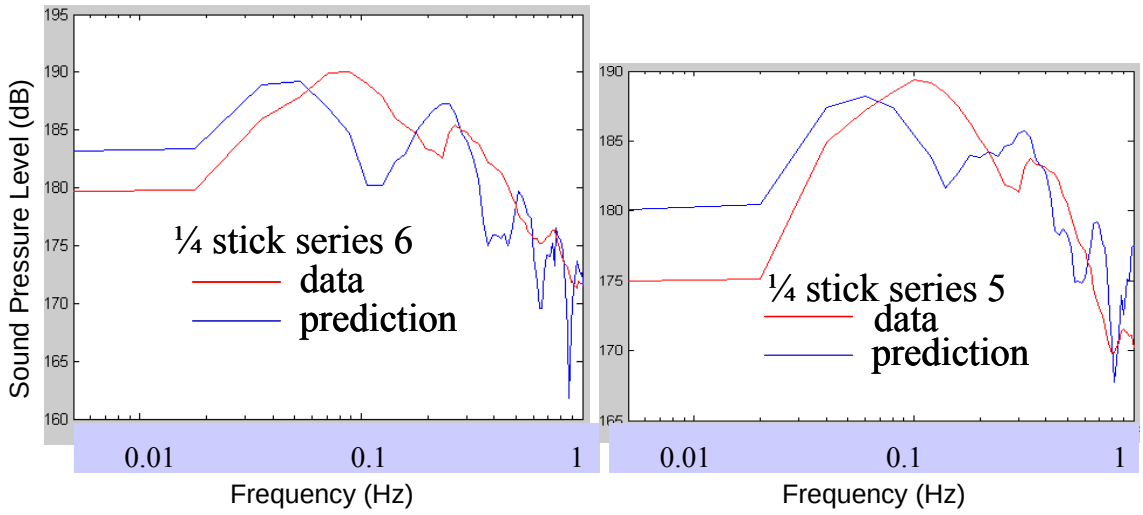

a. Quarter stick, series 6 prediction data. **b. Quarter stick, series 5 prediction data.**

Figure 36. Measured and predicted spectra at the sensor mounted on the surface of the gravel in pit 2 for the quarter-stick charge without adjusting the estimated incident pulse duration.

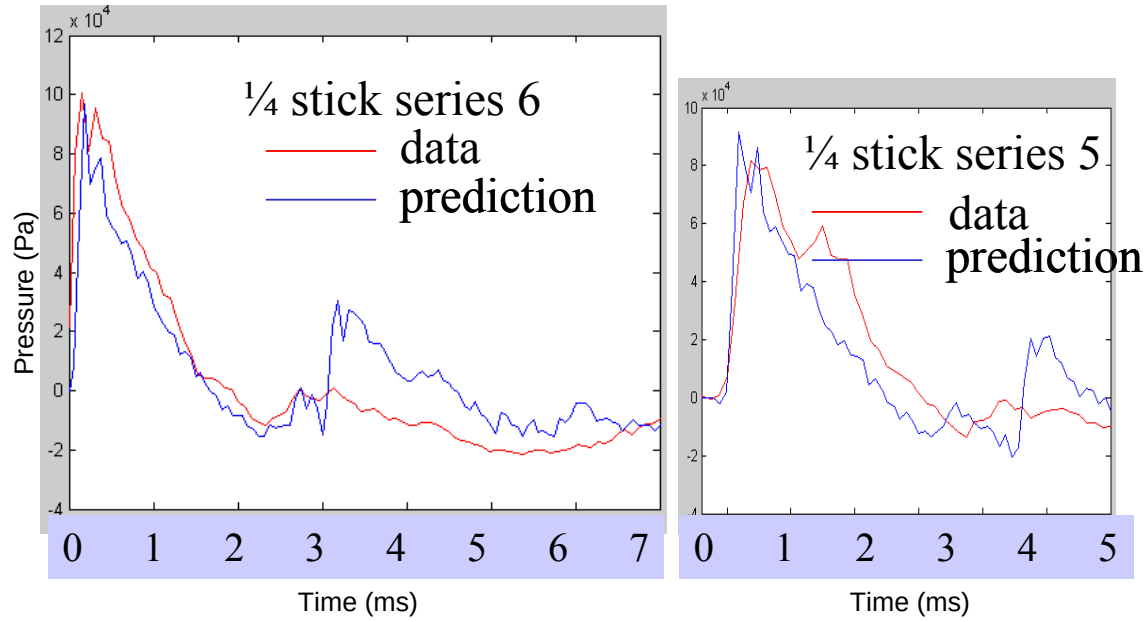

a. Quarter stick, series 6 prediction data. **b. Quarter stick, series 5 prediction data.**

Figure 37. Measured and predicted blast waveforms for the quarter-stick charge at the sensor mounted on the surface of the gravel in Pit 2 after adjusting the estimated incident pulse duration.

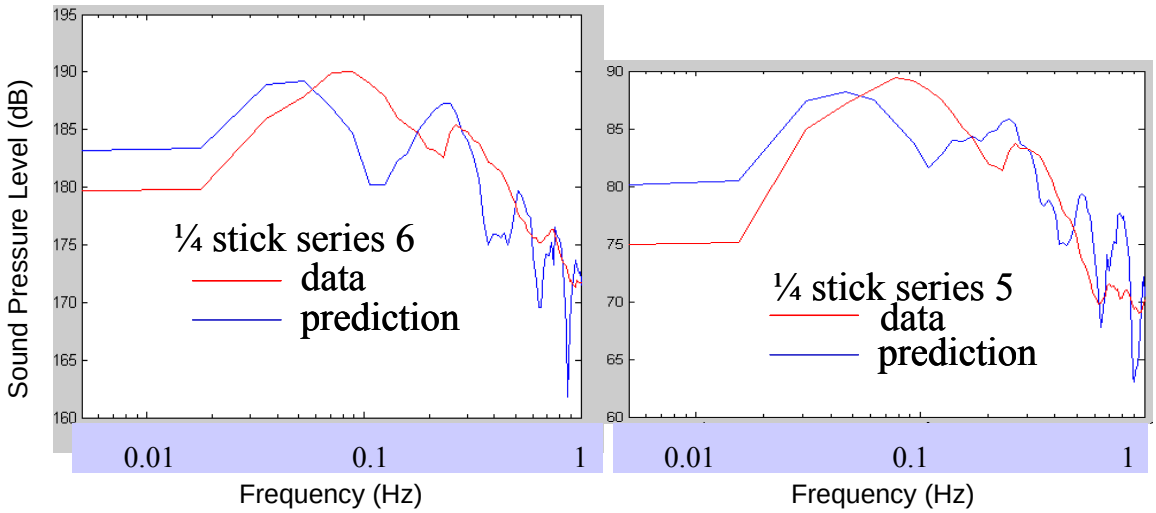

a. Quarter stick, series 6 prediction data. **b. Quarter stick, series 5 prediction data.**

Figure 38. Measured and predicted spectra at the sensor mounted on the surface of the gravel in Pit 2 for the quarter-stick charge after adjusting the estimated incident pulse duration.

Given the assumptions made for these calculations, the agreement between measurement and prediction is good. The main discrepancies are noticeable in the tails of the pulse waveforms and correspondingly at low frequencies in the spectra. The strong absorption in the 8- and 16-Hz octave bands for the quarter-stick charges was observed for the half- and one-stick charges also. Figure 39 shows an example waveform comparison. Note the change in the negative part of the waveform, as well as the peak at the surface of Pit 2 compared with the signal at the surface of the control site.

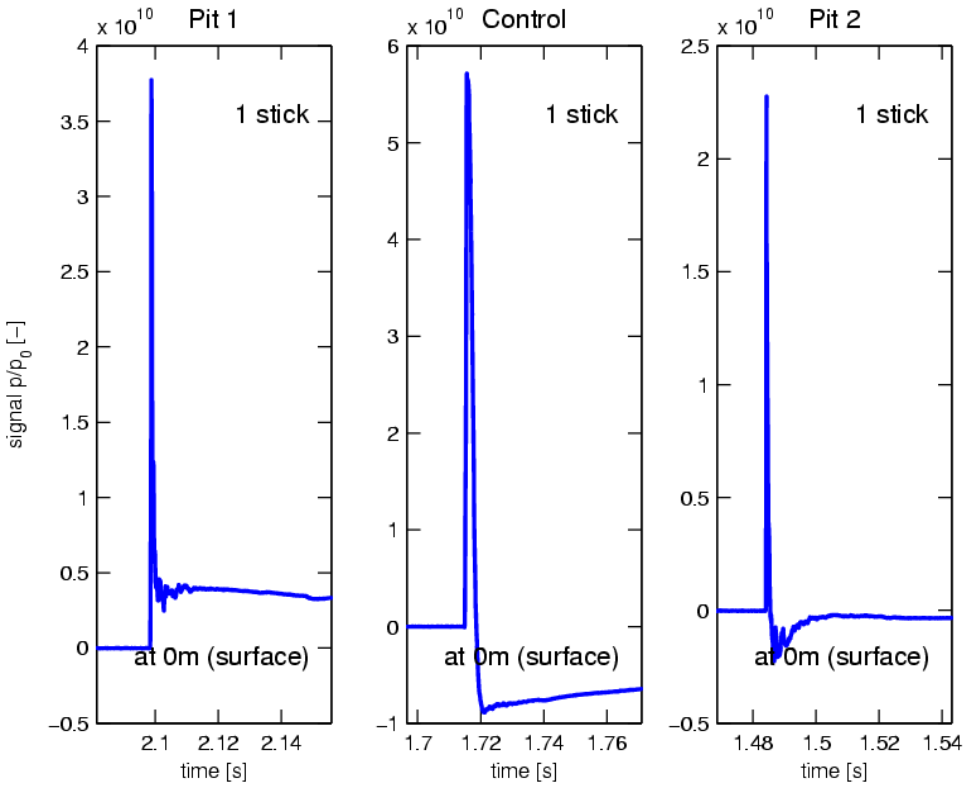

Figure 39. Waveforms recorded at the surface for the one-stick charge.

Figure 40 shows octave band spectra measured at the surface of Pits 1and 2 (Channel 8) for various charge sizes. With the exception of the data for the eighth-stick charge at the 2-m height, the spectra show a net reduction above the pits at frequencies below 125 Hz. For the eighth-stick charge there is a small net reduction in the spectra above the pits between OBCF 16 Hz and 125 Hz and a net enhancement below OBCF 16 Hz. Again, except for the eighth-stick charge, there is a consistently greater reduction due to Pit 2 below 63 Hz. The reduction at the Pit 2 surface is particularly great between 4 and 16 Hz for charges greater than an eighth stick.

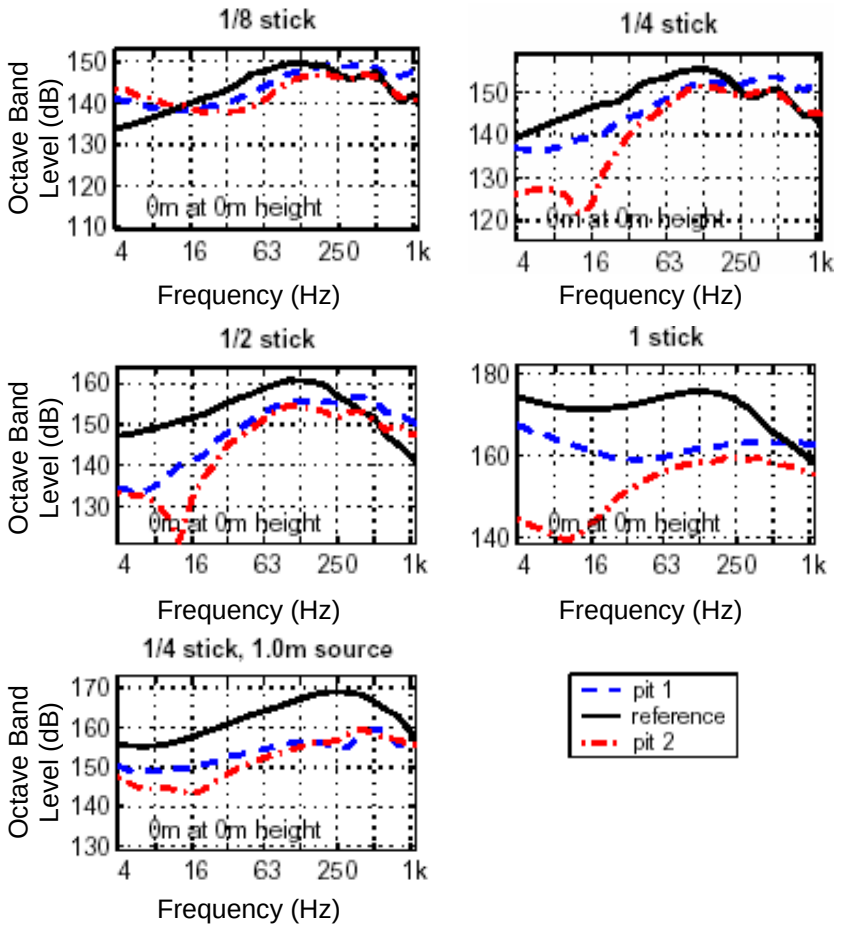

Figure 40. Octave band spectra measured at the reference site surface and at the surfaces of Pits 1 and 2 for various charge sizes (all at a source height of 2 m, except the bottom graph, which has a source height of 1 m).

The initial objective of the design of Pit 1 was to achieve good "impedance matching" at 50 Hz. However, the data at the surface-mounted sensor show that Pit 2 performs better, and both pits appear to offer greater reduction than expected from nonlinear rigid-porous theory below 16 Hz. The first resonant frequency for the pore-borne waves calculated for Pit 2 is 46Hz. Another possible mechanism is increased acoustic-to-seismic coupling, and this should be investigated further.

Comparisons with Data Received by Pancake Gauges 2.6 m from the Blast. In cases where the measured waveforms for the smaller charges (one stick, half stick, and quarter stick) show clear direct and ground-reflected arrivals (see, for example, Figure 41) at Pit 2, and similar arrivals with a comparable direct peak pressure at the reference site, it is possible to calculate the difference in attenuation due to ground surface reflection between the reference site and Pit 2.

Only data for the smaller charges are considered since nonlinear theory 2 is for weak shocks. It is assumed that for each explosion there is a reduction in the positive peak pressure of the measured reflected pulse because of spherical spreading and hydrodynamic distortion in the air over the greater path length and (because of nonlinear reflection at the ground surface. It is assumed also that the nonlinear attenuation caused by the path length difference is the same at the reference site and at the Pit 2 site.

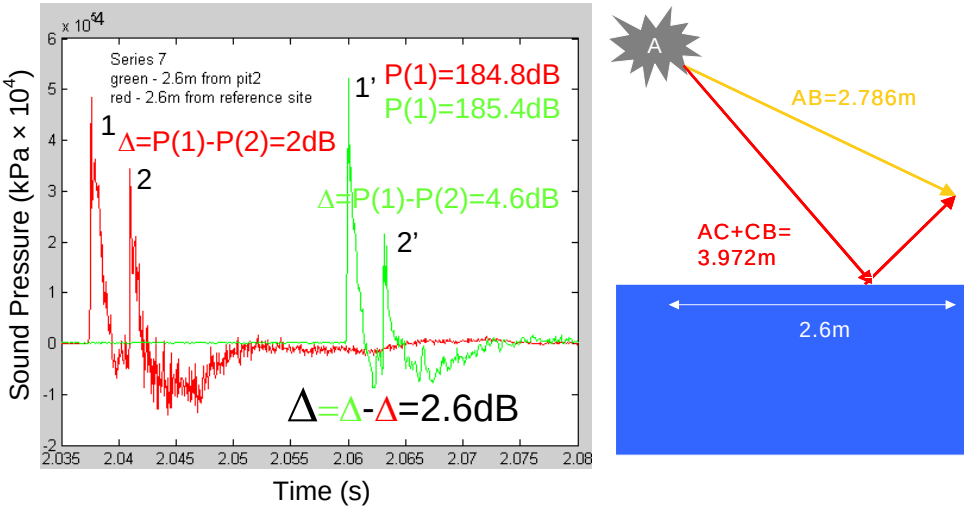

Figure 41. Method for estimating that the attenuation due to reflection at Pit 2 for a half-stick explosion at 2-m range and 1-m height when the source is at the 2-m height is 2.6 dB.

A similar procedure can be applied to Pit 1 data. The results of this procedure for Pit 1 (explosive charge of one stick) and Pit 2 (explosive charges of a quarter stick and one stick) are shown in Tables 10 and 11.

Table 10. Attenuation due to reflection from pit 2 (quarter-stick charge).

Reference site			Pit 2			Attenuation due to reflection from the pit	
Series	P(1), dB	Δ_0, dB	Series	P(1'), dB	Δ_2, dB	$\Delta=\Delta_2-\Delta_0$	
6	182.5	2.6	6	180.8	6.3	3.7	2-m source height
6	182.5	2.6	5	180.8	6.7	4.1	
14	180.3	1.9	15	178.4	5.6	3.7	1-m source height
15	180.2	3.2	15	178.4	5.6	2.4	

Table 11. Attenuation due to reflection from both pits (one-stick charge).

Reference site			Pit 2			Attenuation due to reflection from the pit
Series	P(1), dB	Δ_0, dB	Series	P(1'), dB	Δ_2, dB	$\Delta=\Delta_2-\Delta_0$
11	190.5	2.9	11	189.4	4.8	1.9
11	190.5	2.9	12	188.3	2.5	–1.4
Reference site			**Pit 1**			**Attenuation due to reflection from the pit**
Series	**P(1), dB**	**Δ_0, dB**	**Series**	**P(1'), dB**	**Δ_2, dB**	**$\Delta=\Delta_2-\Delta_0$**
11	190.5	2.9	11	188.9	4.9	2
11	190.5	2.9	12	189.3	6.1	3.2

According to these results, Pit 2 gives a greater extra reduction on reflection for a quarter stick than for a half stick and one stick. This observation is consistent with the prediction shown in Figure 42.

The results for Pit 2 may be compared with predictions of nonlinear theory 2 if it is assumed that the incident and reflected waves are plane. The comparisons are shown in Figure 42. Contrary to predictions, the measured reduction for a lower source height is smaller. On the other hand, the data are for the difference in reductions in reflection between Pit 2 and the reference site, whereas the predictions are for the reduction in reflection due to Pit 2 only. For one of the 1-m-high explosions, the difference between the direct and reflected peak levels at the reference height is particularly high. As mentioned earlier, the data for series 14 and 15 exhibit twin peaks in the direct arrival waveform. It should be noted also that the plane wave assumption will be less valid for the lower source height. Moreover there is the problem that the direct pressure peaks are not strictly the same at the different sites as assumed by the analysis.

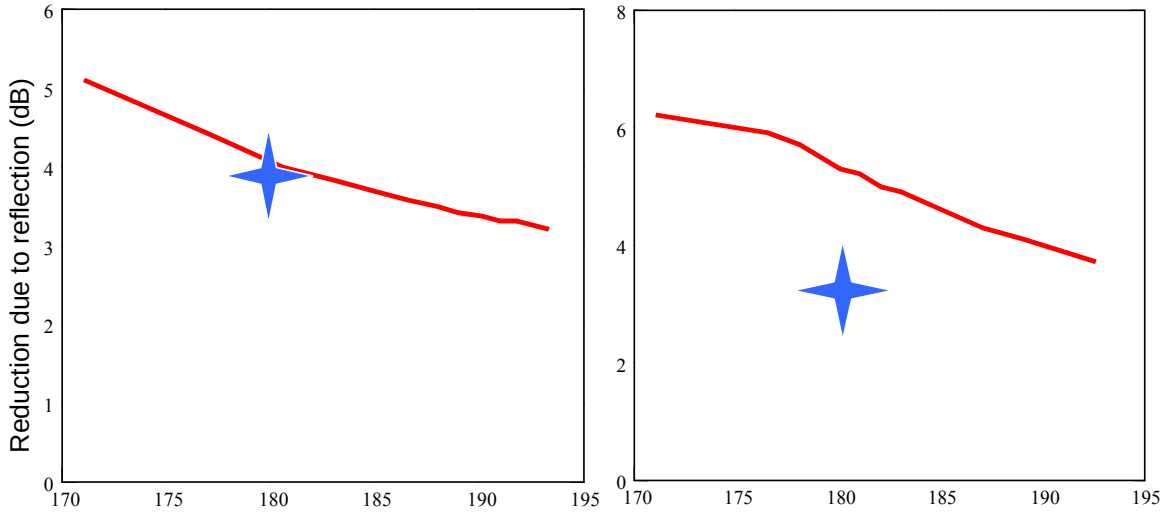

a. 2-m source height **b. 1-m source height**

Figure 42. Predictions (red lines) for reduction in amplitude due to reflection from Pit 2 compared to data (blue stars) for a quarter stick.

Linear Predictions of the Far-field Effects of the Pits and Pit Size

According to the De Jong et al. (1983) model the excess attenuation over the single discontinuity between portions of ground with impedance Z_1 and Z_2, the source being over Z_1 (see Figure 43), is given by

$$EA = 20\log\left|\frac{P}{P_1}\right| \tag{3}$$

where

$$\begin{aligned}\frac{P}{P_1} &= 1+\frac{R_1}{R_2}Q_{1,2}\exp\left\{ik\left(R_2-R_1\right)\right\} \\ &+\left(Q_2-Q_1\right)\frac{\exp\left(\frac{-i\pi}{4}\right)}{\sqrt{\pi}}\frac{R_1}{R_3}\left\{F_{31}\pm F_{32}\exp\left\{ik\left(R_2-R_1\right)\right\}\right\}\end{aligned} \tag{4}$$

$Q_{1,2}$ is replaced by Q_1, the spherical wave reflection coefficient for the portion of the ground with impedance Z_1, and the plus sign in the curly brackets is used when the point of specular reflection falls on that portion of ground. Conversely $Q_{1,2}$ is replaced by Q_2, the spherical wave reflection coefficient for the portion of

the ground with impedance Z_2, and the minus sign in the curly brackets is used when the point of specular reflection falls on that portion of ground.

$$F_{31} \equiv F\left[\sqrt{k\left(R_3 - R_1\right)}\right] \tag{5}$$

and

$$F_{32} \equiv F\left[\sqrt{k\left(R_3 - R_2\right)}\right] \tag{6}$$

are Fresnel integrals, and the path lengths R_{i3} are defined in Figure 43.

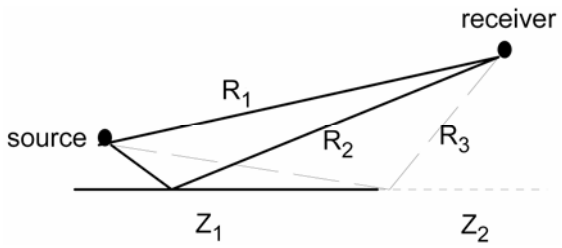

Figure 43. Definition of the various path lengths in the De Jong formula.

The impedance spectra used for the pits and the (unplowed) ground are the result of direct impedance fitting to short-range excess attenuation spectra and are shown in Figure 44.

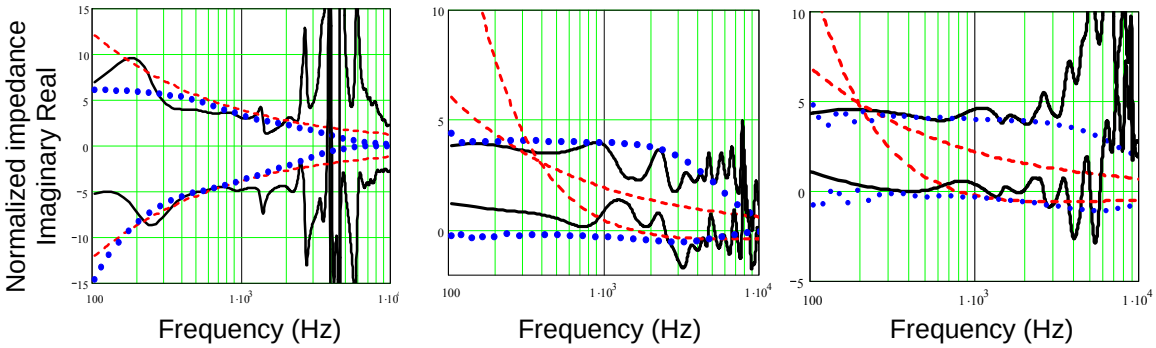

a. Ground b. Pit 1. c. Pit 2.

Figure 44. Impedance spectra used to describe pits and ground.

The predictions shown in Figures 45 and 46 are (a) for the source height at 2 m and the discontinuity at 2.6 and 9 m from the source and (b) for the source height at 1 m and the discontinuity at 2.6 and 9 m from the source.

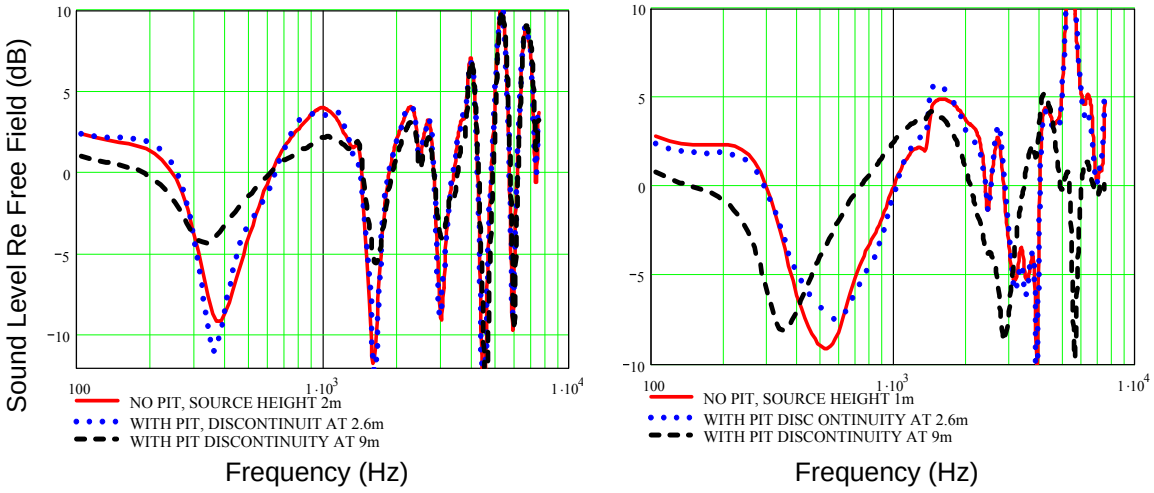

a. Source height 2 m. **b. Source height 1 m.**

Figure 45. Predicted excess attenuation spectra: source over Pit 1.

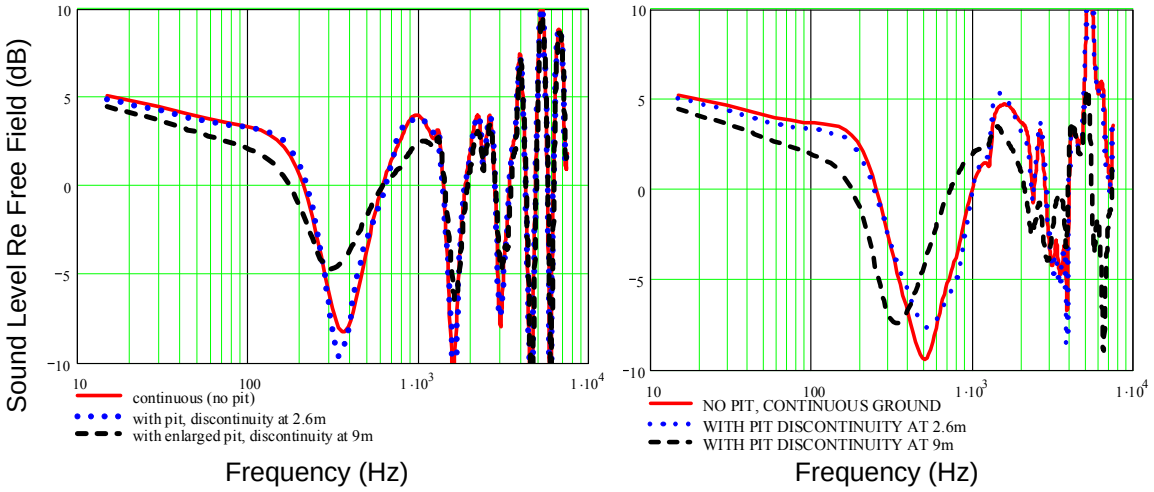

a. Source height 2 m. **b. Source height 1 m.**

Figure 46. Predicted excess attenuation spectra: source over Pit 2.

It is predicted that the influence of the 2.6-m-wide pits on the excess attenuation spectra at a 15-m range is small but is more noticeable when the source height is 1 m. With the discontinuity at 2.6 m, the main ground effect for Pit 1 is

predicted to be at a lower frequency than for Pit 2 and so should be more noticeable for a blast noise spectrum. Hypothetical extension of the pits to 9 m from the source is predicted to have a significant effect on the sound level at 15 m. Nonlinear FCT simulations (presented later in this report) support this conclusion.

Further Discussion of Test II Results

Conclusions drawn from the data analysis of Test II are that

- The plowed ground attenuates at all frequencies (but particularly in the 8- and 16-Hz octave bands at 50 m) out to 100 m, but
- At further distances the propagation is attenuated for frequencies above 100 Hz whereas the propagation is enhanced for frequencies below 100 Hz.

Previous research on the propagation of blast sound at distances up to 110 m has indicated that a snow-covered surface significantly reduces peak levels and energy levels and elongates waveforms compared with summer conditions (Albert 2002). Experiments with continuous broadband sound from a loudspeaker have shown that plowing reduces broad-band sound levels at short range (up to 50 m) compared with those at the same distances over unplowed ground (Attenborough et al. 2000). The latter finding can be understood in terms of the influence of plowing on the ground surface. First, the air permeability of the ground surface is increased (flow resistivity is reduced). Second, the surface is made rough; predictions and measurements have indicated that surface roughness that is small compared with the wavelength lowers the effective impedance of the ground surface (Boulanger et al. 1998, Attenborough and Waters-Fuller 2000).

The impedance spectra plots shown previously indicate that it is necessary to include roughness parameters to obtain good agreement with the impedance spectra. The plowed ground data are fitted by much lower flow resistivity values and larger roughness values than are required to fit the impedance spectra before plowing. Using the fitted impedance spectra for unplowed and plowed ground, calculations of sound levels with respect to the free field have been carried out for distances of 15, 50, and 250 m (Fig. 47). Classical linear models predict that the main effects of the change in ground impedance between unplowed and plowed ground are in the 250- and 500-Hz octave bands. These results are consistent with conclusion above. Also there is evidence in these linear predictions of a surface wave around 200 Hz at 250 m range before plowing which changes its main frequency content to near 100 Hz after plowing. However, this does not account completely for the observed change in the 16-Hz octave band.

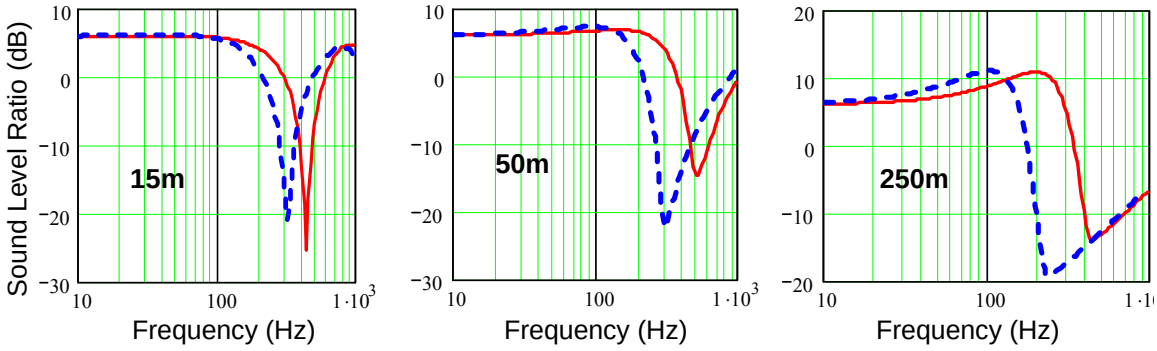

Figure 47. Predicted excess attenuation (sound level re free field) spectra at 15, 50, and 250 m using a linear propagation model.

During the tests reported here there was a fluctuating crosswind of between 1 and 3 m/s (Fig. 48a and b). There was a strongly upward-refracting temperature gradient between the ground and a height of 7 m (Fig. 48c). In the early afternoon the gradient was as much as 1°C/m. The mean RH during these tests was 70%.

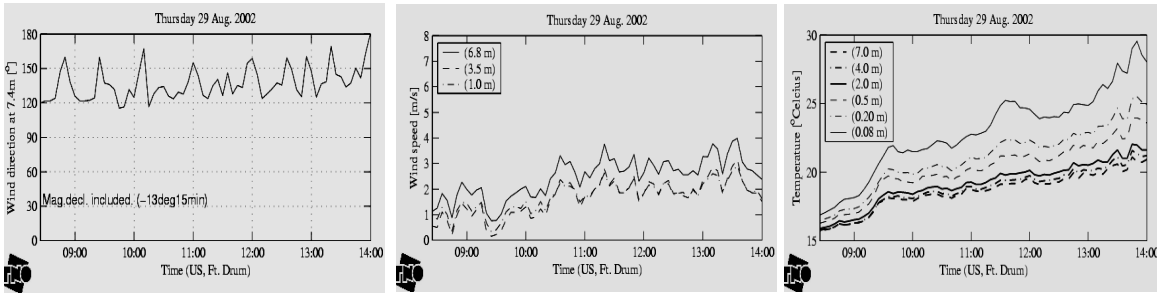

a. Wind direction [247.5° (WSW) is along the receiver line].

b. Wind speeds at three heights.

c. Temperatures at five heights.

Figure 48. Variation of meteorological conditions with time during the tests.

The effective speed of sound is a function of the temperature (T in kelvins):

$$c = 331.6 \times \sqrt{(273/T)} \text{ m/s.} \quad (7)$$

The effect of the temperature gradient is to alter the effective sound speed profile as a function of height. By using the measured temperature gradient, the speed of

sound as a function of the height z, can be described approximately with the following exponential function:

$$c(z) = c_0 + b\left(\left(\frac{z}{z_0}+1\right)^{\alpha} - 1\right);\ b = 3.67\ \text{m/s},\ \alpha \cong 0.595 \qquad (8)$$

with the roughness parameter $z_0 = 0.1$m.

Figure 49 shows the speed of sound as a function of the height and a number of rays traced according to this profile. When the effect of atmospheric turbulence is neglected, a shadow zone exists where no rays are present. Notice that the microphone at 100 m at 1.0 m is located in this shadow zone and that the one at a height of 5.0 m is not. At the 250-m range, both microphones (at 1- and 5-m heights) are predicted to be in the shadow zone.

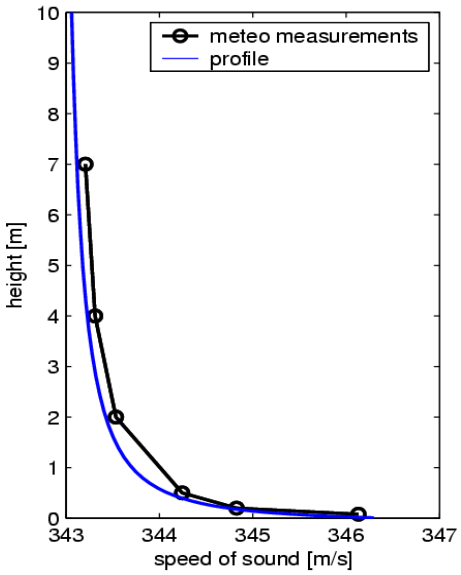

a. Measured temperature profile and logarithmic fit.

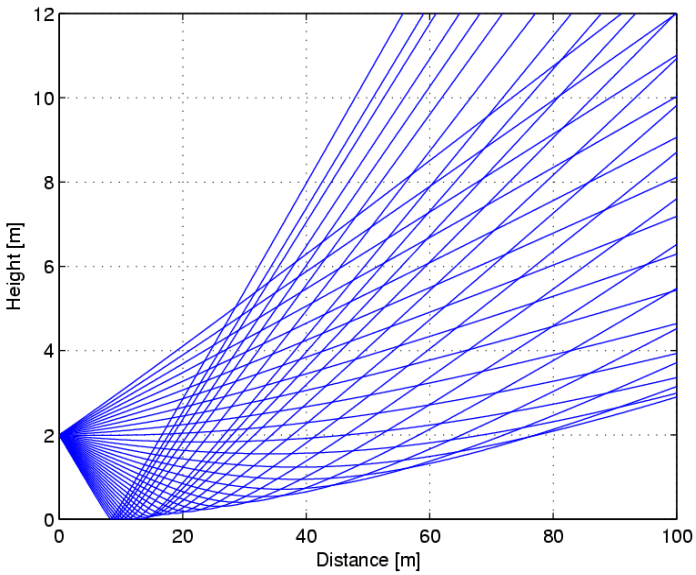

b. Ray trace for fitted logarithmic profile.

Figure 49. Speed of sound as a function of height, and effect of the temperature gradient on sound rays.

Residue series calculations (Li et al. 1998) for a broad-band source, assuming a bilinear sound speed versus height profile, have been used to investigate whether the strong upwardly refracting conditions can account for the transition between significant extra attenuation at 50 m and enhancement at 250 m over the plowed ground observed at 1-m-high receivers. Figure 50 indicates that they do not.

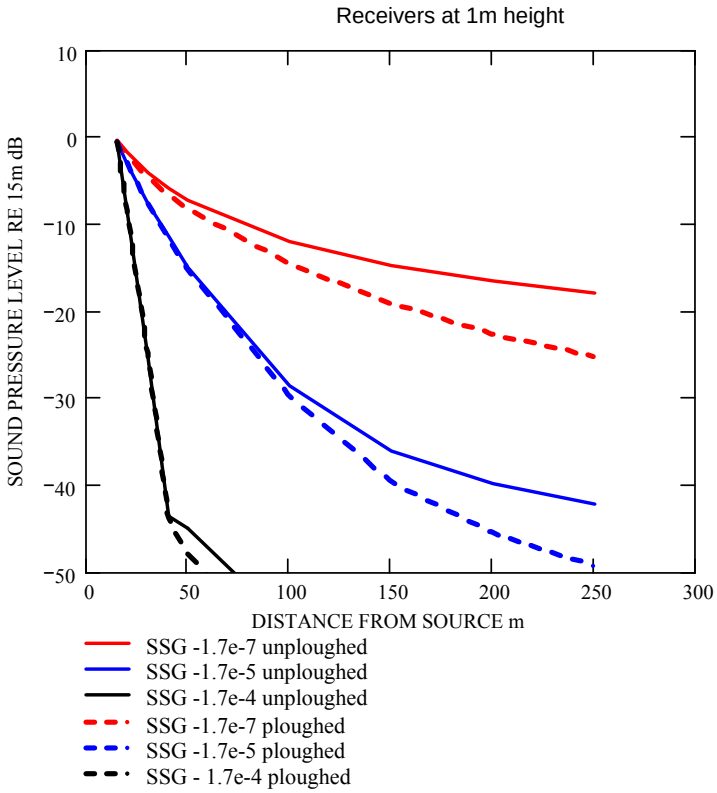

Figure 50. Residue series predictions of the sound levels relative to 15 m at 1-m-high receivers for three different effective sound speed profiles and for a broad-band source.

Figure 50 shows predictions of sound pressure levels relative to 15 m as a function of range before and after plowing. The measured energy levels over the unplowed ground correspond approximately to an effective linear sound speed gradient of -1.7×10^{-5} m/s m. The calculations suggest that the extra attenuation due to plowing should continue to increase with distance.

It is particularly interesting to investigate the waveforms above the plowed ground area. Figure 51 displays the time signals at 50 and 250 m at 1.0 m high. On one hand, the peak of the blast wave at 50 m is largely reduced due to plowing. On the other hand, the positive pressure duration has increased at 250 m. This is due to an elongation of the positive phase above the porous ploughed area. A similar result was seen for sound propagation over porous snow. The interaction with the porous ground has a smoothing effect on the waveform, i.e. the "sharpness" of the waveform is reduced. Also note the evidence of "slow" wave arrival, i.e. the small amplitude oscillation in the "tail" of the waveform, at the 250-m range and the 1-m height above the plowed area.

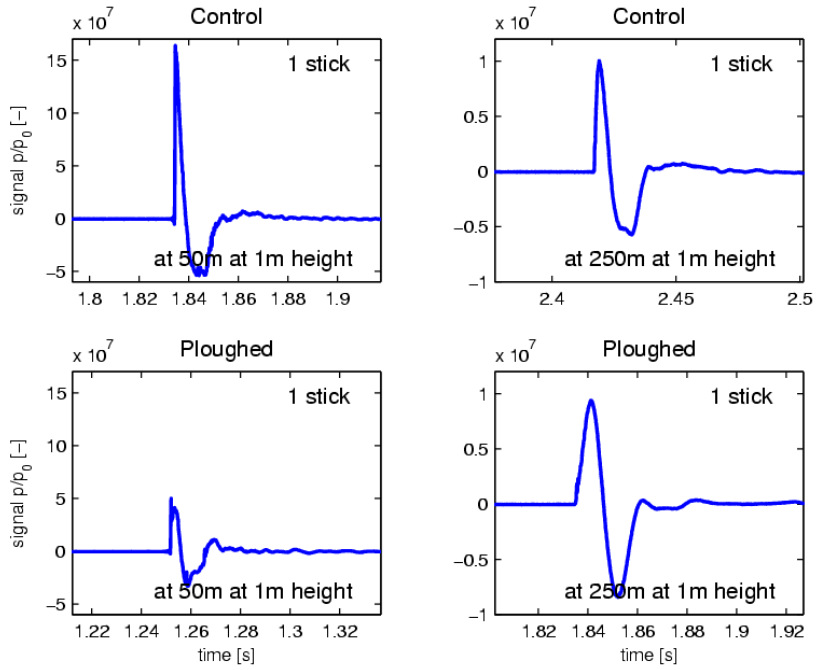

Figure 51. Pressure–time signals at 1.0 m high. The upper two graphs are for the reference site; the lower two are for the ploughed site, all for one stick.

A possible explanation for the observed results may be the influence of acoustic-to-seismic coupling. Figure 52 shows data for the ratio of blast sound pressures to vertical particle velocities measured above and just below the surface during long-range trials in Norway (Attenborough et al. 2002). Also shown are calculations for propagation from a point source that take ground elasticity, porosity, and layering into account (Tooms et al. 1993). The clear reduction in the ratio of pressure to velocity observed and predicted between 1 and 10 Hz may be associated with the formation of an air-coupled Rayleigh wave. The effect is determined largely by the seismic wave profile within the ground and the near-surface layering. In the case of the Ft. Drum trial, the effect of plowing may have been to increase the degree of acoustic-to-seismic coupling. At close range this would have the effect of reducing the sound energy above the surface. However, it could also lead to the formation of an air-coupled Rayleigh wave, which would carry low-frequency energy at longer ranges and result in an enhancement compared with the unplowed surface.

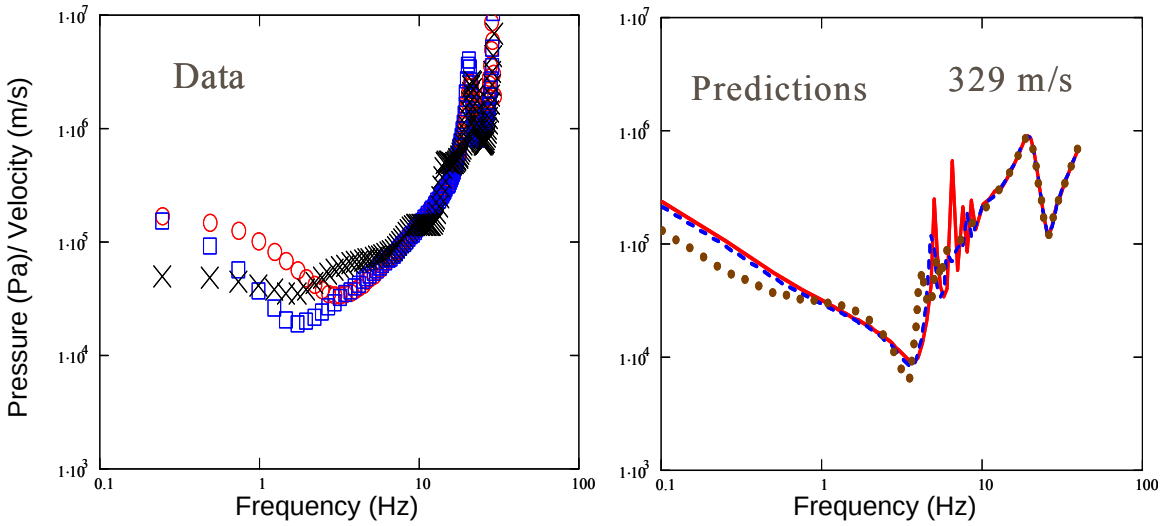

Figure 52. Acoustic-seismic coupling ratios deduced from measurements and predicted by FFLAGS at ranges of 6300 m (circles and solid line), 7200 m (boxes and broken line), and 12600 m (crosses and dotted line) assuming a sound speed in air of 329 m/s.

Test of FCT code

Calculations at the pit

This part compares the FCT code predictions of shock waves over a porous area with Test I measurements for the control site and Pit 2. Previous work has been reported on the Flux Corrected Transport method for solving the flow equations in open air and porous materials (Védy 2002b). The FCT technique is now used to predict the propagation of the shock wave over a relatively small porous area. The three-dimensional sound propagation over the porous surface can be described with a rectangular grid for the FCT code with the use of spherical coordinates. Pressure–time histories of the measurements are compared to the FCT results for distances of 2.6 and 15 m from the source. Also, numerical data for an enlarged pit are presented to indicate further mitigation effects.

Figure 53 shows the geometry used for the measurements for Pit 2.

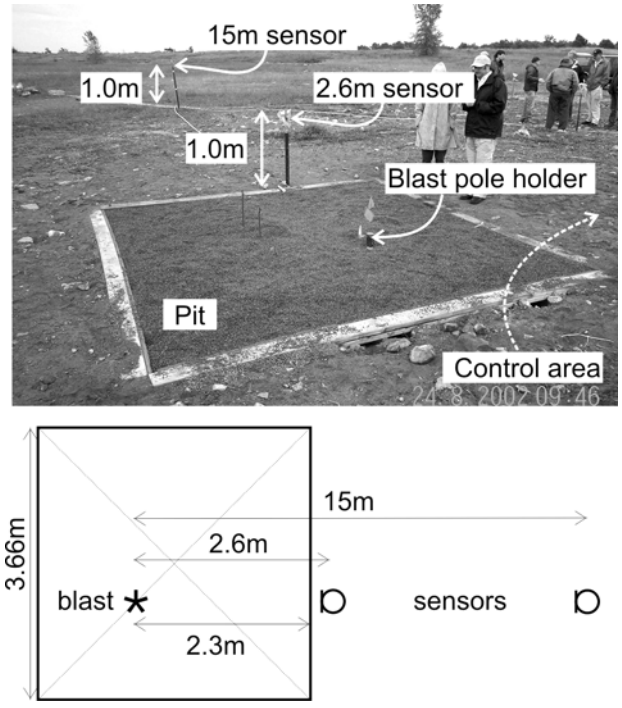

Figure 53. Measurement set-up for C4 explosives above Pit 2.

Figure 54 shows the geometry for the numerical FCT method. As cylindrical symmetry is assumed, the calculation is in principle valid for a cylindrical pit. It is expected that this geometry resembles the measurement set-up well, as the same vertical planes are considered.

For the pit the flow resistivity was measured at the site and was found to be 850 kPa s/m^2, with a porosity of 0.4 and a tortuosity of 1.5. The tortuosity had been set to 1.0 for the FCT method, though, as it corresponds better with the expected results. The Forchheimer non-linearity parameter was determined under laboratory conditions and was found to be 5.26 s/m. For the control area and the area beyond the pit, an acoustically rigid boundary condition was used.

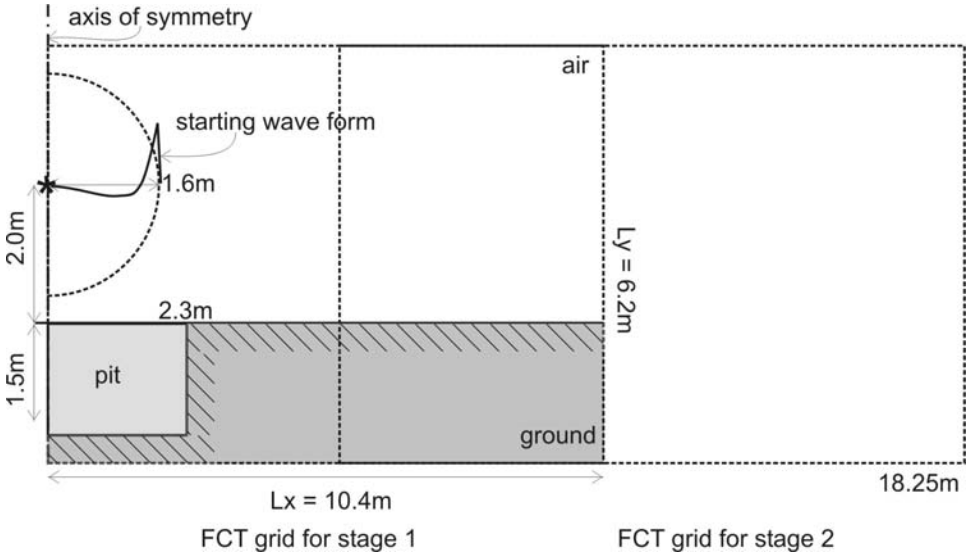

Figure 54. Numerical set-up for the FCT method. Stage 2: 4.99 to 18.25 m.

As a first step (stage 0), the initial conditions for the starting waveform, up to 1.6 m from the source origin, have to be determined. This is done by calculating the waveform up to 2.6 m in the free field and comparing these results at 2.6 m to the measurements. The FCT results at 2.6 m are obtained with an efficient one-dimensional method with spherical coordinates, where analytical distributions for the pressure, velocity, and density are used as starting conditions. For all the calculations, the starting pressure follows a Gaussian distribution. For the eighth-stick case, the maximum pressure is set to 27 GPa, while it is 147 GPa for the half-stick case. In both cases the Gaussian width is set to 2.5 mm, the velocity is set to zero, and the density is deduced from the pressure, assuming an adiabatic relation and a perfect gas law. These settings produce pressure pulses at 2.6 m, which are comparable, in terms of amplitude and positive phase durations, to the measurements.

For stage 1 a two-dimensional grid was used with a length of Lx = 10.4 m and a height of Ly = 6.2 m (number of grid points: Nx = 520, Ny = 310). The flow variables, pressure, density and velocity, are initialized using analytical distributions according to the results given with the one-dimensional simulations performed during stage 0. The grid for stage 2 starts at 5.0 m (Lx = 13.4 m, Nx = 670). For the Control site a similar grid was used, with Ly = 4.2 m and Ny = 210. At the top of the grid and at the right side a non-reflection boundary condition is used.

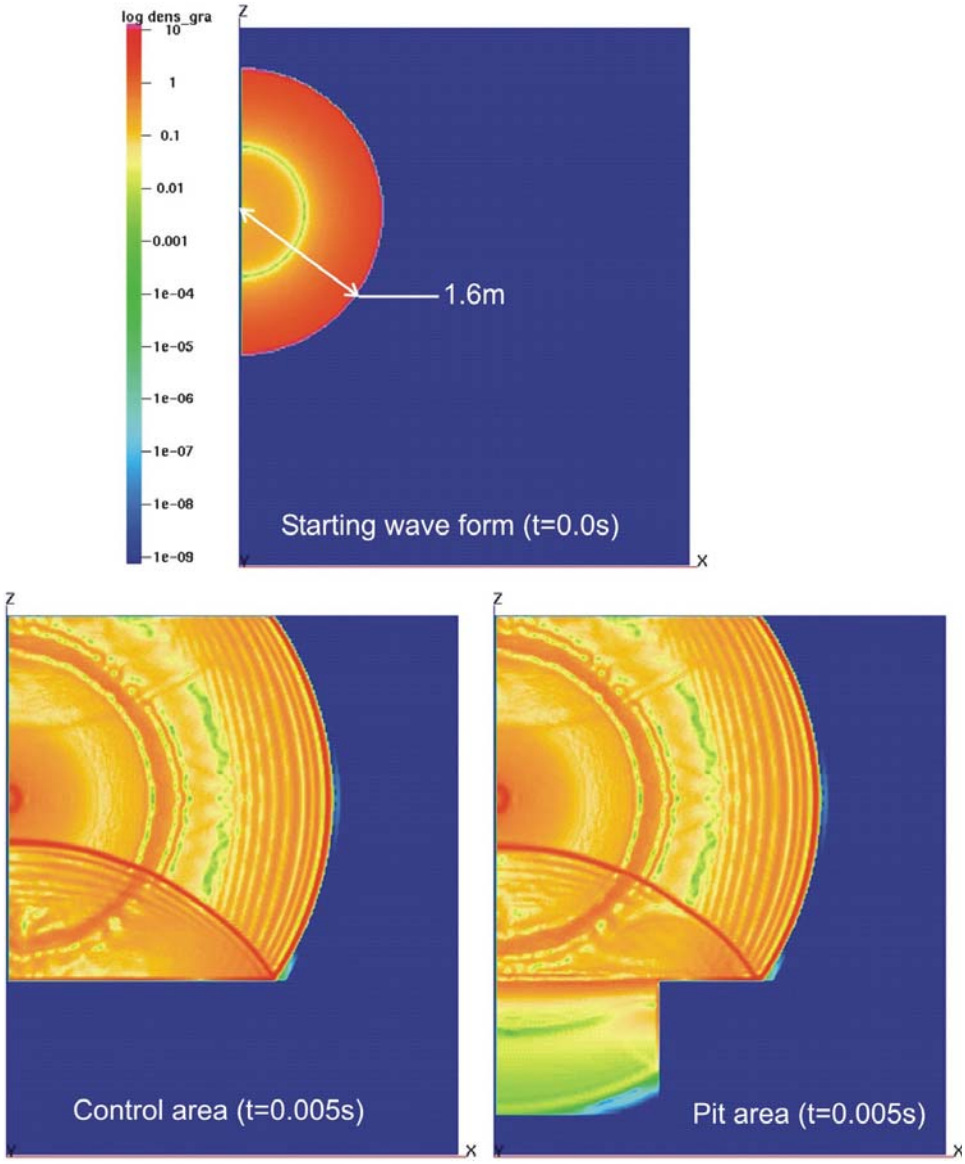

Figure 55. Density gradient calculated with the FCT code. The top image shows the starting condition, with a source at a height of 2.0 m at time t = 0.0 s. The bottom left image shows the shock wave above a rigid surface. The bottom right image shows the shock wave above absorbing Pit 2.

It is illustrative to show the density gradient above the control area and the pit at 5.0 ms from the starting condition, as determined in stage 0, which is set to t = 0.0 s for stage 1 (Fig. 55).

Pressure Perturbations at 2.6-m Distance

Here, pressure perturbations will be shown with respect to the ambient pressure of 101325 Pa, at the sensor positions at a height of 1.0 m. The direct and reflected waves are separate in time at 2.6-m distance. Figure 56 shows the FCT results and the results of three measurements for the eighth-stick size for the control area as well as for Pit 2.

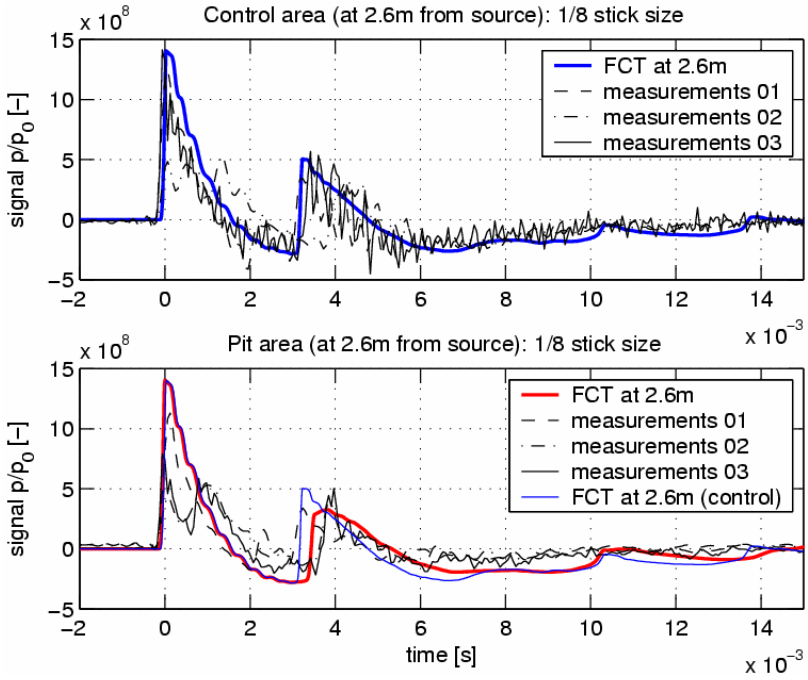

Figure 56. Comparison of numerical and measured pressure–time histories for the eighth-stick size at 2.6-m distance. The upper graph shows the control data, while the lower graph shows Pit 2 data. The first peak of the normalized pressures (p_o = 20 µPa) has been shifted in time and set to zero for comparison. The microphone height is 1.0 m.

The arrival times of the direct waves have been set to zero. A good resemblance of the numerical and measured results can be seen. The starting condition for FCT was set so that a good resemblance with the direct wave measurement for series 01 ("measurements 01") was obtained. Measurements "01" have the highest peak level.

The reduction of the peak pressure for the reflected wave due to the pit is more pronounced for the FCT results, although the measurements show a high degree of scatter.

For the control area the arrival time of the reflected wave shows good agreement with the measurements. With a pit the arrival times for both measurements and FCT results are later for the reflected wave, compared to the control area, due to a reflection inside the pit.

Figure 57 shows similar results, but now for the half-stick charge. The results of the measured direct wave "03" have been used to create a starting condition for the FCT method. Compared to the other measurements, this peak level is rather high, so the FCT results are structurally higher, compared to the other measurements. The reproducibility of the measurements is much better than for the eighth-stick size.

The resemblance between numerical and measured results is fair. The FCT method predicts a smaller peak of the reflected wave for the control area. For these higher levels, this may be due to the numerical damping. A similar effect is seen for the porous area. Nevertheless, for the porous area the FCT method predicts a similar reduction of the peak amplitude as for the measurements.

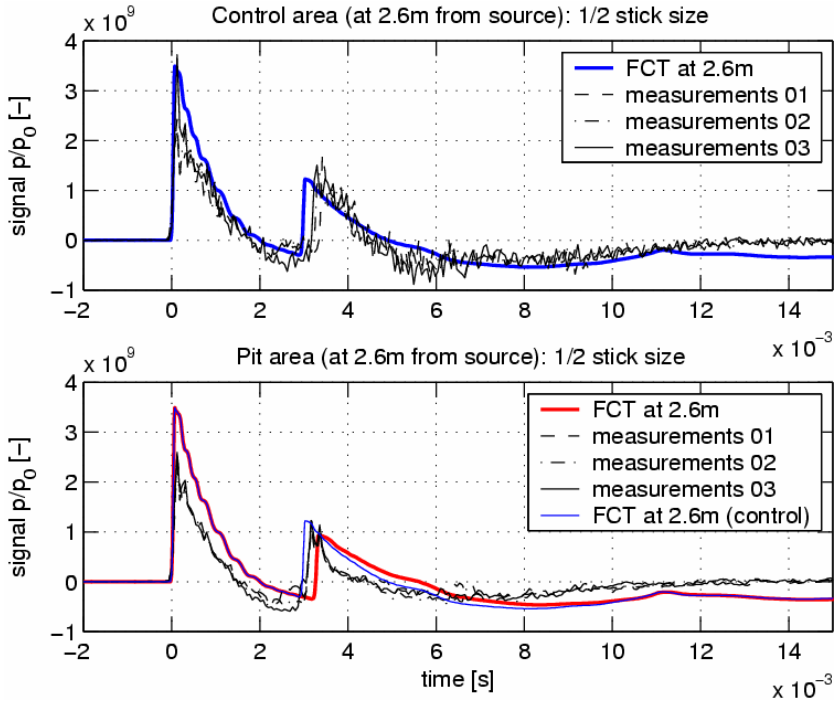

Figure 57. Comparison of numerical and measured pressure–time histories for the half-stick size at 2.6-m distance. The upper graph shows the control data, while the lower shows the Pit 2 data. The first peak of the normalized pressures (p_o = 20 µPa) has been shifted in time and set to zero for comparison. The microphone height is 1.0 m.

Pressure Perturbations at 15-m Distance

Figures 58 and 59 show the pressure–time histories at 15-m distance from the source. The FCT code results are shown as well as the three measurement series as used in the previous section. For the eighth-stick size a good resemblance is obtained. The effect of the pit is negligible at this distance due the small size of the pit. The measurements show some scatter for this charge size. This may be due to an explosion of the charge in two stages, because at this distance the arrival times of the direct and reflected wave should be indistinguishable.

The negative phase of the waveform is shorter for the results of FCT method than for the measurements. However, for the half-stick size it is larger. It is expected that a finer-tuned starting condition can improve the difference.

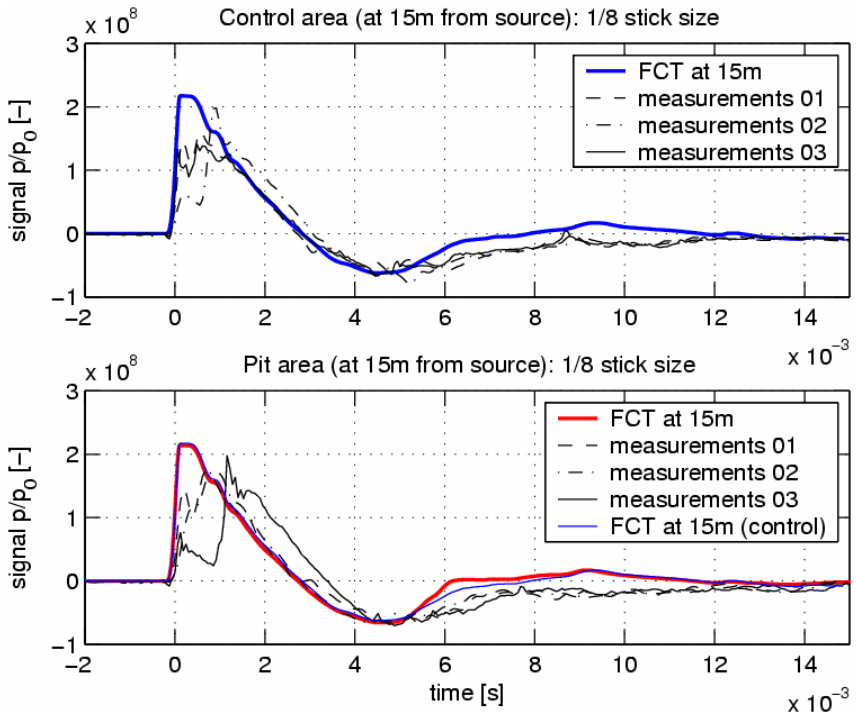

Figure 58. Comparison of numerical and measured pressure–time histories for the eighth-stick size at 15-m distance. The upper graph shows the control data, while the lower graph shows the Pit 2 data. The first peak of the normalized pressures (p_o = 20 µPa) has been shifted in time and set to zero for comparison. The microphone height is 1.0 m.

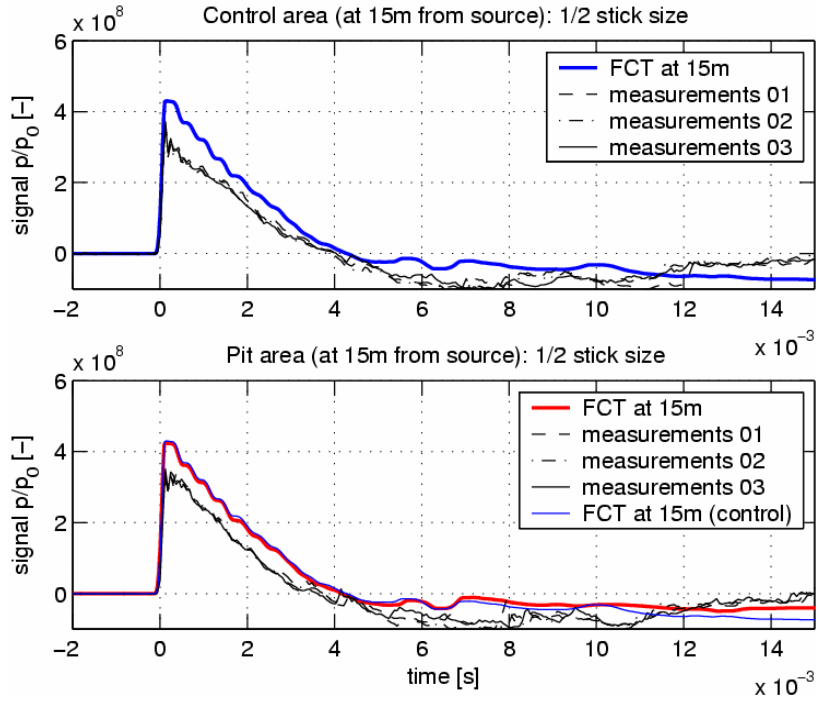

Figure 59. Comparison of numerical and measured pressure–time histories for the half-stick size at 15-m distance. The upper graph shows the control data, while the lower graph shows the Pit 2 data. The first peak of the normalized pressures (p_o = 20 µPa) has been shifted in time and set to zero for comparison. The microphone height is 1.0 m.

For the half-stick size it was explained in the previous section that the overestimation of the pressure is due to too high a starting condition for the FCT method. For this charge size the waveform of the measurements corresponds well to the expected waveform. The numerical waveform resembles the measurements fairly well.

Effect of an Enlarged Pit

It was shown that the FCT method can predict shock waves traveling over a porous area well. In this section the calculated effect of an enlarged pit is shown. For the FCT method an axisymmetric two-dimensional coordinate system was used, so the surface of the pit is in fact circular. Figure 60 depicts the waveforms at 15 m for three pit sizes: radii of 2.3, 4.5, and 9 m. Also, the source is at 2.0-m height, and the receiver is at 1.0-m height.

As expected, the sound pressure decreases for increasing pit size. The sound exposure level (unweighted), as mostly used for impulse sound, is defined as:

$$L_X = 10\log\frac{1}{T_0}\int_{-\infty}^{+\infty}\frac{p(t)^2}{p_0^{\,2}}\mathrm{d}t \qquad T_0 = 1.0\ \mathrm{s};\ p_0 = 20\ \mu\mathrm{Pa}. \tag{9}$$

Table 12 lists the L_X values for the eighth- and half-stick sizes. A rectangular time window of 6 ms has been used for the shock waves. For the half-stick size, only the energy of the positive phase of the shock wave has been taken into account. This was done because the wake of the shock wave is not well predicted with FCT yet. Also, C-weighted values are given, as well as the sound reduction with respect to the control site.

Table 12. Sound exposure levels of the shock wave for different pit radii and reduction with respect to control site. A rectangular time window of 6 ms has been applied for the shock waves.

Pit radius (m)	1/8-stick size			1/2-stick size		
	LX [dB]	LX(C)	Reduction [dB(C)]	LX	LX(C)	Reduction [dB(C)]
0.0	137.4	137.0		143.5	142.4	
2.3	137.2	136.8	0.1	143.3	142.3	0.1
4.5	136.2	135.7	1.3	142.9	141.8	0.6
9.0	133.4	132.6	4.4	141.3	140.0	2.4

Table 12 shows that 4.4 dB(C) can be gained by using a porous surface of 9-m radius under the source for the eighth-stick size. For half-stick size the reduction is 2.4 dB(C). There is extra energy present in the negative phase of the waveform. Snapshots of the pressure field show that the pressure does not come to rest after the shock wave. This effect stems from the starting condition. It is expected that fine tuning the wake of the shock wave for the starting condition can prevent this.

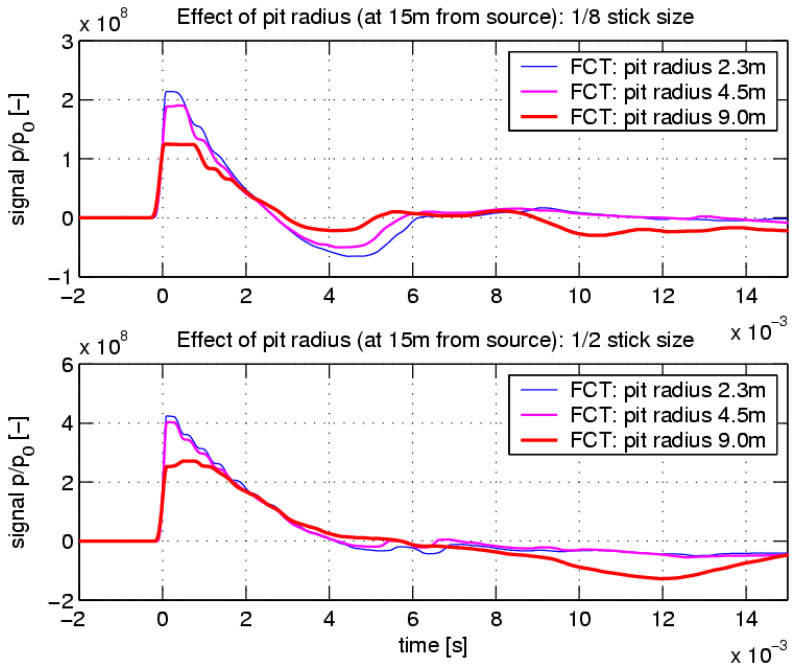

Figure 60. Calculated pressure–time histories for three pit sizes. Upper: eighth-stick size. Lower: half-stick size. Normalized pressure (p_o = 20 μPa) at 15 m from the source. The source was at a height of 2 m. The receiver was at a height of 1 m.

Conclusions

A means to mitigate shock waves, via a porous surface directly beneath the source, has been investigated experimentally and numerically. The results predicted with the FCT method agreed well with the measurements. The FCT method uses axisymmetric two-dimensional coordinates and was used up to 15 m from the source in two stages. To start the calculation, a starting condition has to be found. The starting waveform was chosen to be a 1.6-m length and such that the peak level and positive phase duration matched the measured direct wave at 2.6 m from the source.

The initial relatively small size of the porous surface, i.e. with a radius of 2.3 m, has been extended numerically to a radius of 9 m. The FCT method predicts a considerable reduction of the peak pressure at 15-m distance. However, the wake of the waveform requires further investigation.

Test of Coupling of FCT with NPE and PE

In this part two techniques are demonstrated:

- Coupling of FCT results to the NPE method (non-linear PE), and
- Coupling of NPE results to the PE method.

The FCT code uses multi-dimensional Euler equations. For this test a rectangular grid and axisymmetrical coordinates are used. As a result absolute pressure, velocity, and density data on a rectangular grid are available. For the NPE code a similar rectangular grid can be used because it uses the same axisymmetrical coordinates. The NPE method is based on a single equation for the pressure perturbation for shock waves that are not too strong (less than 10 kPa). Furthermore, NPE has a small angle approximation for the propagation so that shock waves can be described at angles smaller than 10º with respect to the horizontal axis. Atmospheric refraction and sound absorption can be taken into account. The NPE code is suitable for moderate distances from the source, typically hundreds of meters. Further, NPE uses a moving frame that propagates with a time-step dt.

When the pressure amplitude of the shock wave is below 1 kPa, the linear PE method can be applied. The PE, or parabolic equation, is based on the linear wave equation in the frequency domain. As a consequence, the shock wave, described in the time domain with NPE, needs to be transformed to the frequency domain. This transformation is performed as a function of the height. As for the NPE method, the PE method takes into account atmospheric refraction and sound absorption.

Figure 61 shows a schematic overview of the sequential methods.

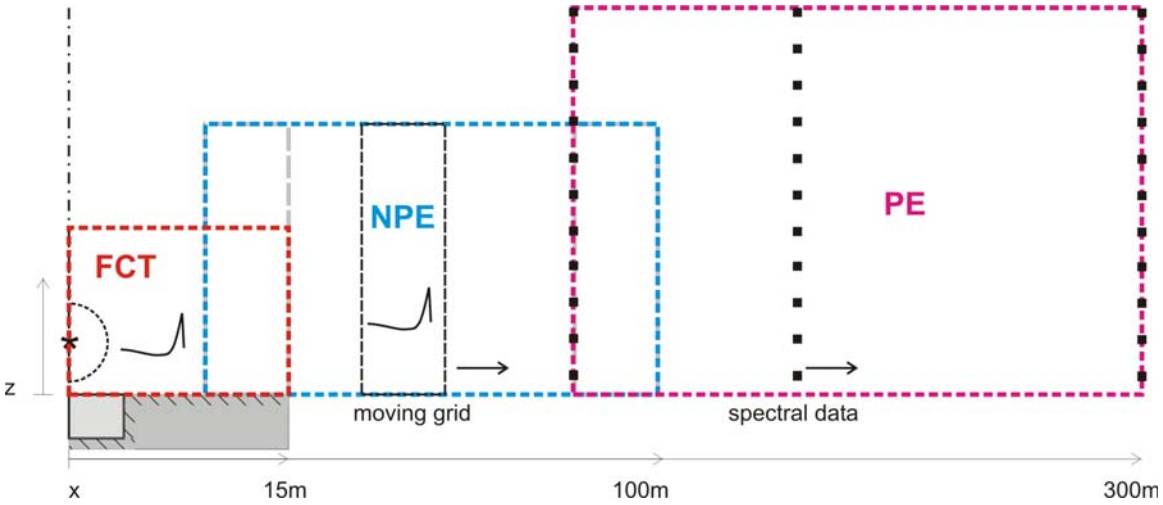

Figure 61. Schematic overview of coupling of FCT with NPE and PE.

Coupling FCT and NPE

Figure 62 shows snapshots of the pressure as calculated with the FCT-code. At time t = 0 s a starting pressure/velocity/density field with a radius of 1.6 m and a source height of 2.0 m was used. The ground was assumed to be rigid. For this case the starting condition for eighth-stick size was used. The atypical wake of the waveform at 2-m height (lower right figure) is due to this starting condition.

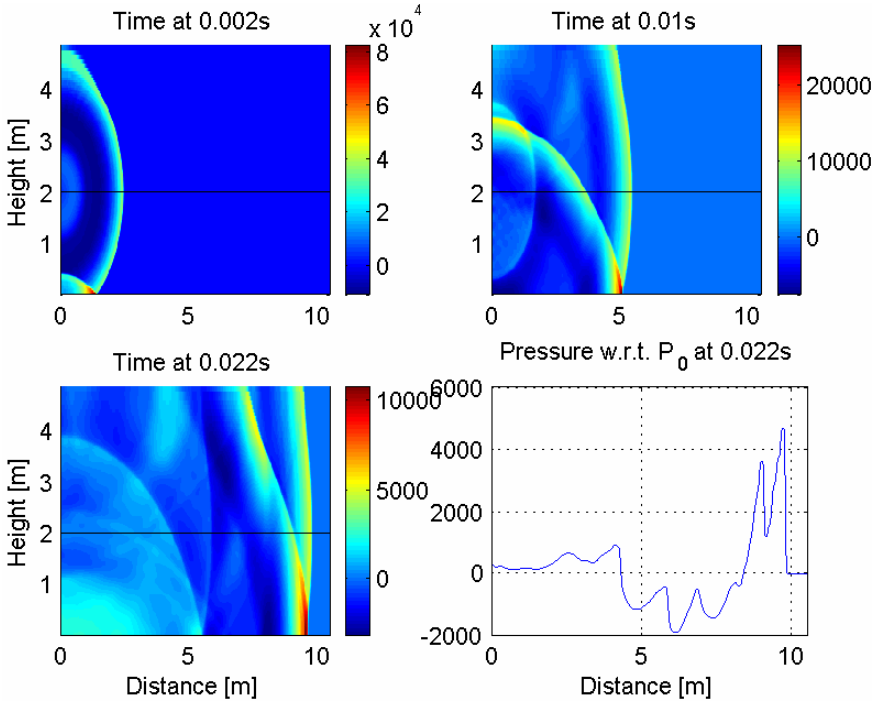

Figure 62. Three snapshots of the pressure as a function of height and distance, calculated with the FCT code. The lower right figure depicts the pressure at time t = 0.022 s from the start at a height of 2 m.

For the NPE code, which uses a larger grid as well as a coarser grid, a section of the FCT results for the pressure is used as a starting condition. To this end the FCT pressure field is interpolated onto the grid as used for the NPE code. Figure 63 shows the pressure field for the NPE code as well as the pressure–time history at 2-m height. For this test case a relative small width of the moving grid is used for the NPE code, i.e. a part of the wake of the wavelength as calculated with FCT is neglected.

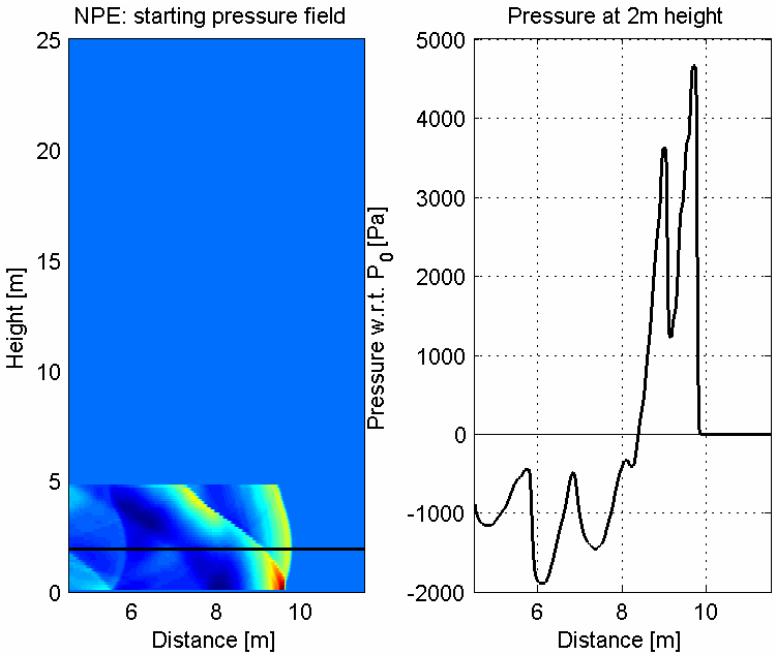

Figure 63. Starting pressure for the NPE code as a function of height and distance.

For the NPE code a grid spacing of dx = 0.25 m and dz = 0.125 m was used, with a horizontal x-coordinate and a vertical z-coordinate. The speed of sound was set to 340 m/s, and a time step of dt = 0.3 ms was used.

Figures 64 and 65 show the NPE results at 25 and 100 m, respectively. At 25 m, pressure information has entered higher regions (above 5 m). However, due to the narrow angle approximation of NPE, these pressures are not yet accurate. At 100-m distance, and using a maximum angle of 10º and an image source at –2 m, pressures up to 15 m can be used for further analysis. Also, to suppress reflections from the top of the grid, a numerical absorbing layer between 15 and 25 m was used.

The right-hand side of the figures shows the pressure at 2-m height. Besides the non-linear results, the linear and free-field pressures are shown as well. When the non-linear wave is compared to the linear one, the typical increase in the positive phase duration for the non-linear wave can be seen as well as an increased speed of sound. Salomons (2000) showed that NPE results are accurate up to 200 m for a free-field situation.

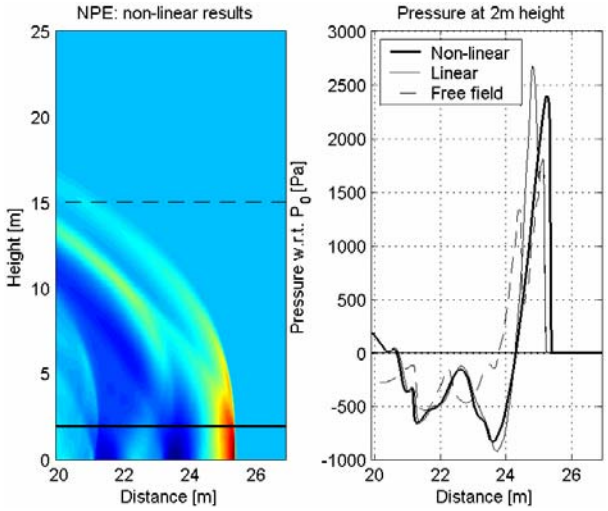

Figure 64. NPE results at 25 m from the source.

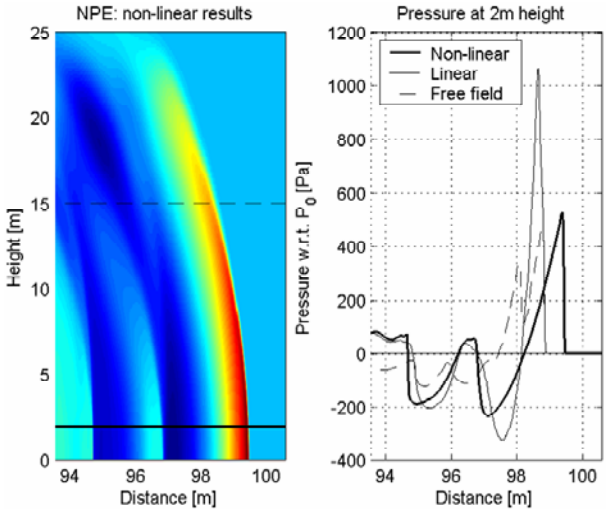

Figure 65. NPE results at 100 m from the source.

Coupling NPE and PE

For testing purposes a pressure–time history for NPE was chosen as shown in Figure 66. The bottom left graph shows the free-field pressure–time history at 2-m height. The bottom right graph shows the pressure as a summation of the free-field pressure and the reflected pressure as a function of height. With these calculated starting conditions, the linear excess attenuation can be calculated analytically, so that the linear NPE results as well as PE results can be compared to a

simple analytical two-ray solution. A rigid ground was assumed. The grid spacing and time step for NPE are dx = 0.25 m, dz = 0.125 m, and dt = 0.3 ms.

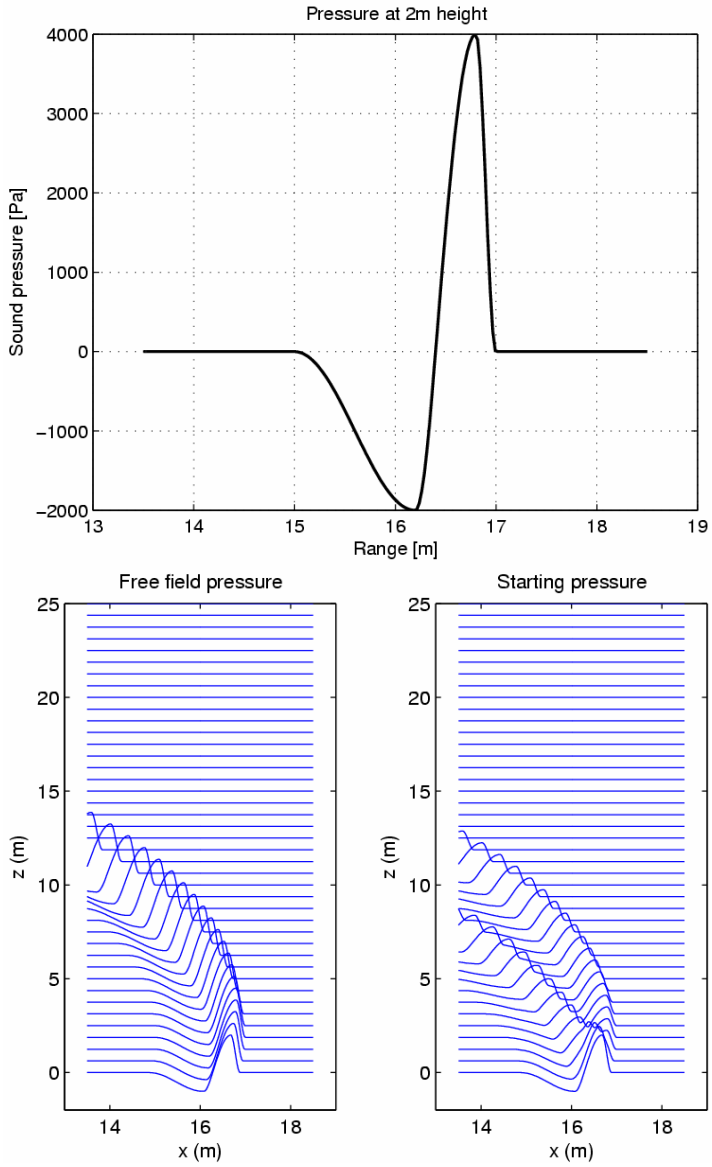

Figure 66. NPE results for a given pressure–time history. The bottom left graph shows the free-field starting pressure at 15-m distance from the source at 2-m height. The source was at 2-m height. The bottom right graph shows the free-field pressure–time histories as a function of height and histories with a reflected wave included.

The NPE calculations started at 15-m distance from the source. By using the NPE code up to 100 m from the source, the non-linear, linear, and free-field pres-

sures are obtained (Fig. 67). The upper graph shows the pressure–time history for a receiver at 100 m. The lower graph shows the sound exposure levels as a function of frequency. The initial wavelength of the shock wave was set to 2 m, so the peak level for the linear propagating wave lies near 170 Hz.

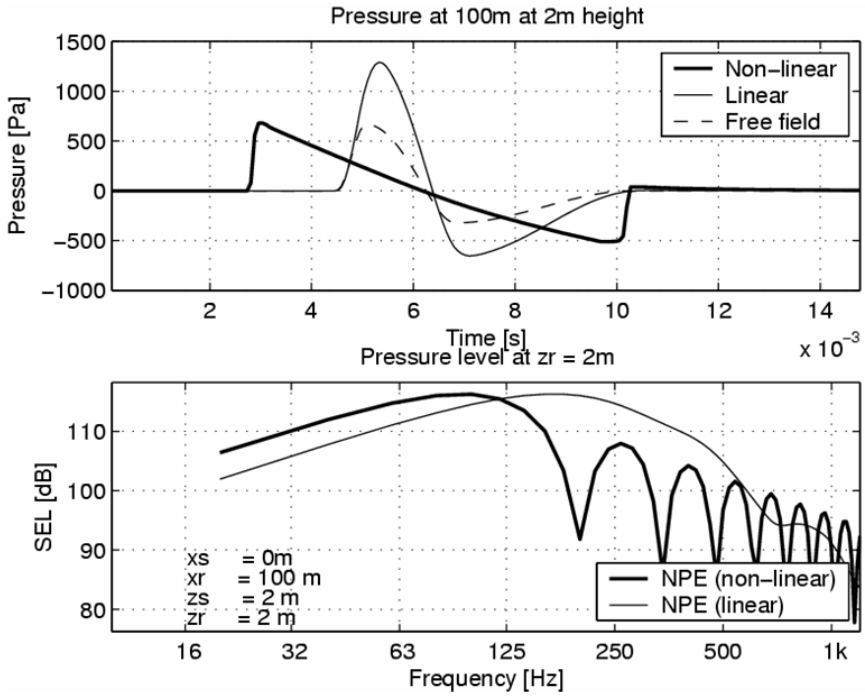

Figure 67. NPE results at 100 m for non-linear propagation above a rigid ground, linear propagation above a rigid ground, and linear free-field propagation. The upper graph shows the pressure–time history. The lower graph shows the spectrum (linear frequency spacing of 20 Hz).

The linear excess attenuation at 100-m distance is shown in Figure 68 for three heights: 2, 5, and 10 m. These linear results compare well with analytical ones, although for frequencies above 500 Hz the energy content of the shock wave is much lower, so deviations occur. The slightly lower results for NPE at 10-m height are due to the small angle approximation.

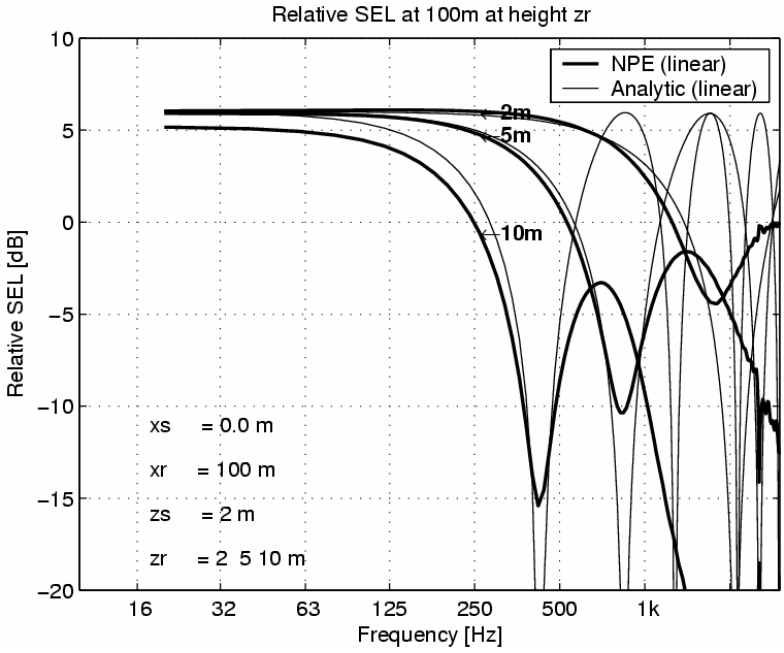

Figure 68. Comparison of the linear excess attenuation for NPE and an analytical two-ray model. The source was at 0 m at a height of 2 m. The receiver at 100 m at heights of 2, 5, and 10 m.

The sound level as a function of frequency and height, calculated with NPE at 100 m, is used as a starting condition for PE. A Fourier transform of the time data as shown in Figure 67 results in a complex spectrum. In this way phase information of the wave is preserved, and the interaction of direct and reflected waves is described accurately. The existing vertical grid spacing dz imposes an upper boundary for the frequency in PE (about six grid points per wavelength). In this case dz = 0.125 and PE results are accurate up to 500 Hz. Alternatively, vertical interpolation can be used to increase this frequency.

Figure 69 shows the unweighted sound exposure level at 300 m at heights of 2, 5, and 10 m. These PE results compare well with the analytical results. However, the accuracy can be increased as shown in Figure 70. For NPE a lower height for the grid is required than for PE (50 and 150 m, respectively), due to the shorter distances for NPE (Fig. 61). No pressure information is available for the upper region of the PE grid, and these spectra are set to zero. As a result, numerical noise is introduced. When a new arbitrary starting condition is used at 100 m for the complete height of the PE grid, then the noise is largely reduced at 300 m. Due the linear relations, the obtained amplitude and phase information, calculated with PE at 300 m, can be added to the NPE results at 100 m to get the results at 300 m.

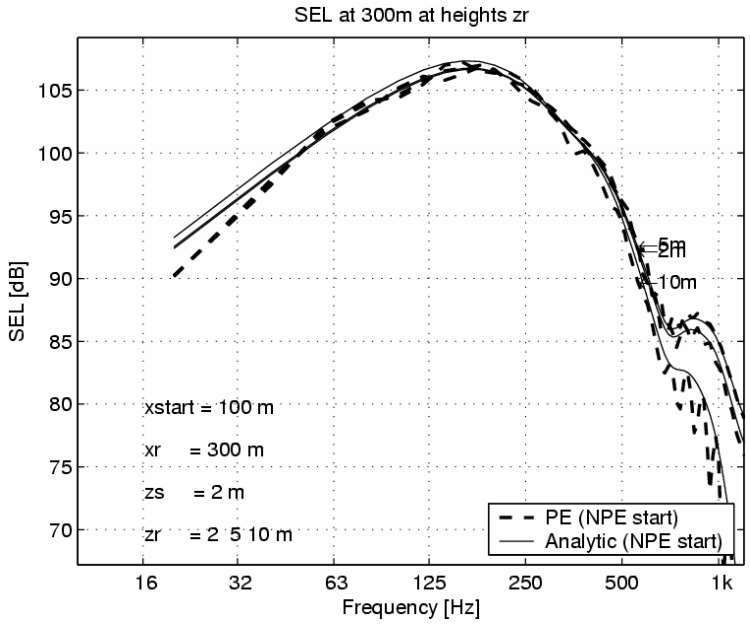

Figure 69. Linear sound exposure level at 300-m distance from the source, with the NPE start at 100 m for a maximum height of the NPE grid.

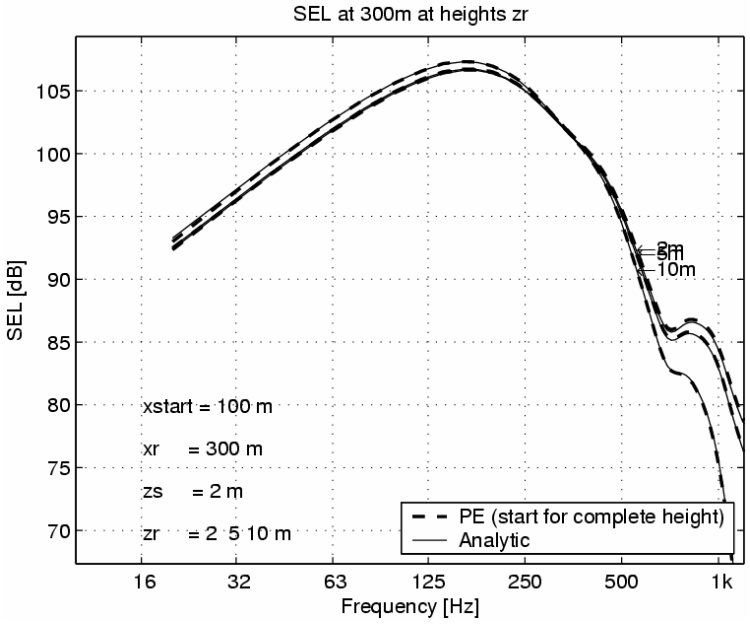

Figure 70. Linear sound exposure level at 300-m distance from the source, with the start at 100 m with maximum height as used for PE grid.

Discussion

The coupling of the FCT method and the NPE method has been demonstrated to work. With the NPE code, shock waves can be calculated up to moderate distances. Refraction and air absorption can be included.

As Test II included a ploughed area up to 250 m, it is recommended that sound absorption for the ground be included in NPE. In NPE the flow resistivity and porosity can be included for the ground as an additional boundary condition at the air–ground interface. The ground is then also included in the code. However, no satisfactory results have been found yet.

The coupling of the NPE method and the PE method has also been demonstrated to work. When the amplitude of the shock wave has decreased to a linear level, as calculated with the NPE code, the shock wave is transformed to the frequency domain as a function of height. These complex spectra are then used in PE for further propagation of the wave up to several hundreds of meters. Again, refraction and dissipation can be taken into account, as well as a complex acoustic impedance boundary condition for, for instance, a soil with heather or grass.

6 CONCLUSIONS AND RECOMMENDATIONS

Conclusions

The principle that blast source absorbers can be designed has been realized and validated.

Analytical methods have been developed to calculate the surface impedance of multiple-layered rigid porous materials in the presence of high-amplitude (non-linear) acoustic excitation.

The principle of reducing blast source sound by means of granular absorbers has been demonstrated.

A code (FCT code) has been formulated to describe the propagation of a blast shock wave at short distances from the source (typical 1–15 m). It is based on the non-linear version of the Euler equations.

An approach for calculating starting conditions for this FCT code for muzzle blasts has been developed. Calculations made using this code correspond well with results found in the literature.

The FCT code has been coupled to two other models (NPE and PE) in order to predict sound levels at larger distance (including meteorological effects).

The FCT code has been used to describe the non-linear theory for rigid porous materials (Forchheimer non-linearity). The use of the FCT code has been validated by measurements performed with high explosives.

Several approaches were investigated for using the NPE code to account for the interaction of a blast shock wave with absorbing rigid-porous materials. However, the accuracy of the calculated results remains insufficient.

A field test was conducted at Ft. Drum, NY, USA, and it demonstrated the following results:

- Measured absorption in pits agrees with theory (40 dB loss at 1 m into the material).
- Reflections at Pit 2 (measured at 2.6 m) agrees with plane wave theory.
- Waveforms are predicted reasonably well by the FCT method.
- Pit 2 (2.6 m and maybe 0 m) gives good absorption between 8 and 500 Hz.
- There is a small reduction from Pit 1 at 15 and 250 m.
- FCT calculations give an indication that a larger pit will yield greater absorption.

- The quarter-stick data indicate that a shorter distance between the blast source and the absorbing surface leads to a greater absorption. The plowed field test yielded a noticeable effect. The main absorption occurs at short distances (up to 50 m) and occurs even below 100 Hz. Absorption occurs at 250 m at the higher frequencies (over 100 Hz).

Recommendations

Blast Sound Attenuation at the Source

The basic ability to design and optimize blast source sound-absorbing surfaces has been developed, and it is recommended that research be conducted to provide requisite proof of concept and breadboard validation. The possible steps in such research might include:

- Optimizing materials and geometry for a given source. Here it is recommended that the FCT code and the analytical methods be refined and extended to optimize the size, shape, extent, and material make-up of absorbing surfaces. For practical configurations, such topics as starting conditions and muzzle brake effects must be considered.
- Optimizing the standoff distance for a given source. Here it is recommended that field trials of candidate materials be tested to ensure minimal damage and that non-planer surfaces be investigated using the FCT code and analytical means in order to maximize absorption.
- Designing a practical configuration for armor fire. Here, the results from the first two steps will be used to design a practical blast-sound-absorbing surface for an armor range.
- Conducting a full-scale test. Here the results will be compared with theory and with calculations in order to further validate the design methods.
- Documenting the design method protocol and creating a corresponding manual.

Blast Sound Attenuation along the Propagation Path

The plowed-field test demonstrated some unexpected results at the lower frequencies. It is recommended that further research be conducted to understand the observed effects at low frequencies, including the large attenuation at 50 m and the apparent increase in low frequency levels with distance. Possible mechanisms might include acoustic-to-seismic coupling.

Ultimately, one objective is the far-field prediction of blast sound energies. To this end the NPE should be extended to better include rigid porous ground effects.

REFERENCES

Albert, D.G. (2002) Reduction of blast noise by snow cover. *Noise Control Engineering Journal,* **50**(6), 200–203.

Albert, D.G., and J.A. Orcutt (1990) Acoustic pulse propagation above grassland and snow: Comparison of theoretical and experimental waveforms. *Journal of the Acoustical Society of America,* **87**: 93–100.

American National Standards Institute (1999) *Template Method for Measuring Ground Impedance*. ANSI S1.18-1999, New York.

Attenborough, K. (1992) Ground parameter information for propagation modeling. *Journal of the Acoustical Society of America,* **92**: 418–427.

Attenborough, K., and T. Waters-Fuller (2000) Effective impedance of rough porous ground surfaces. *Journal of the Acoustical Society of America,* **108**(3): 949–956.

Attenborough, K., S. Taherzadeh, and C. Madshus (2002) Preliminary results from comparisons of infrasonic acoustic-seismic coupling data with predictions using FFLAGS. *Proceedings of the 10th Long Range Sound Propagation Symposium*, Grenoble.

Attenborough, K., T. Waters-Fuller, K.M. Li, and J.A. Lines (2000) Acoustic properties of farmland. *Journal of Agricultural Engineering Research,* **76**: 183–195.

Auregan, Y., and M. Pachebat (1999) Measurement of the nonlinear behavior of acoustical rigid porous materials. *Physics of Fluids,* **11**: 1342–1345.

Boris, J.P. (1976) Flux-corrected transport modules for solving generalized continuity equations. NRL memorandum report 3237, Naval Research Laboratory, Washington, D.C.

Boulanger, P.M., K. Attenborough, S. Taherzadeh, T. Waters-Fuller, and K.M. Li (1998) Ground effect over hard rough surfaces. *Journal of the Acoustical Society of America,* **104**: 1–9.

Cummings, A. (1989) A review of the use of porous materials to absorb sound at high levels. Consultancy report, Commins-BBM Partnership, London/ European Space Agency.

De Jong, B.A., A. Moerkerken, and J.D. Van Der Toorn (1983) Propagation of sound over grassland and over an earth barrier. *Journal of Sound Vibration,* **86**: 23–46.

Delany, M.E., and E.N. Bazley (1970) Acoustic properties of fibrous absorbent materials. A*pplied Acoustics,* **3**: 105–116.

Forchheimer, P.H. (1901) Zeitschrift des vereines deutscher. *Ingeneieure*, **45**: 1782–1788.

Gilbert, K.E., and M.J. White (1989) Application of the parabolic equation to sound propagation in a refracting atmosphere. *Journal of the Acoustical Society of America,* **85**: 630–637.

Johnson, D.L., J. Koplik, and R. Dashen (1987) Theory of dynamic permeability and tortuosity in fluid-saturated porous media. *Journal of Fluid Mechanics,* **176**: 379–402.

Kuntz, H.L., and D.T. Blackstock (1987) Attenuation of intense sinusoidal waves in air-saturated bulk porous materials. *Journal of the Acoustical Society of America,* **81**: 1723–1731.

Lambert, R.F., and J.D. McIntosh (1990) Nonlinear wave propagation through rigid porous materials. II. Approximate analytical solutions. *Journal of the Acoustical Society of America,* **88**: 1950–1959.

Li, K.M., Q. Wang, and K. Attenborough (1998) Sound propagation over convex impedance surfaces. *Journal of the Acoustical Society of America,* **104**(5): 2683–2691.

McDonald, B.E., P. Caine, and M. West (1994) A tutorial on the nonlinear progressive wave equation (NPE). Part 1. *Applied Acoustics,* **43**(2), 159–167.

McIntosh, J.D., and R.F. Lambert (1990) Nonlinear wave propagation through rigid porous materials. I. Nonlinear parameterization and numerical solutions. *Journal of the Acoustical Society of America,* **88**: 1939–1949.

McIntosh, J.D., M.T. Zuroski, and R.F. Lambert (1990) Standing wave apparatus for measuring fundamental properties of acoustic materials in air. *Journal of the Acoustical Society of America,* **88**(4): 1929–1938.

Salomons, E.M. (2000) NPE method for propagation of non-linear waves. TNO memorandum, HAG-MEM-000128. The Netherlands Organization for Applied Scientific Research.

Standley, E., O. Umnova, K. Attenborough, and A. Cummings (2002) Shock wave reflection measurements on porous materials. *Noise Control Engineering Journal,* **50**(6): 224–230.

Taherzadeh, S., and K. Attenborough (1999) Deduction of ground impedance from measurements of excess attenuation spectra. *Journal of the Acoustical Society of America,* **105**(3): 2039–2042.

Tooms, S., S. Taherzadeh, and K. Attenborough (1993) Sound propagation in a refracting fluid above a layered porous and elastic medium. *Journal of the Acoustical Society of America,* **3**(1): 173–181.

Umnova, O., K. Attenborough, and A. Cummings (2002) High amplitude pulse propagation and reflection from a rigid porous layer. *Noise Control Engineering Journal*, **50**(6): 204–210.

Umnova, O., K. Attenborough, A. Commings, and E. Standley (2003) Behavior of porous layers at high levels of continuous acoustic excitation: Theory and experiment. *Journal of the Acoustical Society of America*, **114**(3): 1346–1356.

Védy, E. (2002a) Numerical simulations of strong shocks. *Noise Control Engineering Journal*, **50**(6): 211–217.

Védy, E. (2002b) Simulations of flows in porous media with a flux corrected transport method. *Noise Control Engineering Journal*, **50**(6): 218–223.

Wilson, D.K., J.D. McIntosh, and R.F. Lambert (1988) Forchheimer-type nonlinearities for high-intensity propagation in air-saturated porous media. *Journal of the Acoustical Society of America*, **84**: 350–359.

APPENDIX A: PIT DESIGN

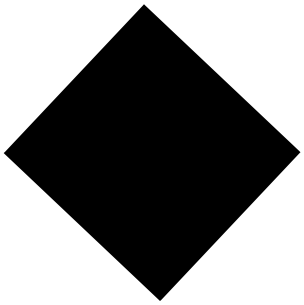

Pit
1.5-m below grade
3.66-m square
1.5-m depth
C-4, ~570 g max on pole
2-m above pit lip

Direction of Measurement

We use 3.66 m on a side which is exactly 12 ft. We need to fit to USA construction materials.

This gives us 2.6 m from the center to the corner.

Wall Sections

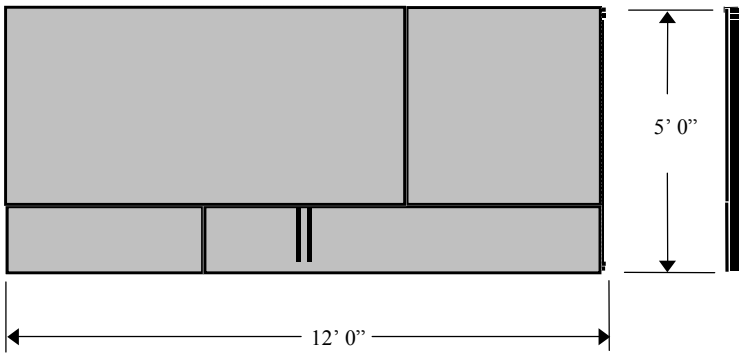

All dimensions are “outside”
All lumber is 2” x 6” nominal
Stud spacing is 12”, studs are approximately 4’ -6” long
Plates are 12’ -0” long
2” x 6” angle iron (3/16”) affixed to inside of top plate and pl ywood
1” plywood screwed to inside of wall .(SEE BLACK OUTLINE)
NO plywood for the last 1 -1/8” on right side of wall
Dual studs at ends; triple studs in center

Wall Sections--Metric Values

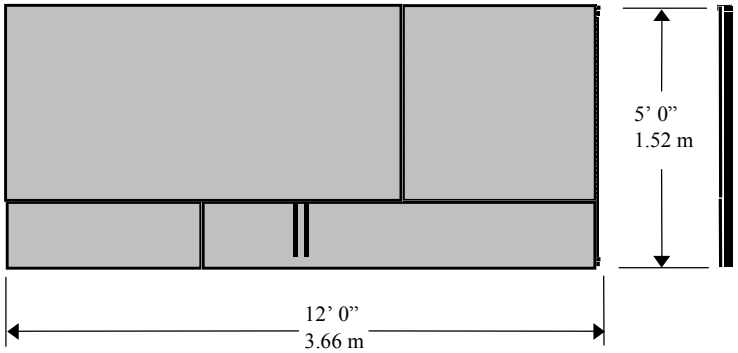

All dimensions are “outside”
All lumber is 2” x 6” nominal (approximately 38 X 140 mm as mill ed)
Stud spacing is 12” (30.5 cm), studs are approximately 4’ -6” long (1.372 m)
Plates are 12’ -0” long (3.66 m)
2” x 6” (51 x 152 mm) angle iron (3/16” [10 mm]) affixed to insi de of top plate and plywood
1” (25.4 mm) plywood screwed to inside of wall.(SEE BLACK OUTLIN E)
NO plywood for the last 1 -1/8” on right side of wall
Dual studs at ends; triple studs in center

Wall Sections --Studs and Plates Only

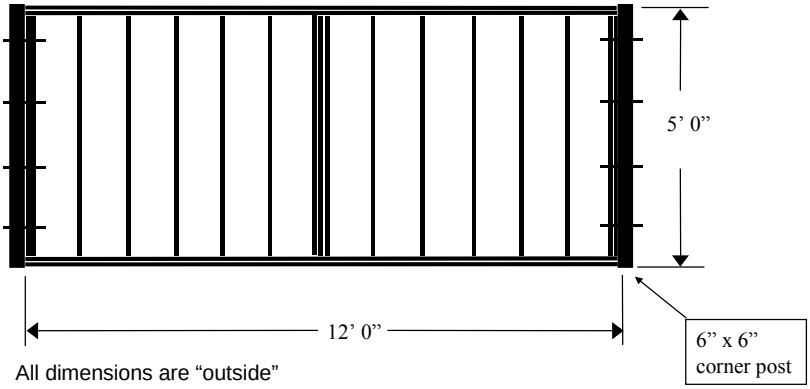

All dimensions are “outside”
All lumber is 2” x 6” nominal
Stud spacing is 12”, studs are approximately 4’ -6” long
Plates are 12’ -0” long
1” plywood **SCREWED** to inside of wall with large washers over screw heads.
Dual studs at ends bolted to (red) 6” x 6” corner posts
Triple studs in center for metal cross bracing

Wall Layout--Plan

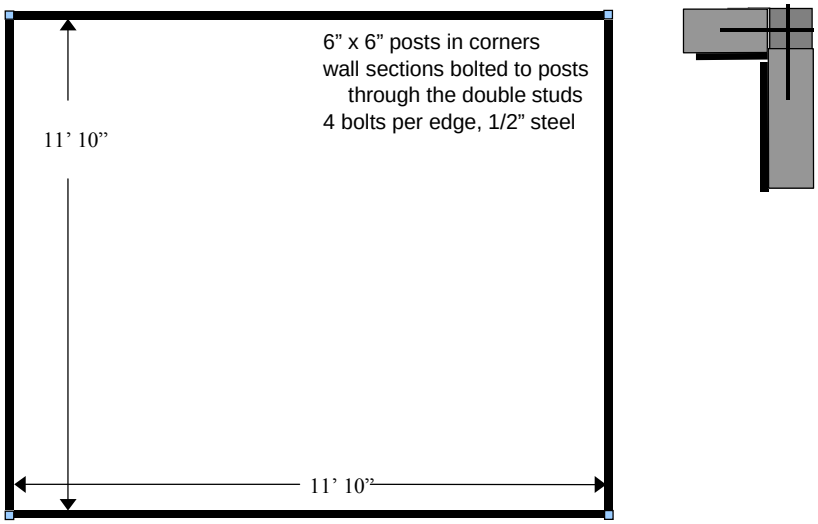

C-4 and Gages Placement

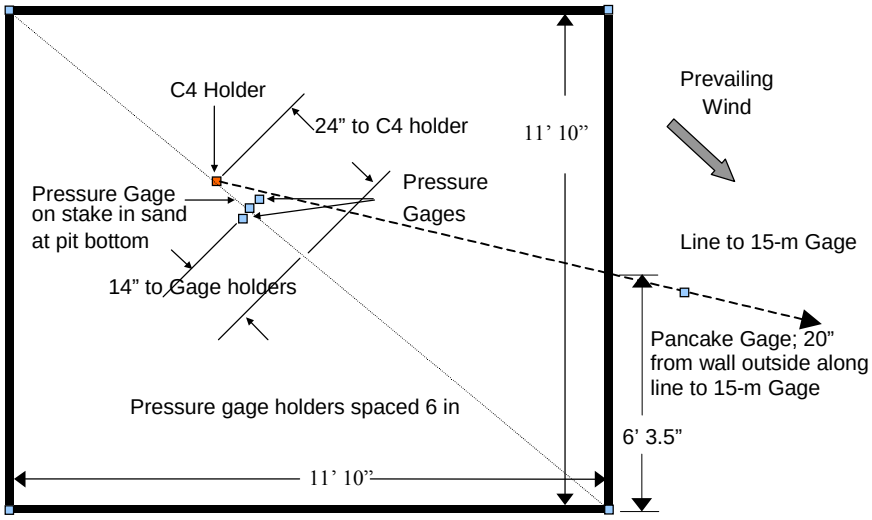

Pancake Gage is 156.2” (~4 m) from C-4 post.

APPENDIX B: PRESSURE–TIME HISTORIES FOR THE THREE PANCAKES AT 2.6 M USED FOR TEST I

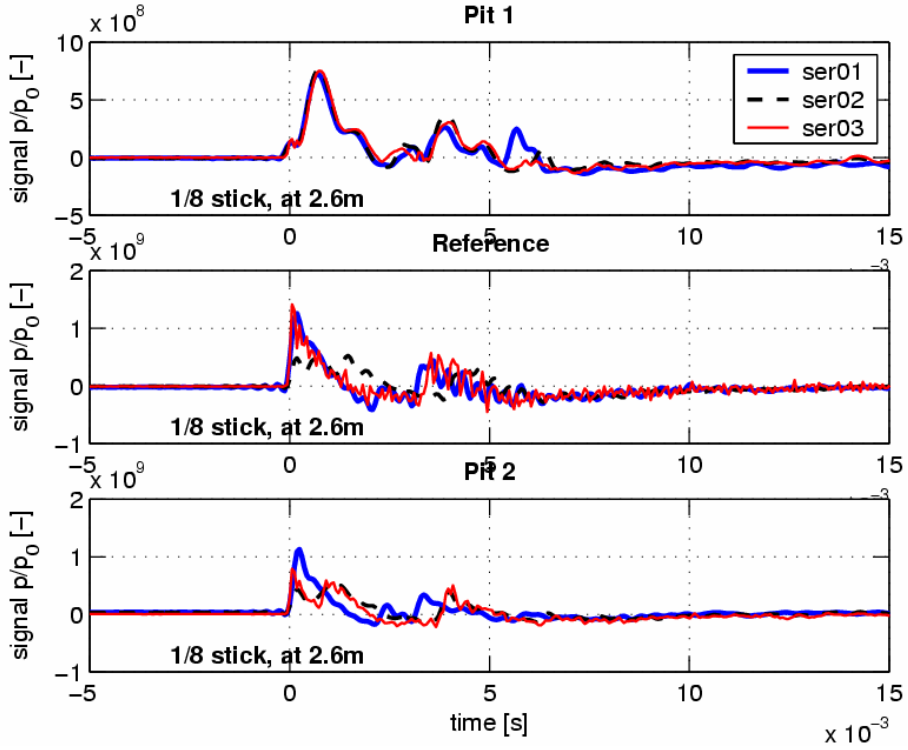

Figure B1. Pressure–time histories for the eighth-stick size at 2.6 m. The source was at 2.0-m height.

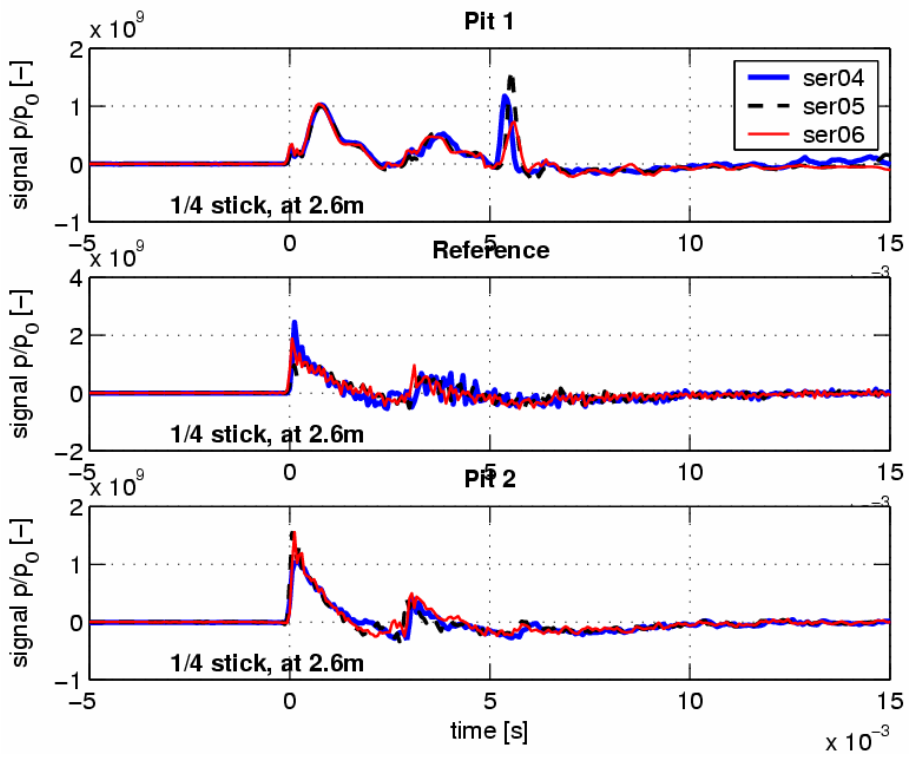

Figure B2. Pressure–time histories for the quarter-stick size at 2.6 m. The source was at 2.0-m height.

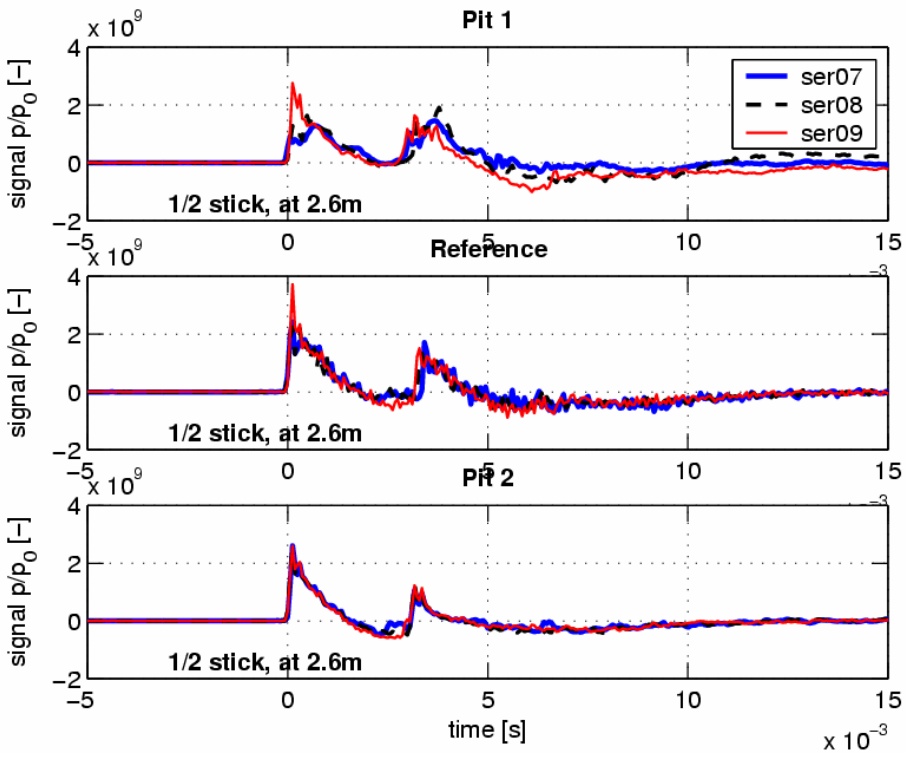

Figure B3. Pressure–time histories for the half-stick size at 2.6 m. The source was at 2.0-m height.

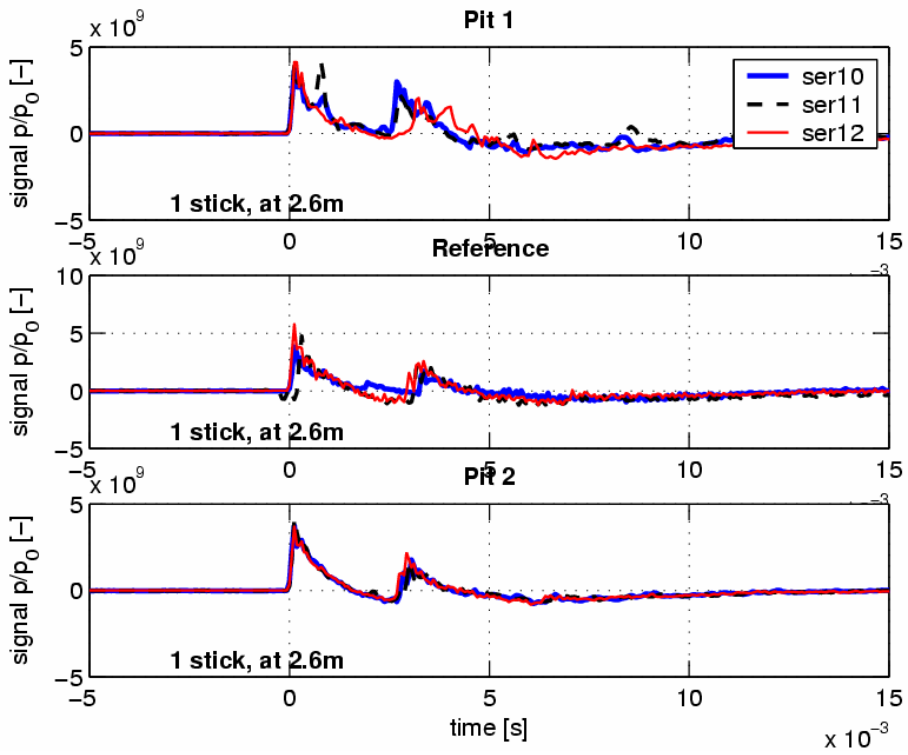

Figure B4. Pressure–time histories for the one-stick size at 2.6 m. The source was at 2.0-m height.

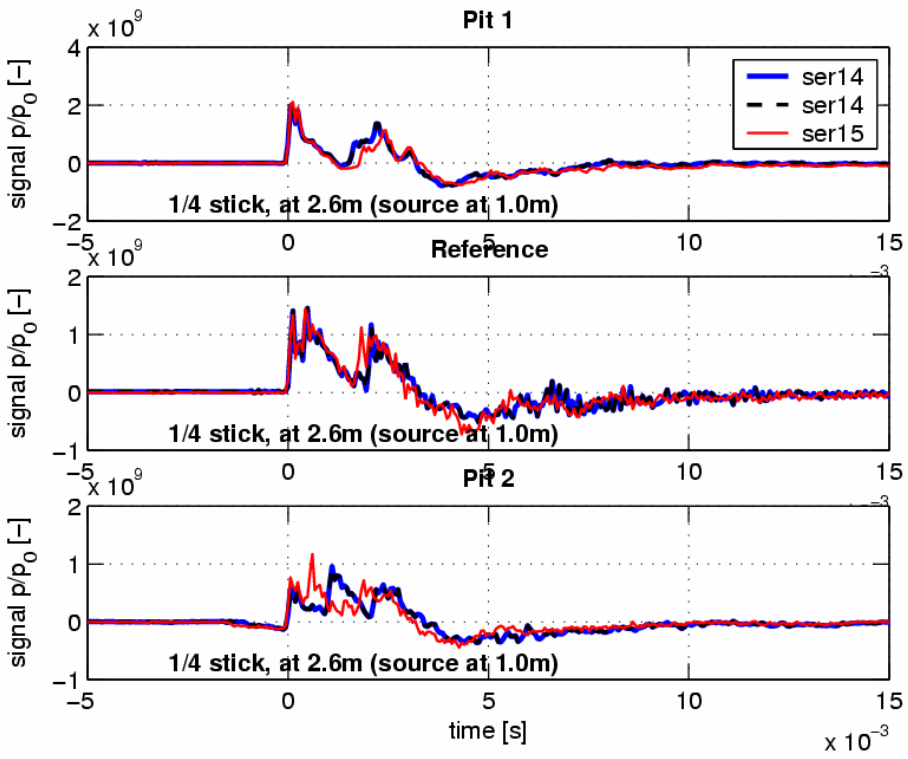

Figure B5. Pressure–time histories for the quarter-stick size at 2.6 m. The source was at 1.0-m height. Note: series 13 could not be used here.

REPORT DOCUMENTATION PAGE

Form Approved
OMB No. 0704-0188

1. REPORT DATE *(DD-MM-YY)*	2. REPORT TYPE	3. DATES COVERED *(From - To)*
September 2004	Technical Report	

4. TITLE AND SUBTITLE

Blast-Sound-Absorbing Surfaces:
A Joint Project of the ERDC and the Netherlands Ministry of Defense

5a. CONTRACT NUMBER

5b. GRANT NUMBER

5c. PROGRAM ELEMENT NUMBER

6. AUTHOR(S)

Keith Attenborough, Alan Cummings, Piyush Dutta, Paul Schomer, Erik Salomons, Edwin Standley, Olga Umnova, Frank Van Den Berg, Frits Van Der Eerden, Pieter Van Der Weele, and Eric Védy

5d. PROJECT NUMBER

5e. TASK NUMBER

5f. WORK UNIT NUMBER

7. PERFORMING ORGANIZATION NAME(S) AND ADDRESS(ES)

U.S. Army Engineer Research and Development Center
Cold Regions Research and Engineering Laboratory
72 Lyme Road
Hanover, NH 03755-1290

8. PERFORMING ORGANIZATION REPORT

ERDC/CRREL TR-04-17

9. SPONSORING/MONITORING AGENCY NAME(S) AND ADDRESS(ES)

10. SPONSOR / MONITOR'S ACRONYM(S)

11. SPONSOR / MONITOR'S REPORT NUMBER(S)

12. DISTRIBUTION / AVAILABILITY STATEMENT

Approved for public release; distribution is unlimited.

Available from NTIS, Springfield, Virginia 22161.

13. SUPPLEMENTARY NOTES

14. ABSTRACT

This research investigated methods of absorbing blast sound, including the development of analytical theories, numerical simulations, laboratory experiments, and a field trial. Prior to this research, no theory existed for the design of sound-absorbing surfaces at low frequencies in a highly non-linear shock environment. The work includes developments of (1) a theory for the non-linear response of rigid-porous materials to high amplitude sound, allowing for a linear variation of flow resistivity with flow velocity (Forchheimer's non-linearity); (2) a time-domain non-linear theory that assumes low frequencies, semi-infinite media, and weak shocks and gives explicit results for incident triangular shock waveforms; (3) an alternative time-domain formulation that enables predictions for a finite layer but requires numerical integration; and (4) a further non-linear theory that predicts the response of multiple rigid-porous layers to continuous high-intensity sound. Numerical work has been carried out to predict the surface impedance of a porous and elastic layer subject to continuous high-intensity sound and including Forchheimer's non-linearity. Measurements have been made on the propagation constant, characteristic impedance, and reflection coefficients for finite-amplitude, low-frequency continuous sound waves incident on porous concrete, porous aluminum, sand, gravel stones, perforated panels, and open-cell polymer foams. In addition, shock tube systems based on membrane rupture have been used to look at the acoustic shock response of materials. Finally, the far-field propagation is modeled using parabolic equation method. A full-scale field test using high explosives was conducted at Ft. Drum, NY. The primary purpose was to test predictions of the blast reflection from and attenuation into a porous medium, and a secondary objective was to test the effect of plowing the ground surface over a larger area. Charges of C4 were exploded over two candidate blast sound-absorbing test surface sections filled with gravel stones. The non-linear theory for response of rigid-porous layers to continuous high amplitude sound has been found to give predictions in good agreement with impedance tube data. The most interesting behavior is that the reflection coefficient decreases at first as incident sound pressure increases. The non-linear theory for the impulse response of single rigid-porous layers has been found to give predictions in good agreement with laboratory measurements of shock wave reflection and transmission. The predictions of the plane wave non-linear theories have been found to be in reasonable agreement with reflection and transmission data from Ft. Drum.

15. SUBJECT TERMS

Acoustic impedance
Blast sound absorber
Forchleimer non-linearity
High-intensity sound
Propagation constant
Reflection coefficient
Rigid porous absorber
Surface impedance
Weapons firing noise

16. SECURITY CLASSIFICATION OF:			17. LIMITATION OF ABSTRACT	18. NUMBER OF PAGES	19a. NAME OF RESPONSIBLE PERSON
a. REPORT	b. ABSTRACT	c. THIS PAGE			19b. TELEPHONE NUMBER *(include area code)*
U	U	U	U	114	